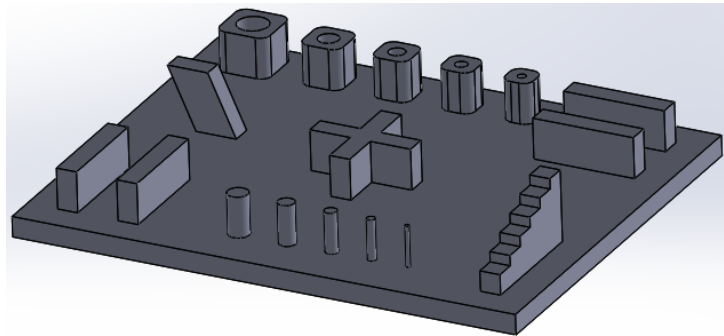




TÉCNICO
LISBOA



Fabrication of a test artifact for WAAM

Lourenço Drumond Dias

Thesis to obtain the Master of Science Degree in

Mechanical Engineering

Supervisors: Prof. Inês da Fonseca Pestana Ascenso Pires
Prof. Eurico Gonçalves Assunção

Examination Committee

Chairperson: Prof. Rui Manuel dos Santos Oliveira Baptista
Supervisor: Prof. Eurico Gonçalves Assunção
Members of the Committee: Prof. Carlos Manuel Alves da Silva
Eng. João Pedro da Fonseca Matos Pragana

October 2020

Acknowledgments

Firstly, I would like to thank Professor Inês Pires and Eurico Assunção not only for the opportunity to work on this subject, but also for the guidance and help provided throughout this challenging project.

I also have to extend my thanks to all the laboratory personnel, that were always available to help, not only with equipment related matters, but also with suggestions that could be beneficial for the development of my work.

Just as importantly, I would like to thank all the friends that I had the luck and privilege to make along this academic adventure. For creating such a close group of supportive people that helped me through the toughest times, a sincere thank you.

On the topic of friends, I must thank one of my longest lasting friends, Matilde, with whom I have shared a lot of moments, and this thesis was yet another one in which she helped me get through. Equally, I have to thank Nuno, which I have known for many years now, and besides helping me to get through the recent lockdown days a bit faster, also contributed as he could for the making of this work.

To my girlfriend Beatriz, a thank you is no way near enough to express the gratitude for continuously picking me up when I was feeling down, and encouraging to keep going through the hardest moments.

Finally, I would like to thank my family, that helped me get to where I am today, and always encouraged me to follow the path that I thought better. As such I would like to dedicate this work to my parents and brother, who have always made sacrifices for my well being and success.

Resumo

Com o aumento do interesse pelo fabrico aditivo em metal, causado pela sua capacidade de reduzir o desperdício de material e tempo de execução a cada peça, vem conseqüentemente um crescimento da necessidade de test artifacts, que permitem aumentar ainda mais o impacto destas vantagens. Apesar deste facto, atualmente ainda não existe um *test artifact* exclusivamente dedicado à análise de peças produzidas por WAAM. Como tal, neste trabalho foi desenvolvido um *test artifact* constituído por uma parede inclinada de 60°, um conjunto de pinos finos que reduzem progressivamente o seu diâmetro até a instalação não conseguir replicar as dimensões do modelo CAD, um conjunto de furos finos cujo diâmetro também é reduzido progressivamente até atingir uma falha dimensional, dois conjuntos de paredes retas orientadas ao longo dos eixos do X e Y, uma intersecção em forma de cruz e um incremento vertical em forma de escada.

Após a otimização dos parâmetros de deposição, os resultados revelaram os elementos mais pequenos que são possíveis de imprimir na instalação selecionada, assim como o intervalo de inclinação no qual é possível produzir paredes inclinadas. Para além disso, foi possível avaliar a forma como a instalação lidava com intersecções e geometrias com um aumento de calor interno. Mais importante ainda, o test artifact criado permitiu identificar várias limitações quer de software e de hardware, além de permitir avaliar o desempenho do braço robótico ao longo dos eixos X, Y e Z e averiguar a existência de erros de calibração ou desvios.

Palavras-chave: Wire Arc Additive Manufacturing (WAAM), test artifact, geometrias padrão, avaliação da instalação, limitações de hardware/software, precisão dimensional, desvios dos eixos.

Abstract

With the current increasing interest in metal additive manufacturing, caused by its capacity to reduce both material waste and lead times of each part, comes a subsequent growing need of test artifacts that allow to further increase the extent of these advantages. Be that as it may, there isn't a test artifact dedicated to the exclusive analyses of WAAM produced parts. As such, in this work a test artifact was developed comprised of a 60° inclined wall, a set of thin pins that progressively reduced in diameter until the setup failed to replicate the CAD model's dimensions, a set of thin resolution holes whose diameter also progressively reduced until dimensional failure was achieved, two sets of straight walls oriented both along the X and Y axes, a cross shaped intersection and a staircase vertical increment.

Upon deposition parameters optimization, the results revealed the thinnest features possible to print on the selected setup, as well as the range of inclination at which was possible to produce inclined walls. Moreover, it was possible to assess how the setup dealt with geometries with intersections and cross-overs, as well as geometries with increasing internal heat accumulation. More importantly, the test artifact created allowed to pinpoint several hardware and software limitations in addition to allowing to evaluate the performance of the robotic arm's along the X, Y and Z axes, and look for any existing miscalibrations or deviations.

Keywords: Wire Arc Additive Manufacturing (WAAM), test artifact, benchmark geometries, setup evaluation, hardware/software limitations, dimensional accuracy, axes deviations.

Contents

- Acknowledgments iii
- Resumo v
- Abstract vii
- List of Tables xi
- List of Figures xiii
- Glossary xvii

- 1 Introduction 1**
- 1.1 Motivation 1
- 1.2 Objectives 2
- 1.3 Thesis Outline 2

- 2 Literature Review 5**
- 2.1 Additive Manufacturing 5
- 2.2 Wire Arc Additive Manufacturing 6
 - 2.2.1 Deposition Strategies 8
- 2.3 Test Artifacts 11
- 2.4 International Standard 16

- 3 Materials and Test Methods 19**
- 3.1 Equipment and setup 19
- 3.2 Setup Procedure: User Guide 21
 - 3.2.1 Setup Power On/Off 23
 - 3.2.2 Kuka’s Manual Movement 23
 - 3.2.3 Referencing the Base’s Position 25
 - 3.2.4 Wire, Gas and Welding Process Selection 25
 - 3.2.5 Changing the Wire Feed Speed 25
 - 3.2.6 Transferring a deposition path to the KUKA 25
 - 3.2.7 Running a Deposition Path 27
 - 3.2.8 Opening the Gas Valve 28
- 3.3 Experimental Procedure 29
 - 3.3.1 Overhanging Structures 30

| | | |
|----------|--|-----------|
| 3.3.2 | Thin Pins | 32 |
| 3.3.3 | Thin Vertical Resolution Holes | 32 |
| 3.3.4 | Straight Walls and Cross Shaped Intersection | 33 |
| 3.3.5 | Staircase Vertical Increment | 35 |
| 4 | Results and Analyses | 37 |
| 4.1 | Overhanging Structures | 37 |
| 4.2 | Thin Pins | 44 |
| 4.3 | Thin Resolution Holes | 48 |
| 4.4 | Straight Walls and Cross Shaped Intersection | 53 |
| 4.5 | Staircase Vertical Increment | 57 |
| 4.6 | Setup Limitations | 59 |
| 4.6.1 | Hardware Limitations | 59 |
| 4.6.2 | Software Limitations | 61 |
| 4.7 | Test Artifact | 65 |
| 5 | Conclusions | 69 |
| 5.1 | Future Work | 70 |
| | Bibliography | 73 |
| A | Deposition paths | 77 |
| A.1 | Inclined Walls | 77 |
| A.2 | Thin Pins | 78 |
| A.3 | Thin Resolution Holes | 80 |
| A.4 | Straight Walls | 83 |
| A.5 | Cross Shaped Intersection | 84 |
| A.6 | Staircase Vertical Increment | 85 |

List of Tables

| | | |
|------|--|----|
| 4.1 | Voltage and current of several depositions at constant velocity. | 40 |
| 4.2 | Heat input for three distinct cases where WFS=TS | 42 |
| 4.3 | Thin pins final parameters. | 47 |
| 4.4 | Thin pin's final measurements and respective deviations from the CAD. | 47 |
| 4.5 | Thin vertical resolution holes final parameters. | 50 |
| 4.6 | Thin vertical resolution hole's final measurements and respective deviations from the CAD. | 51 |
| 4.7 | Heat input per square millimeter values for each part. | 52 |
| 4.8 | Final parameters for both the deposition strategies of the straight walls. | 54 |
| 4.9 | Straight wall's final measurements and respective deviations from the CAD. | 55 |
| 4.10 | Cross shaped intersection final dimensions and respective deviations from the CAD. | 57 |
| 4.11 | Staircase vertical increment final dimensions and respective deviations from the CAD. | 59 |
| 4.12 | Distances, in millimeters, between walls for both X-axis and Y-axis aligned walls. | 67 |

List of Figures

| | | |
|------|--|----|
| 2.1 | Types of Metal Additive Manufacturing. | 6 |
| 2.2 | The Phases of Cold Metal Transfer [6]. | 7 |
| 2.3 | Deposition Strategies: a) Unidirectional with a constant start point b) Unidirectional alternating the start point c) Crosswise d) In a spiral form e) Weaving f) Oscillation. | 9 |
| 2.4 | Illustration of the part's heat exchange for both the oscillation and the unidirectional parallel depositions [13]. | 9 |
| 2.5 | Wall depressions caused by depositions with constant start and end points. [12] | 10 |
| 2.6 | Illustration of the effect of alternating the deposition start and end points, when building cross shaped parts [17]. | 10 |
| 2.7 | Example deposition paths used by Venturini for the production of T-crossings [18]. | 11 |
| 2.8 | Inclined walls problem and solution. [12] | 11 |
| 2.9 | AM test artifact projected by Mahesh et al. [21]. | 13 |
| 2.10 | Examples of test artifacts Moylan et al. [20] | 13 |
| 2.11 | Examples of geometries with intersections and height variations. | 14 |
| 2.12 | Examples of geometries with overhangs and smaller heat exchange sections. | 15 |
| 2.13 | Illustration of the minimum amount of measurements per dimension. Example of thin resolution pins [31]. | 17 |
| 3.1 | Important input parameters for a successful deposition. | 20 |
| 3.2 | Setup's main components and respective controllers. | 22 |
| 3.3 | Setup's main components and respective controllers. | 23 |
| 3.4 | Representation of the 6 axes of freedom of the KUKA 150 L110-2 F 2000 [32]. | 24 |
| 3.5 | Highlight of the buttons and icons needed for the manual use of the KUKA robot. | 24 |
| 3.6 | Setup's main components and respective controllers. | 26 |
| 3.7 | Indication of the parameter needed to change the WFS. | 26 |
| 3.8 | Symbols used to represent the two types of error. | 27 |
| 3.9 | Detail of some of the most important buttons, switches and indications, to perform a deposition. | 28 |
| 3.10 | Both positions of the lever, for closed and open gas valve. | 29 |
| 3.11 | Both positions of the lever, for closed and open gas valve. | 30 |
| 3.12 | Examples of overhanging structures. | 30 |

| | |
|---|----|
| 3.13 Representation of a force model during the fabrication of a inclined wall, [34]. | 31 |
| 3.14 Structure with a fully overhanging feature decomposed into buildable and unbuildable sub-volumes, [35] | 31 |
| 3.15 Thin pins with 10mm, 8mm, 6mm and 4mm respectively. | 32 |
| 3.16 CAD model of the thin vertical resolution holes and respective dimensions in mm. | 33 |
| 3.17 CAD model and respective deposition paths for the straight walls. | 34 |
| 3.18 CAD model of the cross shaped intersection. | 35 |
| 3.19 CAD model of the staircase vertical increment and key dimensions in mm. | 35 |
| | |
| 4.1 Effect of WFS in the deposition of inclined walls. | 38 |
| 4.2 Effect of TS in the deposition of inclined walls. | 39 |
| 4.3 Heat input variation comparison for different values of TS and WFS. | 40 |
| 4.4 Examples of different outcomes for the same $\frac{WFS}{TS}$ ratio, in the deposition of inclined walls. | 41 |
| 4.5 Influence of the layer height in the deposition of inclined walls. | 43 |
| 4.6 Final deposition of a 60° inclined wall, without defects. | 43 |
| 4.7 Original and final dimensions of the inclined wall, in millimeters (mm). | 44 |
| 4.8 Two different deposition paths, for different positions of the guide line. | 45 |
| 4.9 Different geometrical outcomes, for different deposition paths. | 46 |
| 4.10 Two different deposition paths, for different deposition segments distances. | 46 |
| 4.11 Final results for all the attempted pins. | 47 |
| 4.12 Unsatisfactory connection of the two segments, both for a horizontal and vertical single deposition path strategy. | 49 |
| 4.13 Example of the complementarity between odd and even layers. | 49 |
| 4.14 Display of the deposition path in smaller thickness areas and consequent deposited geometry. | 50 |
| 4.15 Final results for all the attempted thin resolution holes. | 52 |
| 4.16 Different custom zones depending on the deposition guide line deposition. | 54 |
| 4.17 Final straight walls. | 55 |
| 4.18 Representation of the custom zones necessary to the manufacture of the cross shaped intersection. | 56 |
| 4.19 Final cross shaped intersection. | 56 |
| 4.20 Profile representation of staircase vertical increment and each deposition segment (S). | 57 |
| 4.21 Different perspectives on the final staircase vertical increment. | 58 |
| 4.22 Effects of the undesired velocity alteration in the last segment of each layer. | 60 |
| 4.23 Material accumulation at the top of the thin pin, due to the arc ignition delay. | 61 |
| 4.24 Example of a start and finish of deposition not coinciding with the ones defined by the user. | 62 |
| 4.25 Similar distance between the deposition parcels and the ends of the part, for two distinct values of deposition parcel distance. | 62 |
| 4.26 The importance of deposition path extensions in a straight wall [44]. | 63 |

| | | |
|------|--|----|
| 4.27 | Deposition guide software limitations. | 64 |
| 4.28 | Deposition guide software limitations. | 64 |
| 4.29 | CAD model of the projected test artifact. | 66 |
| 4.30 | Final outcome of the test artifact. | 67 |
| | | |
| A.1 | Deposition paths for the 60° inclined wall. | 77 |
| A.2 | Deposition paths for the 10 mm pin. | 78 |
| A.3 | Deposition paths for the 8 mm pin. | 78 |
| A.4 | Deposition paths for the 6 mm pin. | 79 |
| A.5 | Deposition paths for the 4 mm pin. | 79 |
| A.6 | Deposition paths for the 15 mm thin resolution hole, with a horizontal guide line. | 80 |
| A.7 | Deposition paths for the 15 mm thin resolution hole, with a vertical guide line. | 80 |
| A.8 | Deposition paths for the 10 mm thin resolution hole, with a horizontal guide line. | 81 |
| A.9 | Deposition paths for the 10 mm thin resolution hole, with a vertical guide line. | 81 |
| A.10 | Deposition paths for the 8 mm thin resolution hole, with a horizontal guide line. | 82 |
| A.11 | Deposition paths for the 8 mm thin resolution hole, with a vertical guide line. | 82 |
| A.12 | Deposition paths for the straight wall, with a horizontal guide line. | 83 |
| A.13 | Deposition paths for the straight wall, with a vertical guide line. | 83 |
| A.14 | Deposition paths for the cross shaped intersection, with a vertical guide line. | 84 |
| A.15 | Deposition paths for the staircase vertical increment, up until layer 10. | 85 |
| A.16 | Deposition paths for the staircase vertical increment, for layers 11 e 12. | 85 |
| A.17 | Deposition paths for the staircase vertical increment, for layers 13 e 14. | 86 |

Glossary

| | |
|-------------|----------------------------------|
| AM | Additive Manufacturing. |
| CMT | Cold Metal Transfer. |
| DED | Direct Energy Deposition. |
| EWT | Effective Wall Thickness. |
| GMAW | Gas Metal Arc Welding. |
| GTAW | Gas Tungsten Arc Welding. |
| MAG | Metal Active Gas. |
| MIG | Metal Inert Gas. |
| PAW | Plasma Arc Welding. |
| SW | Surface Waviness. |
| TS | Travel Speed. |
| WAAM | Wire Arc Additive Manufacturing. |
| WFS | Wire Feed Speed. |

Chapter 1

Introduction

1.1 Motivation

Over the past few decades, there has been a dramatic increase over the amount of research and development done over the subject of additive manufacturing (AM). Such is justified by the advantages that come with this relatively new manufacturing method, such as the production of near-net shaped geometries, whilst simultaneously reducing the respective lead times, as well as the wastage of material.

One of these AM techniques, that's dedicated to the manufacture of metal parts, is the wire arc additive manufacturing (WAAM). This process combines the use of an electric arc as a heat source and wire as feedstock, through the use of welding equipment (torch, feeding system and power source) [1]. WAAM is a process that is better fitted for medium to low complexity geometries and normally abstains from the production of small feature parts.

As it's always advantageous to have a way to test the performance of a manufacturing setup, as well as different deposition parameters, sets of benchmark geometries are developed for this purpose, forming the so called test artifacts. These artifacts allow to, not only test several types of geometries all at once, but also identify potential flaws and limitations within the setup, thus saving time and material that would be otherwise wasted on several attempts of manufacture of a potentially large part.

However, although there are some clear differences in geometric complexity and tighter dimensional tolerances, between generic AM test artifacts and metal AM test artifacts, due to their different nature, the same is not always verified for different manufacturing processes within metal AM. This means that a user might have to turn to the same test artifact to analyse both a part produced by an electric arc-based process and another produced by a laser-based process.

As previously explained, WAAM is not as efficient when building small or complex geometries. However, there isn't a test artifact aimed at analysing the output geometries of this process, and instead, the current alternatives are to utilize generic metal AM test artifacts. Since WAAM cannot match the same level of geometrical accuracy of other metal AM processes, these artifacts are naturally not an efficient tool to a process such as this. As an example, the current international standard aiming at the plan and creation of metal AM test artifacts, holds a section destined to the evaluation of the thinnest feature

feasible to perform by a setup. However, as it shall be presented further on this work, the dimension of the standard's biggest test element matched the thinnest feature produced by a basic WAAM setup.

There's, thus, a need for a test artifact that allows an accurate evaluation of WAAM produced parts, respecting the limitations that are induced by the process and respective setups.

1.2 Objectives

The main objective that this thesis sets out to accomplish, is to satisfy the existing need of a WAAM focused test artifact. In order to satisfy said objective, the test artifact must be capable of the following:

- Select and test several types of geometries that are possible to produce using WAAM, providing the user with information regarding the outcome of a potential final part, as well as the difficulties that might arise during its manufacture;
- Present the user with multiple ways to check the performance and accuracy of each axis, thus allowing to identify any possible miscalibrations or deviations, and consequently, a need to perform some maintenance work on the equipment;
- Pinpoint any manufacturing limitation, either related to the setup's hardware or software.

1.3 Thesis Outline

This thesis is divided into 5 different chapters. Chapter 1 is the current one, where an introduction to the motivation behind the present work is bestowed.

Chapter 2 focusses on briefly presenting the concept of additive manufacturing, and subsequently introducing the subject of metal additive manufacturing and its respective different processes available. An overview of WAAM is then presented, introducing its variants and inherent defects. A brief compilation of several of the WAAM's deposition strategies is also shown, describing the associated advantages and disadvantages, in addition to some geometry specific deposition paths. The chapter then advances to an introduction on test artifacts, their purpose and requirements that must be accomplished when designing new ones. This information is further complemented at the end of the chapter with a brief overview of the ISO-ASTM 52902 standard.

Chapter 3 starts by presenting the setup used throughout this thesis, describing both the software and hardware setup procedures. The other main focus of this chapter is to introduce the selected benchmark geometries, presenting the respective dimensions, associated problems and the features that will be evaluated once built.

Chapter 4 exhibits the results obtained and an analysis of the deposition parameters and their influence on the deposited geometries, as well as the dimensional deviations between the projected CAD models and the final parts. A description of the software and hardware limitations is then presented, followed by a presentation of the suggested test artifact, and information that it allowed to gather.

Chapter 5 displays the conclusions assembled through the course of this work and finalises by presenting some suggestions for future work aimed at continuing the development of the test artifact created.

Chapter 2

Literature Review

2.1 Additive Manufacturing

Additive manufacturing (AM), also known as three-dimensional (3D) printing, rapid manufacturing or layer manufacturing, has allowed for great developments in the manufacturing industry, with great benefits to, for example, the medical and the aerospace sectors. Although AM encompasses several material options, this thesis will focus solely on metal manufacturing.

Among others, there are two main groups in which metal manufacturing processes can be separated in: subtraction techniques and additive manufacturing. The first is also called the "traditional process", in which, material is removed from a stock part until it has the desired geometry. The latter refers to processes that join material, usually by melting raw feedstock and adding it layer upon layer, over a substrate, until the final part is achieved. Levy et al. [2] describes AM as a process specially indicated for medium to high geometrical complexity parts and for low quantities for production.

Metal additive manufacturing is an attractive fabrication technology as it provides near net shape components, with complex geometries, greater individual customization and both a lower lead time and associated costs, when compared to traditional methods. However some machining might be needed in the final stages, for a better finish. The heat sources used in this process, are similar to those found in the most common welding processes.

Within metal AM, there are several approaches available, the four main ones being via Binder Jetting, Direct Energy Deposition (DED), Powder Bed Fusion (PBF) or Sheet Lamination. Binder Jetting operates using the principle of depositing binder material on a metal powder, curing the binder to hold the powder together, sintering or consolidating the bound powder and, optionally, infiltrating with a second metal [3]. Sheet Lamination takes another approach, stacking precision cut metal sheets into 2D part slices from a 3D object. After stacking, these sheets are either joined using adhesives or metallurgically bonded using an adequate joining process [3]. The main difference between the other two processes lies in the feeding mechanism: while PBF melts a layer of metal powder, using a laser or an electron beam, DED utilizes a focused energy source (laser, arc or electron beam) to melt the feed-stock that can be either wire or powder. An overview of the several types of metal AM is shown in figure 2.1.

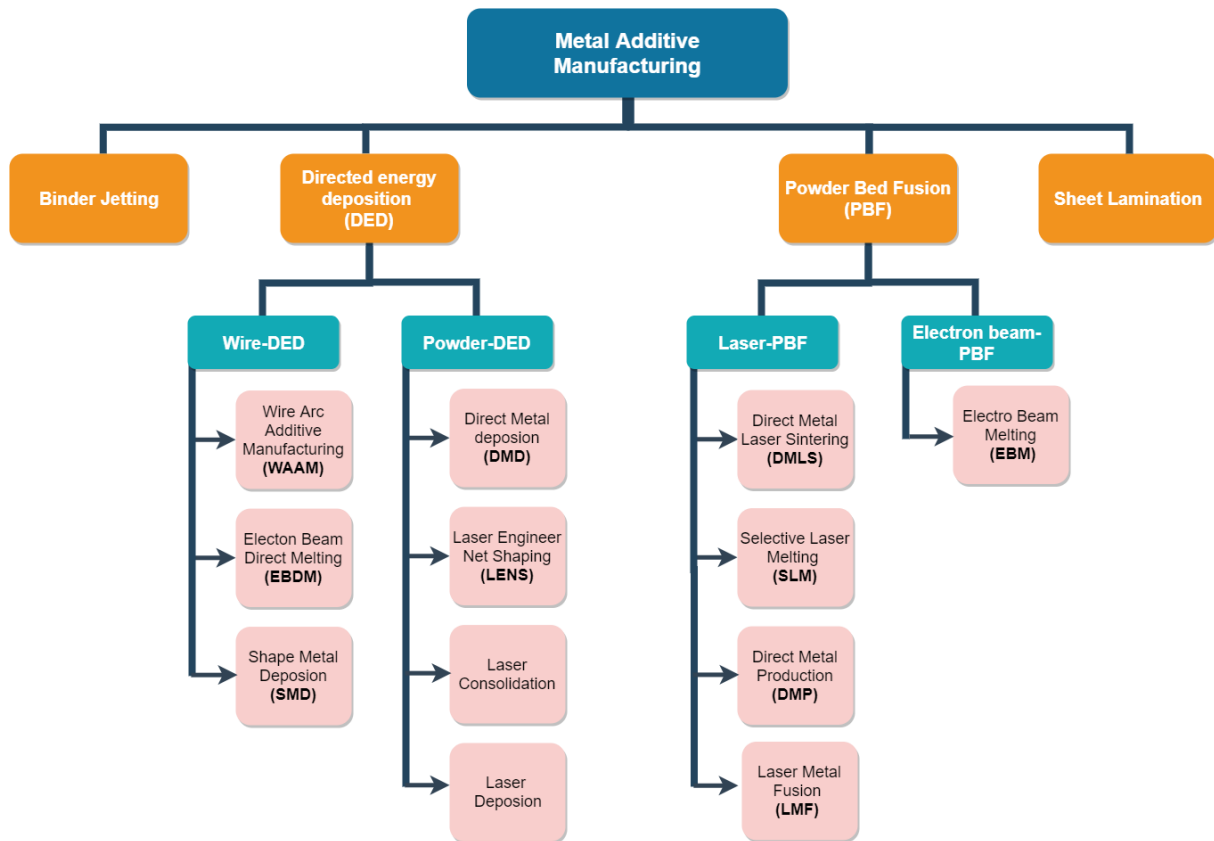


Figure 2.1: Types of Metal Additive Manufacturing.

2.2 Wire Arc Additive Manufacturing

After analyzing figure 2.1, it can be inferred that Wire Arc Additive Manufacturing (WAAM) is a DED technique that uses an electric arc as heat source to melt the wire feedstock. As stated in the previous subsection, Metal additive manufacturing processes, such as WAAM, use the same equipment used in welding (wire feeding mechanisms, heat sources, protective atmospheres). This leads to some variants within the process, depending on the type of equipment being used:

- Gas Tungsten Arc Welding (GTAW);
- Plasma Arc Welding (PAW);
- Gas Metal Arc Welding (GMAW) or Metal Inert Gas/ Metal Active Gas (MIG/MAG).

The GMAW variant is the most used for WAAM, not only due to its high deposition rate, that allows for smaller lead times, but also because it's the only variant in which the wire feedstock is fed from within the torch, requiring a less complex code for the robotic arm or adapted CNC machine, responsible for the movement of the torch. GMAW uses a protective atmosphere of an active or inert gas, in order to protect the molten pool and the adjacent material.

In order to overcome problems inherent to GMAW, such as the instability of the arc and a great amount of spattering, Fronius introduced a variant of GMAW: Cold Metal Transfer (CMT). CMT regulates the dip transfer with the aid of sensors to measure arc length, short circuiting phase and thermal input.

When the wire is moved forward and touches the molten pool, the mechanism detects the resultant short-circuit, reduces the current and signals the wire feeder to retract. The drawback of the wire forces the droplet to detach, and the process is then repeated (figure 2.2). According to Almeida and Williams [4], the backwards movement of the wire reduces significantly the spatter, as no droplets transfer from the gap between the wire and the base material.

Selvi et al. [5] separates the CMT process in three main phases:

- **The peak current phase:** the voltage of the arc is constant and there's a pulse of current, which causes the ignition of the welding arc. The arc melts the wire feedstock, creating molten droplets at the tip of wire.
- **The background current phase:** The current is lowered to avert the transfer of the droplet, which could cause spattering.
- **The short-circuiting phase:** The arc voltage is null and the wire feeder receives a signal to pullback the wire. This back-drawing force facilitates the detachment of the droplet and transfer of material into the welding pool.

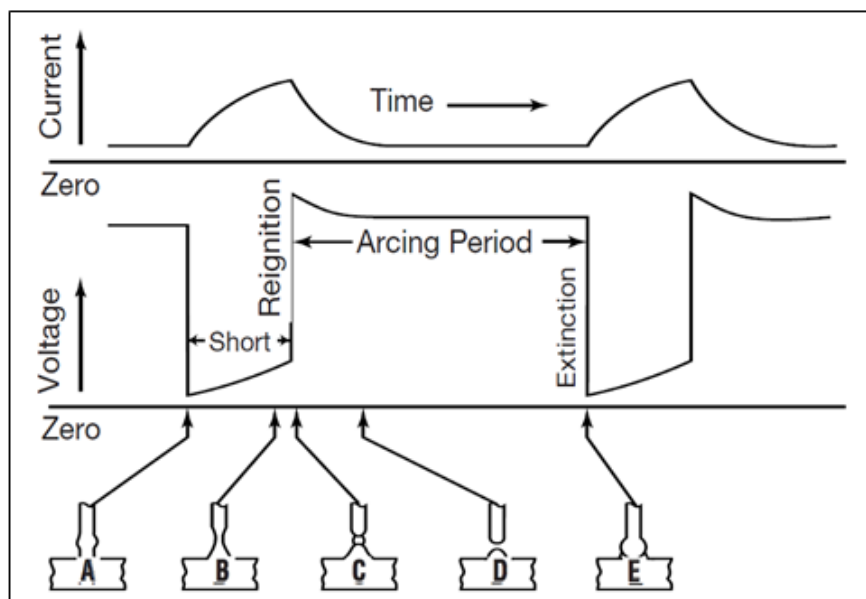


Figure 2.2: The Phases of Cold Metal Transfer [6].

As WAAM is an electric arc process, its susceptible to the same type of defects usually associated with electric arc-based welding, such as pin hole voids, incomplete melting, incomplete filling, hot/cold cracking, spattering and lamellar tearing. In addition to these, some other problems are known to be associated with WAAM as stated by Oliveira et al. [7], such as:

- **Side collapse**, due to the great heat dissipation at the start of the layers, and low dissipation at the end of each layer. This leads to unflattened surfaces;
- **Bending distortion after unclamping**, a consequence of excessive heat input and accumulation;

- **Porosity**, which can be a result of poor wire batch quality, inadequate process parameters or the use of the wrong shielding gas;
- **Unmelted wire stuck to the final part**, due to a wire stick-out that is too long, causing the current to detach the wire without melting it.

Most of these problems can be minimized, or even eliminated, by simply readjusting process parameters and the tool path. These parameters include: current intensity, voltage, shielding gas type and flow rate, contact-tip-to-work distance, wire feed speed, travel speed, and torch angle.

Using pre/post-processing heat treatment can also be advantageous, allowing to alleviate residual stresses in the part. Roman et al. [8] successfully tested the validity of the use of analytic expressions to predict a part's deformation and stress redistribution. With said expressions, the part designer can adapt the parts geometry or the process parameters in order to reduce the deformation, without the need to actually deposit it. Besides this, the authors also discuss the existence of a "critical height". This term refers to the height of a deposited wall from which the increase of stiffness of the cross-section reduces the bending distortion. This minimum height is said to be independent of the material or manufacturing process selected.

Some adversities can be overcome when using add-ons, such as sensors to guarantee a constant tip-to-workpiece distance and inter-layer temperature. Compressed CO₂ and thermoelectric cooling can also be used to enforce identical heat dissipation conditions in each layer.

When optimal parameters are achieved, WAAM can revolutionize the manufacturing industry, and its potential has already been recognized by some important industries, one of which being Lockheed Martin. This company has produced large titanium domes for satellite's fuel tanks, measuring 1.16 meters in diameter and managed to reduce the building schedule in 87 percent [9].

More recently, a company designated Relativity has created the world's largest indoors metal 3D printer, with the capability of creating parts with a diameter of 2.74 meters and a height of 4.58 meters. The company is aiming to create the first space rocket entirely composed of 3D printed parts. The capability of this process to reduce the part count, of a typical rocket, from 100000 to 1000 parts is highlighted. Furthermore, the versatility of a metal 3D printer is praised by Relativity who classifies this equipment as a flexible tool, as opposed to the conventional fixed tools, that serve only one function, leading to a greater investment cost in equipment [10, 11].

These cases, depicted in the last two paragraphs, demonstrate that WAAM can, with some financial investment, excel in the manufacture of medium to large dimension parts. However, when it comes to smaller scales, WAAM faces a few difficulties. Adding to the fact that this process is not as precise as Laser Powder Bed Fusion, WAAM also struggles to extract heat from the fabricated parts, making geometric features, such as small holes or protrusions, hard to achieve.

2.2.1 Deposition Strategies

The tool path, during the deposition of the metal, has a great influence not only in the geometry of the final part, but also in its properties, as stated by Kazanas et al. [12], Xu et al. [13], Venturini et al.

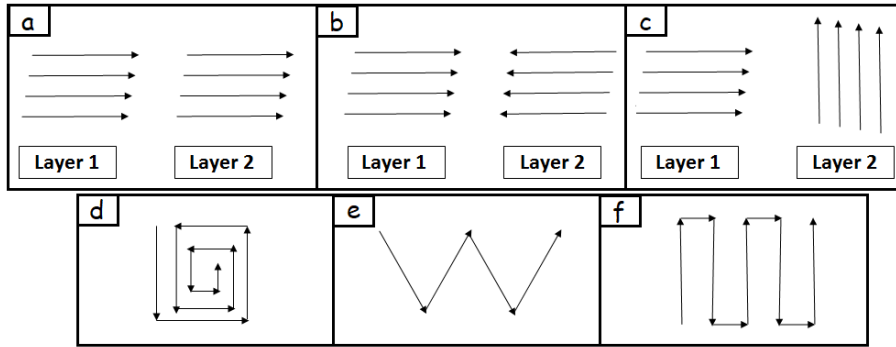


Figure 2.3: Deposition Strategies: **a)** Unidirectional with a constant start point **b)** Unidirectional alternating the start point **c)** Crosswise **d)** In a spiral form **e)** Weaving **f)** Oscillation.

[14]. Every material has its own properties and every geometry has its own details that make each case unique, therefore, there are no predefined right or wrong deposition strategies. Xu et al. [13] and Israr et al. [15] present different ways to perform the deposition, as seen in figure 2.3.

Nevertheless, the strategies most frequently used for WAAM are the unidirectional, the oscillation and the weaving techniques. Xu et al. [13] presented a direct comparison between these three strategies, listing the respective advantages and disadvantages associated with each one. The oscillating deposition was classified as the one that had the highest amount of heat accumulation. Such was justified, not only by the prolonged time at which the torch remains in the same sections of the part, when compared to the other two, but also by the smaller surface area available to exchange heat. As an example, while during the unidirectional depositions, each layer is deposited next to another one which had time to cool down, during the oscillating deposition strategy, the walls are adjacently deposited without any cool down time between them. Ultimately, this means that while on the first case the heat resulting from the deposition can be extracted both downwards to the substrate, and sideways to the preceding walls, on the second case it's only possible for it to be extracted through the substrate (figure 2.4). This effect, depending on the material used, as well as the type of geometry, might cause some problems for the part, such as the appearance of porosity or, in extreme cases, part collapse.

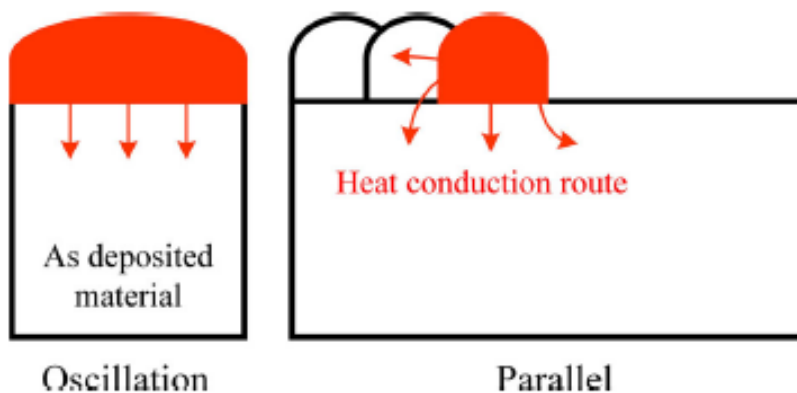
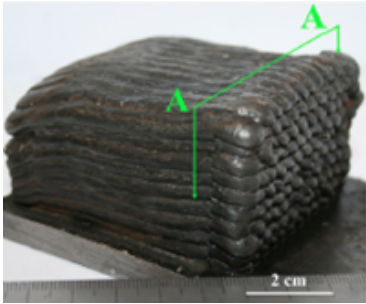


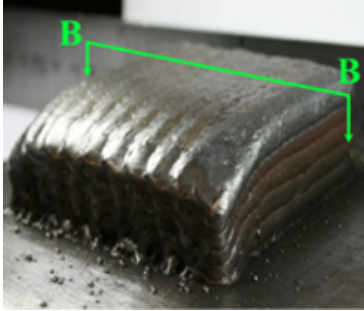
Figure 2.4: Illustration of the part's heat exchange for both the oscillation and the unidirectional parallel depositions [13].

However, the weaving and unidirectional strategies also bring their own problems to the part's ge-

ometry. If the same start and end points are set, the beginning of the bead will generate a heat sink and consequent decrease of the weld penetration. Contrarily, at the end of the same bead, there will be higher temperatures, caused by a lower heat dissipation. This in turn will then result in a bead height drop, which will accumulate, the higher the number of layers stacked up on each other (Figure 2.5), causing the aforementioned side collapse defect. The existence of this phenomenon was also corroborated by Rodrigues et al. [16].



(a) Wall depression caused by a uni-directional deposition with constant start and end points [13].



(b) Wall depression caused by a weaving deposition with constant start and end points [13].

Figure 2.5: Wall depressions caused by depositions with constant start and end points. [12]

It's then easy to conclude that a correct selection of the deposition strategy is fundamental for the part's manufacture success, and it's up to the user to decide what deposition strategy performs best for a certain geometry. Additionally, the location of the start and end of the deposition can also heavily influence the resulting part. Mehnen et al. [17] demonstrated that, when designing a cross shaped part, an alternation between the start and end points of each layer, could mitigate both the appearance of humps and depressions, in the intersection area (Figure 2.6).

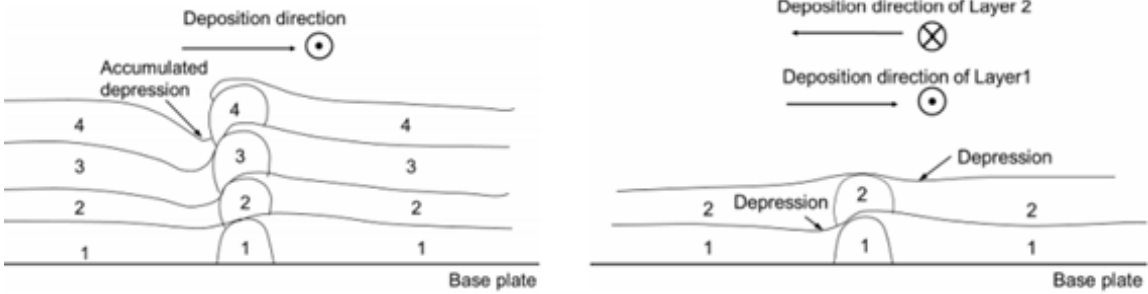


Figure 2.6: Illustration of the effect of alternating the deposition start and end points, when building cross shaped parts [17].

Some geometries might also use customized deposition strategies, combining several of these strategies in order to better fit the desired shape. As an example, Venturini et al. [18] studied and optimized deposition patterns specifically for the case of T-crossings. Throughout his work, several paths were tested, such as a simple combination of both horizontal and vertical uni-directional depositions, as well as a customized "L" shaped trajectory and several other variations (figure 2.7). His findings supported that these custom-made strategies were successful in mitigating the geometries inherent defects, such as heat sinks.

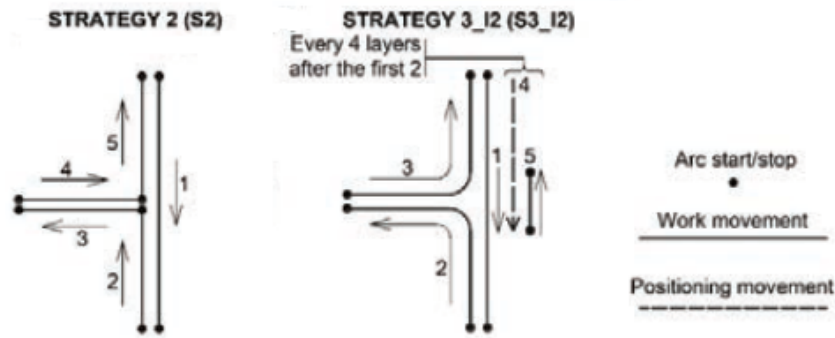


Figure 2.7: Example deposition paths used by Venturini for the production of T-crossings [18].

Additionally, some geometries require further attention as is the case of inclined walls. If the walls have an acute angle not only will there be an increase in the stress the part is subjected to, but also there's a formation of a hump, as shown in figure 2.8 (a).

In order to surpass this problem, Kazanas et al. [12] proposed a pyramid shaped deposition approach (figure 2.8(b)), using an oscillating trajectory, thus creating a smaller radius in the place of the acute angle, reducing the stress concentration and eliminating the hump. However, this technique requires a more complex programming and also leads to a possibility of weld defects.

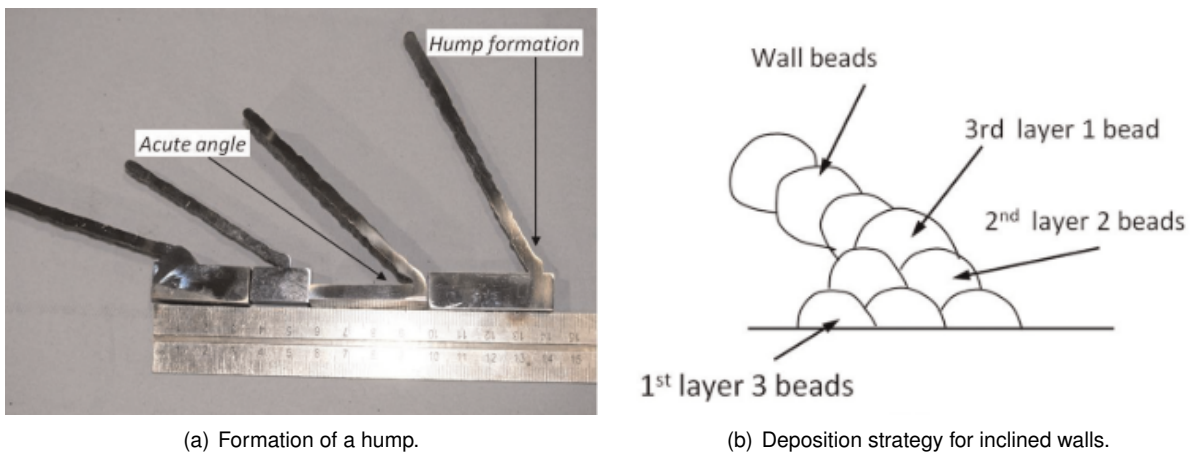


Figure 2.8: Inclined walls problem and solution. [12]

2.3 Test Artifacts

In order to ensure that the parts produced meet the required needs, specifications, and to verify what's the best deposition strategy for a certain material, there are two alternatives available: by performing direct measurements of the produced parts or by using test artifacts. These standardized parts allow to test how reliable is the fabrication of a component with different manufacturing processes, using benchmark geometries. Each of these geometries is developed with the intention of testing the process or the equipment's performance while creating said geometries. This way, a manufacturing process can be selected without as much waste of material, money and time.

These geometries are conceived with the aim to mirror the outputs that the user would get when manufacturing a part using AM. Depending on the purpose intended for each part, it's in the user's best interest to evaluate different properties of the resulting geometry. As reported by Rupal et al. [19], an AM output part has three distinct properties that can be assessed: mechanical properties, geometric properties and surface properties.

Mechanical properties encapsulate all results obtained from mechanical trials, such as tensile strength, compressive strength or impact resistance. The geometric properties cover the dimensional accuracy of the parts, as well as the setup's build limits, like the smallest feature possible to print. Finally, the surface properties concern aspects as the surface roughness or waviness.

Generically, the use of test artifacts is focused on the evaluation of, mainly, geometric and surface properties, thus informing the user if the geometry intended is possible to perform using that specific setup, as well as any uncertainties associated with the AM process. As such, several challenging geometries are selected and repeated, not only to identify the build limits, but also to ensure the consistency of the setup while performing said geometries and thus, comprising the so called geometric benchmark test artifacts, orGBTAs. Aiming at simplifying the text and easing the reader's interpretation, throughout the rest of the present work, all references of test artifacts are specifically in regards toGBTAs.

A test artifact is then an easy and accessible way to not only evaluate a system's manufacturing capability, but also an equally simple way to calibrate the system and know what aspects need further compensating.

According to Moylan et al. [20] a test artifact should have the following characteristics:

- It must be big enough to test the center and the edges of the part.
- Have a substantial number of small, medium and big elements.
- Have holes and protrusions.
- Be quick to produce and have low material requirements.
- Be easy to measure and control the geometry of the part.
- Must not require treatments after its fabrication.
- Have repeated elements, to test the consistency of the geometry.
- Have features of real parts, such as thin walls and flat surfaces.

In accordance, in 2004 Mahesh et al. [21] developed a test artifact designed for testing multiple AM processes. However, as observed in figure 2.9, the intrinsic complexity of the geometries and respective small dimensions and aspect ratios, made it challenging for such artifact to be used in metal AM, as they didn't account for the differences and limitations that were imposed by fabrication with metallic materials, such as different heat conductivity, material viscosity and process precision.

As this was the case with the majority of the generic AM test artifacts, a need arose for the development of artifacts specific to metal additive manufacturing. For this purpose, Kruth et al. [22] and Castillo

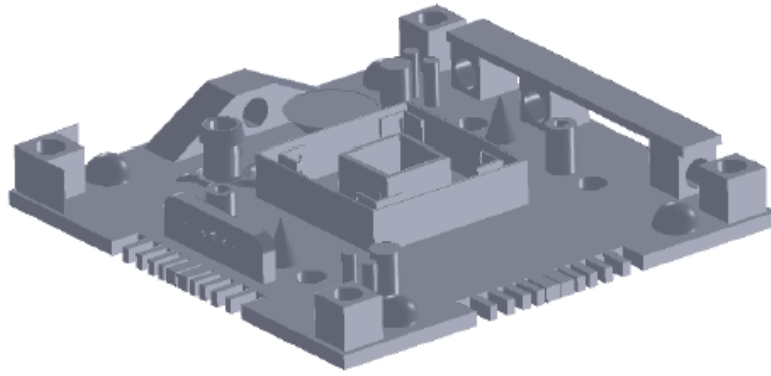
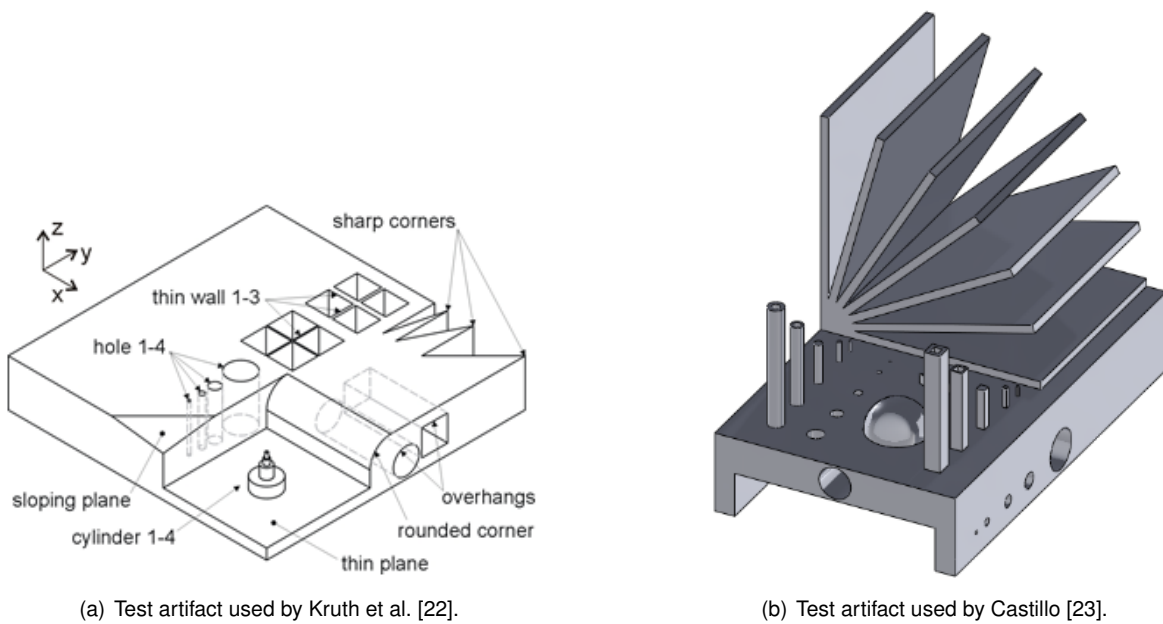


Figure 2.9: AM test artifact projected by Mahesh et al. [21].

[23] both developed a metal AM test artifact each, which are presented in figure 2.10 (a) and 2.10 (b), respectively. It's possible to detect on these more specialized artifacts, that there was a greater concern on gradually increasing the difficulty on the most challenging geometries, such as thin features and overhangs.



(a) Test artifact used by Kruth et al. [22].

(b) Test artifact used by Castillo [23].

Figure 2.10: Examples of test artifacts Moylan et al. [20]

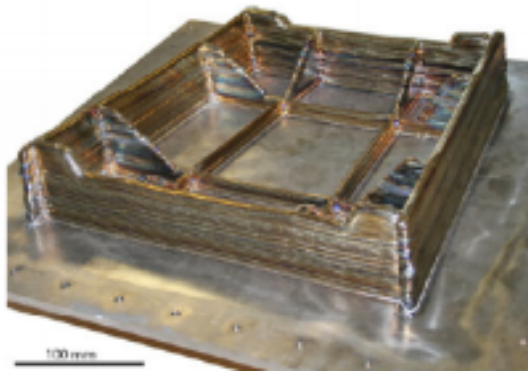
Following the same train of thought, it's natural that different manufacturing processes have different test artifacts, with distinct benchmark geometries, adapted to each processes' capabilities and limitations. As an example, while manufacturing a part with powder bed fusion (PBF), it's possible to achieve much smaller features and tolerances than with the use of WAAM, as the process' accuracy of PBF is vastly higher than the WAAM's. Looking once more at figure 2.10, it's easy to identify features that become problematic when using WAAM, such as small aspect ratio features and overhangs.

However, despite some of these benchmark parts being more adequate for some processes than others, as state Rebaioli and Fassi [24], there is still not a test artifact made specifically for WAAM. In order to project an artifact fit to evaluate WAAM produced parts, the geometries that comprise it should

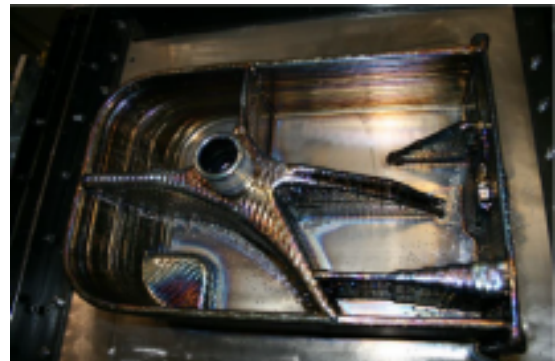
better represent the possible geometrical outcomes of the process, with a corresponding dimensional range.

For this purpose, different elements should be used to test specific aspects: **Linear elements** are used to test the linear positioning accuracy and compensation; **Circular elements** test the method of joining materials, providing a way to search for junctions with lack of fusion or excess material; **Holes or cavities** are fundamental in a WAAM test artifact, as they tackle one of its biggest difficulties, to have the necessary heat flow, allowing the metal to solidify and create cavities with small dimensions. If there is not enough heat transfer away from the metal, the material will collapse, failing to achieve the geometry; **Pins** not only test the ability to create thin features with various aspects ratios, but also informs the dimensions of the thinnest detail that can be printed. This information can also be given incorporating **ribs** in the test artifact, granting the thinnest walls possible to deposit.

The greatest requirement for a WAAM specific test artifact is for it to be able to validate or replicate complex geometries that have been obtained previously with this process. In order to do so, these several geometries must be evaluated and the features that make them difficult highlighted, so they can then be replicated. To facilitate this evaluation, a brief compilation of said geometries is presented hereinafter.



(a) Ti-6Al-4V external landing gear assembly [25].



(b) High complexity demonstrator part built by WAAM [26].



(c) 6 meter long produced by [27].

Figure 2.11: Examples of geometries with intersections and height variations.

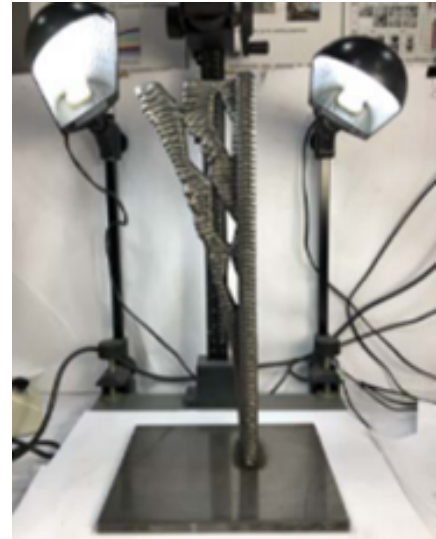
The first group of images shows a group of large parts with some features in common. More specifically, all of them possess a set of straight walls intersecting with each other, some of them at different heights (figure 2.11). It's then highlighted the importance of a WAAM setup to efficiently, and accurately

produce intersections between geometries, as well as precise height variations.

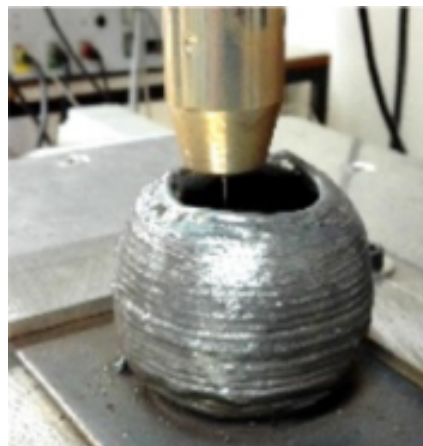
The second group of images presents a completely different type of challenge while manufacturing. These parts contain overhanging features and, in the case of figure 2.12 (c), a part where the section available to exchange heat increases at first, but then becomes progressively smaller with the increase of the part's height. Both these features can lead to part failure if not controlled, thus revealing a great need to test these geometries before building the final part.



(a) WAAM Turbine part [28].



(b) Part made in steel ER70S-6 [29].



(c) Piece obtained by continuous trajectory and growing geometry in z direction [30].

Figure 2.12: Examples of geometries with overhangs and smaller heat exchange sections.

Most of these challenging parts are currently achieved using complementary techniques or materials. For instances, the build of an overhanging structure, as the inclined walls shown in figure 2.10 (b), can be facilitated by the use of rotating tables or more complex and specialized softwares. Additional techniques to optimize the the cooling rate of the parts can also be used, however, these methods come with a large financial investment, and might not be accessible to a majority of users, not only in the manufacturing industry, but also within the scientific research areas. There is thus a need for a test artifact that allows the end-user to inspect the equipment's capabilities, without the need of any other add-ons.

2.4 International Standard

As a means to ensure consistency and coherence with the resulting measurements of the test artifacts, an international standard was developed, the ISO-ASTM 52902 Standard [31]. This grants hegemony to all results and provides a good comparison between all artifacts, and therefore this standard should be taken into consideration and used as a stepping stone when investigating or creating any test artifact.

As the concept behind a test artifact can only work if anyone can replicate it, the norm in question begins by stating that in the making of a new test artifact, all user-defined settings or deposition strategies must be specified, in order to facilitate a consistent replication of the benchmark geometries.

In order to prevent any post-deposition deformations, the use of any support structures or material removal and surface treatment processes are discouraged, as they might cause changes to the parts dimensions and thus tainting the results obtained. However, in the extraordinary circumstance that any of these processes are required, they should be meticulously documented alongside the deposition parameters.

Also in the interest of avoiding any deformation to the parts, the standard advises to perform all the measurements without removing them from the substrate, as well as letting each part cool down to room temperature before measuring them.

Still on the topic of performing measurements, the norm distinguishes 3 different grades that evaluate how uncertain the dimensions obtained are, as well as how difficult and costly to obtain. These are: grade A for simple and easily available measuring tools and methods; Grade AA for intermediate methods, with lower uncertainty but higher cost; Grade AAA for intricate and expensive methods, typically used for laboratory level measurements, that provide the user with the lowest measurement uncertainty possible.

Regardless of the grade of the equipment used to perform the measurements, when measuring a specific dimension, a minimum of three distanced measurements should be performed. The mean value of those values should then be used in order to ensure consistency and avoid inaccurate results. A demonstration on how these measurements should be performed is shown in figure 2.13.

Furthermore, the instrument selected to carry out the measurements should produce a dimensional uncertainty no bigger than 0.2 mm, that is, an equipment with a maximum permissible error (MPE) ≤ 2 .

Regarding the development and arrangement of each geometry within the test artifact, it's highlighted that there should always be at least one benchmark geometry dedicated to testing each of the X, Y and Z axes. This will grant the user with a way to identify any flaws or deviations on the robot's degrees of freedom and posteriorly recalibrate them. It's also possible to have a single benchmark part testing all three of the axes simultaneously. Furthermore, it's also advised to organize these geometries in such a manner that it prevents any collisions or compromises. Collisions might occur if a part is already produced, but is in the welding gun's path to generate another geometry. A compromise to the artifact might happen due to the collapse of a geometry in such a way that affects others nearby. As such, geometries with a high risk of failure should be at a safe distance from other geometries, accounting for the probability of failure. Lastly, in order to facilitate the test artifact's ability to examine the machine's

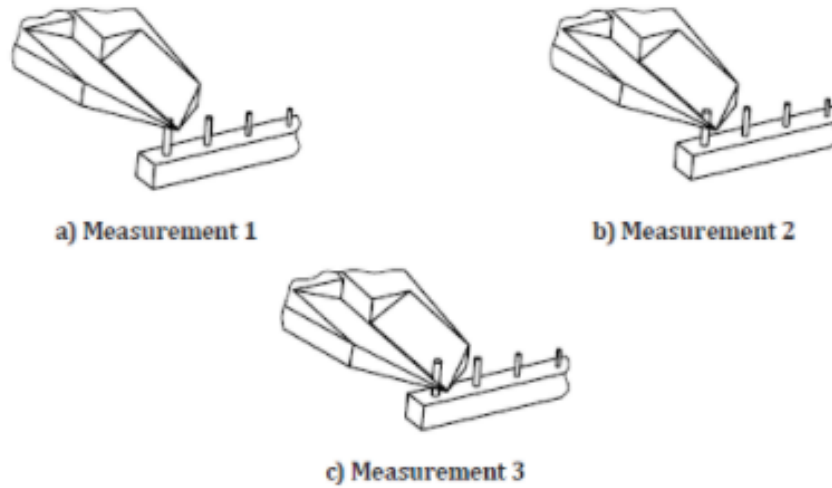


Figure 2.13: Illustration of the minimum amount of measurements per dimension. Example of thin resolution pins [31].

positioning capabilities, geometries should be placed at the center and along the ends of the artifact.

Finally, all measurements should only be performed once all the parts have cooled down to the ambient temperature, and before unclamping the substrate. These precautions will ensure that the resulting geometries are neither dilated, due to high internal heat, nor distorted, as a consequence of residual stresses within the parts.

Chapter 3

Materials and Test Methods

This chapter will present the list of equipment and materials used, as well as the procedure that was followed for the laboratory work. Additionally, a brief overview of the selected geometries to develop as well as the process properties being evaluated are presented.

3.1 Equipment and setup

Generically, in order to produce and test all the parts and geometries, the following steps had to be taken:

- Generation of a 3D CAD model;
- Path planning and generation of code files for the robotic arm;
- Part deposition.

For the case of the present work, the 3D CAD models were made using SolidWorks, but any other program capable to model 3D parts and save them in STEP type files could have been used.

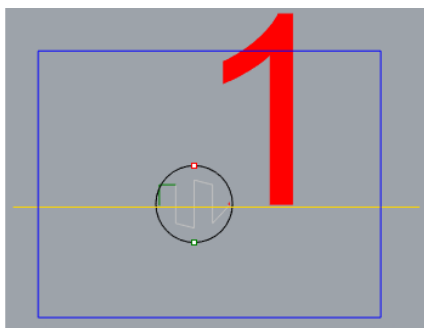
The path planning and file generation was obtained using WAAMSoft, a software developed by Cranfield University, that also uses two other programs: Rhinoceros 5 and Grasshopper. The first is used to open the part in the STEP file and, along side Grasshopper (a visual algorithm editor) generates the deposition path. Within Grasshopper it's possible to insert the desired process parameters such as travel speed, segment distance and layer height. In order to generate the deposition path, in addition to all the aforementioned parameters, the software also requires the user to define the following features:

- Segment area - an area delimited by a blue rectangle, that indicates where the deposition will take place. In the case of a more complex geometry, several segments might be required, dividing the shape into other simpler ones. The red numbers indicate the order at which the deposition will take place, ie, the software will first deposit the first layer of segment 1 and then move on to the first layer of segment 2 and so on;

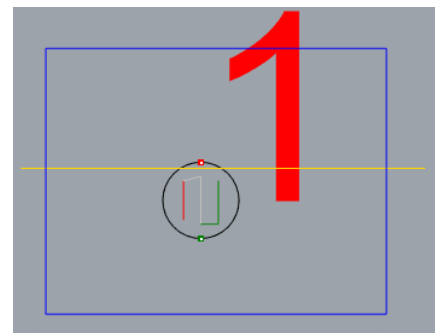
- Deposition guide line - A yellow line that the software will use as a reference, thus creating deposition segments that are perpendicular to this line, for each segment;
- Start / end points - Reference points used to identify where the deposition of each segment should start and finish.

The path that is generated automatically using the software might not be adequate to achieve the desired geometry. As such, the user can change and adapt it and provide the software the best input possible. Within the program, it's possible to adjust the position of the guide line, the yellow line seen in figures 3.1 (a) and 3.1 (b). Further on this work, the mechanics and requirements for the path generation will be explained. Different positions of the line lead to different deposition strategies as seen in the aforementioned images, which will in turn lead to different geometry outputs.

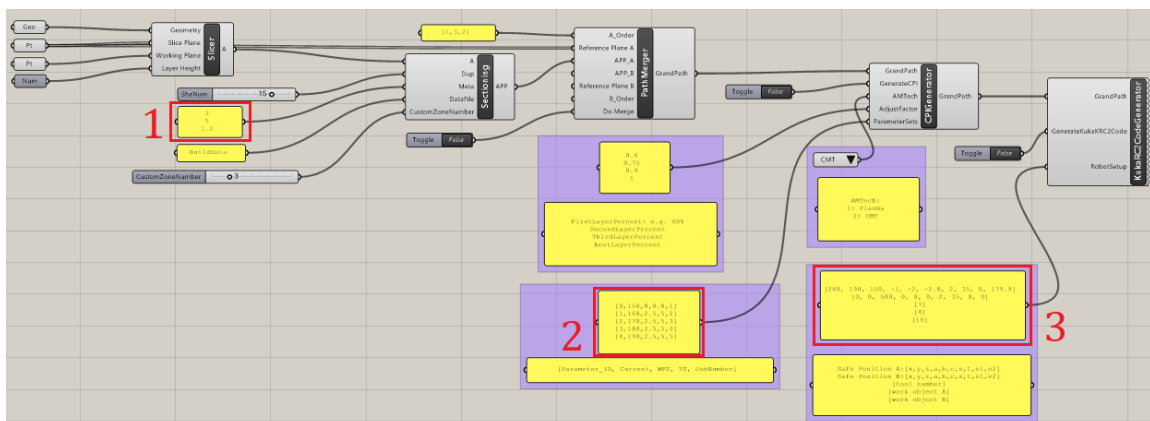
In addition, it's also possible to outline sections ,within a layer, that might need a wire travel speed that's different from the rest of the part. For this purpose it's possible to use costume zones, represented on the software by a light blue rectangle and a pink identification number. Within the same layer, it's possible to have several custom zones with either the same parameters or one that differ from each other. For the first case, the costume zones will all have the same identification number while for the last, they'll be distinguished by their number. For clarification, if the user defines three costume zones, two with a travel speed of 5 m/min and the other with 6 m/min, the first two would be represented with the number one, and the other with the number two.



(a) Inadequate deposition path.



(b) Optimal deposition path.



(c) WAAMSoft deposition parameters.

Figure 3.1: Important input parameters for a successful deposition.

It is also important to note that some important parameters, that have a direct impact on the part geometry, are also set in WAAMSoft, such as the deposition width and the travel speed, represented in figure 3.1(c) with the numbers 1 and 2 respectively.

As a final remark, although the box represented with number 3 in figure 3.1(c) is not important for the parts geometry, it needs crucial input for a safe deposition. In this box, the correct tool (weld gun) and base (substrate) must be indicated, alongside coordinates for a safe position, should the deposition be stopped.

The depositions all took place in Instituto Superior Técnico's facilities utilizing the following resources:

- 6-Axis KUKA KR 150 L110-2 F 2000;
- Fronius CMT VR 700 arc wire feeder;
- AWS A5.18 ER70S-6 $\varnothing = 1.2$ mm consumable welding wire;
- DIN 2391 ST 52 steel substrate plates;
- 18% Carbon Dioxide + 82% Argon protective atmosphere;
- Local exhaust ventilation;
- CMT weld torch;
- Clamps
- Hanna HI 935005 K-Thermocouple Thermometer.

3.2 Setup Procedure: User Guide

In order to properly and safely perform any deposition, the user should follow a series of predetermined steps. Said steps aim at not only guaranteeing a good performance of the equipment, but also ensuring the safety of all the machinery and everyone involved. In addition to all the safety benefits, by following certain guidelines it's easier to assure that the depositions are performed correctly with higher consistency, thus enabling a more accurate display of the setup's performance.

Bearing this in mind and with the absence of an user guide for the setup selected for the development of this work, it was found to be appropriate to create one that could be used not only for the course of this thesis, but also for any future work done at this setup.

It's important to state that this guide is in no way destined to replace the use of each components user guides, provided by the respective companies. It's only intended to provide a quick debrief about the necessary steps to correctly use the present setup. Any specific information regarding one of the component's should be consulted in the brands user guide, which can be provided by the laboratory technicians.

This guide also presupposes that all the pre-processing required to generate the deposition files needed has been done by the user, before reaching this phase.

The main components of the setup are the robotic arm that will follow the predetermined deposition strategy (in this case the 6-Axis KUKA KR 150 L110-2 F 2000) and the welding equipment that works alongside it (Fronius CMT VR 700 arc wire feeder). Within this guide, some references will also be made about components such as the Fronius' remote control console (the RCU 5000i) and the KUKA's remote control console. While the first is primarily used to send the parameters input to the Fronius welding unit, the last can act like a second screen of the KUKA's main unit, giving the user the option to perform certain commands either on the KUKA's PC unit or on the remote control unit (note that some operations, which will be specified further on this guide, are exclusive to either the PC or the remote control console).



(a) Kuka's main controller unit.



(b) Fronius CMT VR 700 arc wire feeder.



(c) KUKA's remote control console.



(d) RCU 5000i.

Figure 3.2: Setup's main components and respective controllers.

3.2.1 Setup Power On/Off

The setup is only active after both the KUKA's and the Fronius' main stations are turned on. Both have the same On/Off mechanism using a switch. The following images show both of the switches possible positions and the respective states. Note that if the Fronius unit is turned before the KUKA, it's possible that an error message is shown, as it could not connect to the KUKA's computer unit. Therefore, it is preferable that the KUKA is turned on first.



(a) KUKA's power off.



(b) KUKA's power on.



(c) Fronius CMT VR 700 power off .



(d) Fronius CMT VR 700 power on.

Figure 3.3: Setup's main components and respective controllers.

3.2.2 Kuka's Manual Movement

Although during the deposition process the movement of the KUKA's robotic arm is automatic, this equipment also allows the user to move it in a manually. To do so, the user should use the KUKA's remote control console and start by turning the switch that's located on the topmost part of the console. This switch indicates whether the robot is in manual or in automatic mode, and for manual use, it should be in the position represented in figure 3.5 (a) box "b".

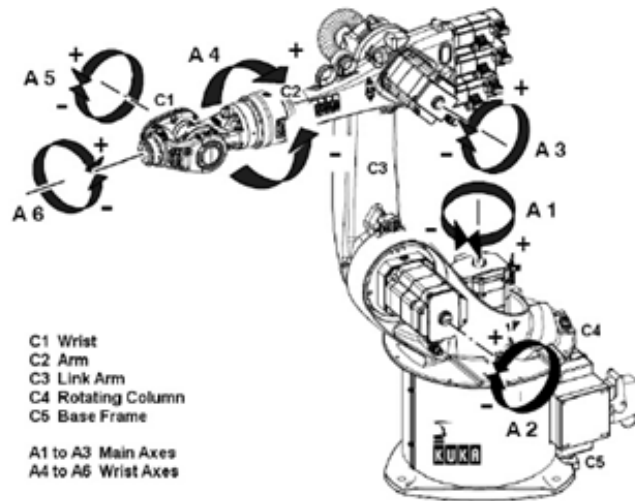
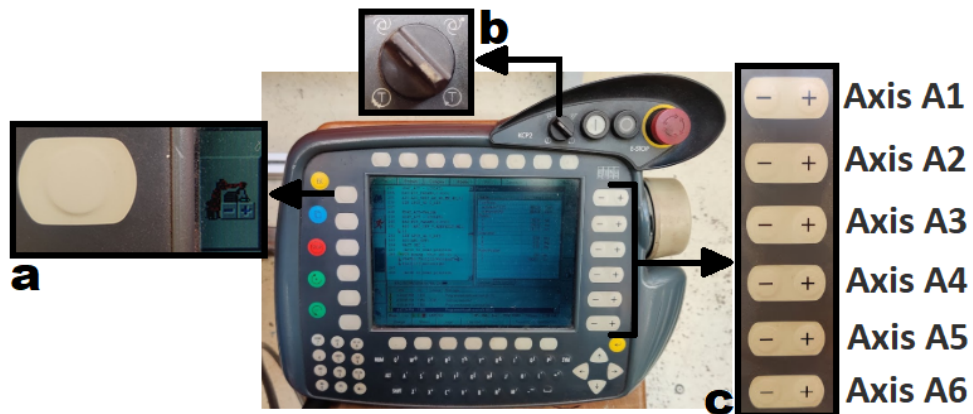


Figure 3.4: Representation of the 6 axes of freedom of the KUKA 150 L110-2 F 2000 [32].

After this step, it's required to change the movement mode to be regulated by each degree of freedom of the robotic arm by pressing the button shown in figure 3.5 (a) box "a", until the same symbol as the one shown in the image appears. This robotic arm possesses 6 degrees of freedom, each one illustrated in figure 3.4.



(a) Detail of buttons and icons relevant to the manual use of the robotic arm.



(b) Highlight of the manual movement safety button.

Figure 3.5: Highlight of the buttons and icons needed for the manual use of the KUKA robot.

To operate it manually, it's simply required to press and hold the safety button at the back of the con-

sole (figure 3.5 (b)) and adjust each axis to the user's preference. The adjustments are made by pressing the "+" and "-" keys on the right side of the remote control console, noting that each set keys corresponds to a specific axis. A simple correspondence between each set of adjusting keys and corresponding axis can be found in figure 3.5 (a) box "c".

3.2.3 Referencing the Base's Position

This step can be skipped when preparing the first deposition for a new substrate, because the data gathered from this step is saved and can be used for latter use. This means that the robot already has some base positions saved and, with the approval of the entity responsible for the equipment, can be re-utilized.

However, should the need arise to generate a all new base position reference, the user should make use of the robot's manual control (3.2.2) and check the 6-Axis KUKA KR 150 L110-2 F 2000's user guide on how to make a new reference.

3.2.4 Wire, Gas and Welding Process Selection

In order to successfully change some operation parameters, such as the wire or the type of welding process selected, the user must first change the systems parameters from external to internal. To do so, with the use of the RCU 5000i, one must press the "Menu" button, scroll until the option "Pré-ajustes da máquina" and then select it (figure 3.6(a)). Once opened, the user should switch the option "Seleção de parâmetros geral" from "Externo" to "Interno" (figure 3.6(b)). Having done so, the user may now press the "Menu" button once again, scroll up to the "Soldagem Synergic MIG/MAG" and select it (figure 3.6(c)).

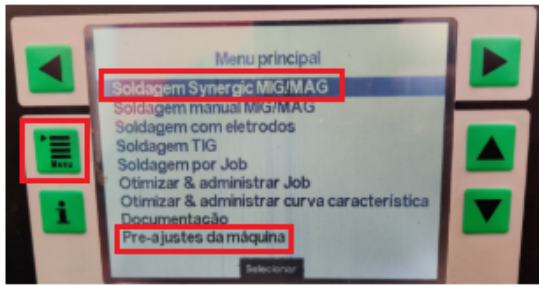
Finally, head to the tab B "Parâmetros de trabalho", and by pressing the "F4" button it is possible to select the welding wire's material, diameter and the composition of the chosen protective atmosphere. Within the same bookmark it's also possible to select the desired welding process in the "Processo MIG" option.

3.2.5 Changing the Wire Feed Speed

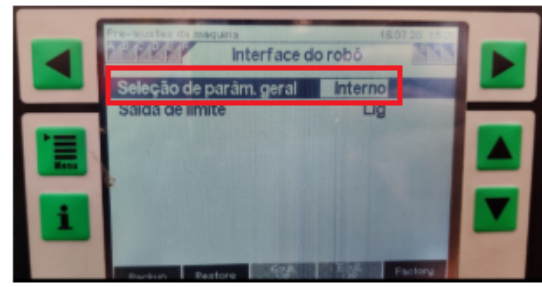
It's possible to regulate the wire feed speed in the tab B "Parâmetros de trabalho". To do so, it's only required to, while having the parameter "Alimentador" selected, scroll until reaching the desired value (figure 3.7).

3.2.6 Transferring a deposition path to the KUKA

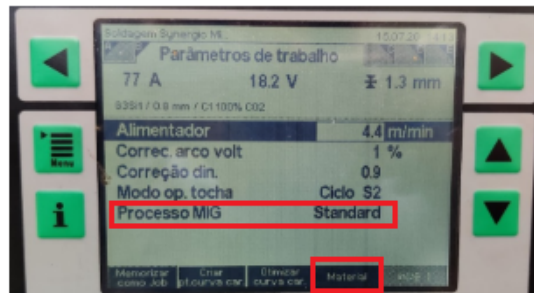
After generating the files containing the deposition trajectory, it's required to transfer them from the user's PC to the KUKA's main control unit. To do this, the user must retrieve the USB flash drive that is kept on the PC lodged in the KUKA's main control station. The next step is to transfer the files into the



(a) RCU 5000i's menu button and options indication.



(b) RCU 5000i's system parameters indication.



(c) RCU 5000i's Material and welding process indication .

Figure 3.6: Setup's main components and respective controllers.



Figure 3.7: Indication of the parameter needed to change the WFS.

flash drive, and then reinsert it into the KUKA's PC unit. Note that the only files required for a deposition are the ones with a .dat and a .src extension.

At this stage it's required to replace any files, from a previous deposition, for the ones with the new deposition trajectory. Accessing the monitor connected to the KUKA's PC unit, start by accessing the previously mentioned flash drive, pressing "(F:\)" while on the KUKA's program, on the left portion of the screen and copy the files. Next, on the left side of the program, look for the tab "Program" and open it, which will lead to the section where the robot will look for the files to use during the deposition. In this menu, paste the files from the flash drive and when a message pops up, asking if it's intended to replace the pre-existing files, click "Yes to all".

At this stage there are three possibilities:

- The software replaces all the files without any error;
- The software replaces all the files but shows a "Compilation error" message and a yellow warning sign. Despite this message, no further action or correction is required, and the program will run

normally;

- The software replaces all the files but shows a "critical error" message and a STOP sign. This message indicates that there is a critical error with the deposition files. Generally, this error is associated with either the deposition path or the robot's home position being defined out of the reach of the robotic arm, meaning that these coordinates are likely wrong and need changing.



(a) Indication of a non-critical error.



(b) Indication of a critical error.

Figure 3.8: Symbols used to represent the two types of error.

3.2.7 Running a Deposition Path

After transferring the files containing the deposition path, it's then possible to run them. It's extremely advised that, before any deposition, the user test the generated path with the weld gun off, thus verifying that the trajectory is as intended. To do this, first go to the previously mentioned tab "Program", then look for the file "Main" and execute it. At this point, the interface of the program changes and now shows, on the left side of the screen, an icon representing a welding gun. To deactivate the weld gun, simply press this button, which will also change the corresponding icon. This operation can also be performed using the KUKA's console by pressing the button highlighted in the figure 3.9, box "a".

To activate the movement of the robotic arm, the user will need to use the KUKA's remote control console, which contains some safety mechanisms that will need some interaction.

Firstly, on the topmost part of the console, there's a switch that indicates whether the robotic arm is in manual or automatic mode. For this case, the switch should be in the automatic position, demonstrated in the figure 3.9, box "d". As a final safety precaution, the user must press the start key, the button directly to the right of the aforementioned switch (3.9, box "e"). Shortly after doing this, on the bottom of the display, two green lights will be presented (3.9, box "g"), indicating that the robotic arm is ready to execute the deposition path. To start its trajectory, press and hold the green button shown in the figure 3.9, box "b" until it reaches the home position. When it does, simply press the same button once more and it will start the deposition path.

As an additional safety mechanism, it's possible to change the approximation velocity, ie, the velocity at which the robotic arm travels from the substrate to the home position and vice-versa. To do this, use the uppermost "+" and "-" keys, on the right side of the console, to adjust the velocity to the desired value (3.9, box "f").

Should the need arise to halt the trajectory of the robotic arm, the console also includes a "STOP" button, also highlighted in the figure 3.9, box "c". By pressing this button, the deposition will be paused and can be resumed by pressing the aforementioned green button once again.

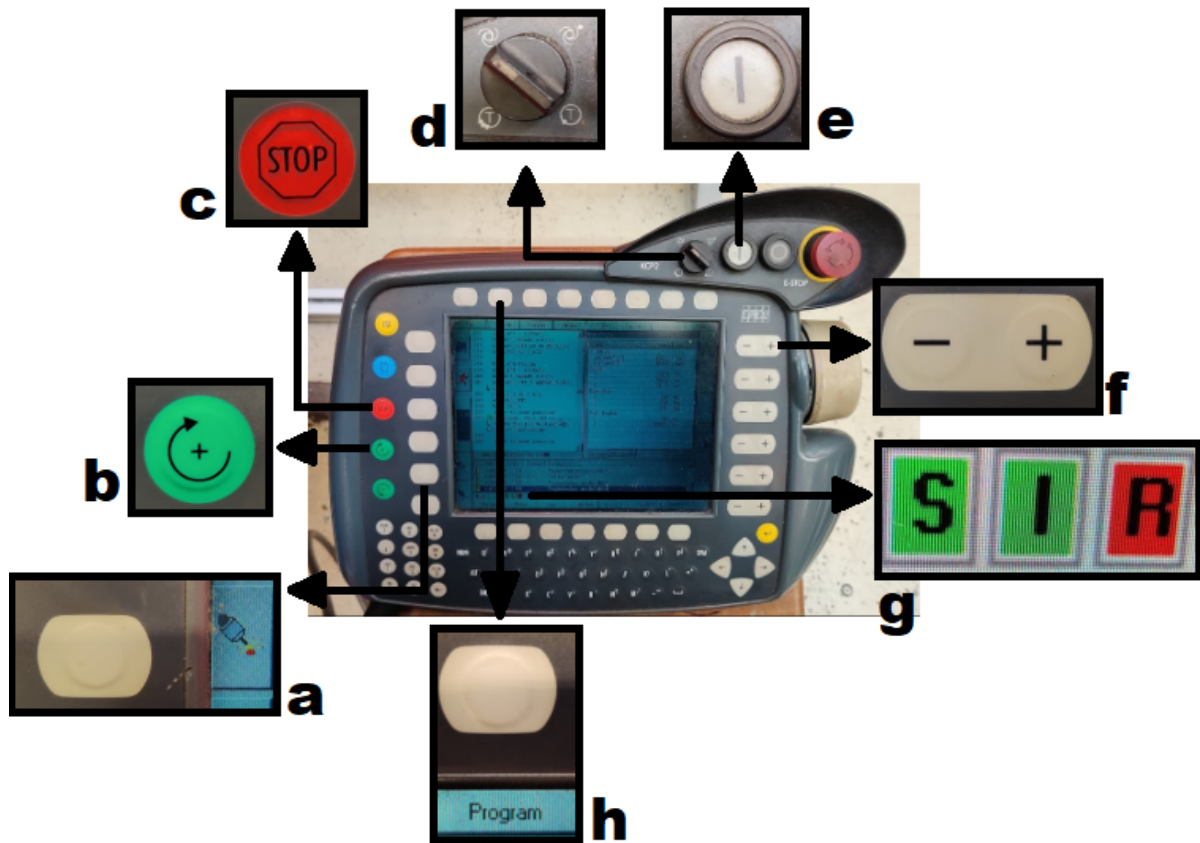


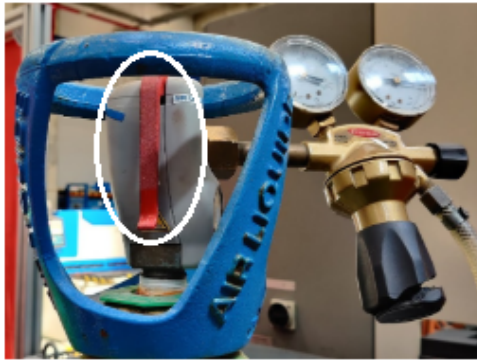
Figure 3.9: Detail of some of the most important buttons, switches and indications, to perform a deposition.

To cancel or resume the program, ie, the current deposition trajectory, the user can either press the button directly above the tab "Program", in the remote console, or click that same tab on the PC and press "Cancel program" or "Reset program" (3.9, box "h").

If the deposition path is the one planned and is functioning correctly, then it's safe to turn the weld gun back on.

3.2.8 Opening the Gas Valve

This simple step is accomplished by, firstly ensuring that the Fronius' welding unit tube is connected to the correct gas cylinder and then opening the valve at it's top. The valve is opened by pulling the red lever up, ie, if the lever is in a horizontal position, the valve is open; if the lever is in a vertical position, the valve is closed.



(a) Gas valve closed.



(b) Gas valve opened.

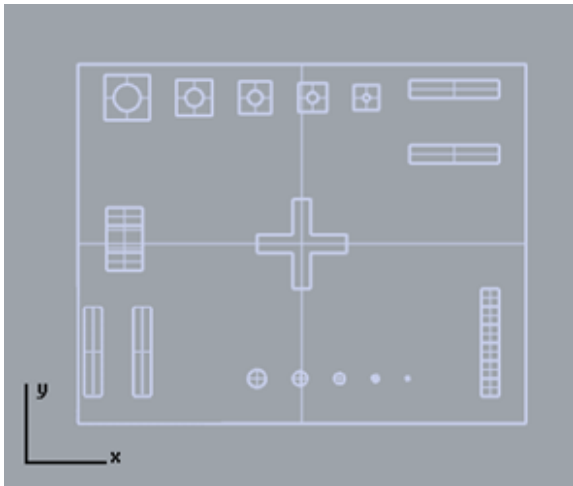
Figure 3.10: Both positions of the lever, for closed and open gas valve.

3.3 Experimental Procedure

In this section, it is intended to test the limitations of a basic WAAM setup, as shown in section 3.1, without the auxiliary use of other resources, such as a revolving table or part cooling aid, such as compressed air. The geometries must be achieved only by the regulation of parameters, ensuring that every WAAM setup can create these parts, thus creating a universal reference of quality for this process. In this context, a set of different geometries were projected, with the objective of reaching the process and the setup's limitations. These geometries were: overhanging structures; thin pins; thin vertical resolution holes; straight walls; cross shaped intersection; staircase vertical increment.

For future reference, and as a means to facilitate the user's interpretation, the following disclaimers are provided:

- Throughout the following chapters, there will be references of vertical directions or movements. It's important to retain that during the deposition path planning phase, as Ding et al. [33] mentions, we are faced with a 2.5D environment, as despite each layer having an associated height, the Z coordinate is neglected. That being said, when regarding the deposition path generation software, the vertical direction is referencing the Y coordinate as demonstrated in figure 3.11 (a). However, when referencing a vertical movement or direction outside the software, it's in regards to the Z coordinate, ie, in the direction that's perpendicular to the substrate. To clarify, both exiting axes are presented in figure 3.11.
- Due to a limitation induced by the software, all depositions are simplified by exclusively altering X, Y and Z coordinates. In other words, despite the KUKA robotic arm allowing changes to its six degrees of freedom, these changes are done in such a way that the welding torch remains perpendicular to the substrate at all times. Ultimately, this means that throughout all the depositions, there were no alterations in the inclination of the torch, always maintaining it at a 90° degree with the substrate, as observed in figure 3.11.



(a) Coordinate axes within the software.

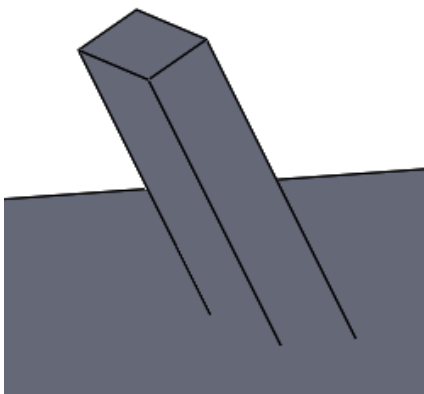


(b) Coordinate axes outside the software.

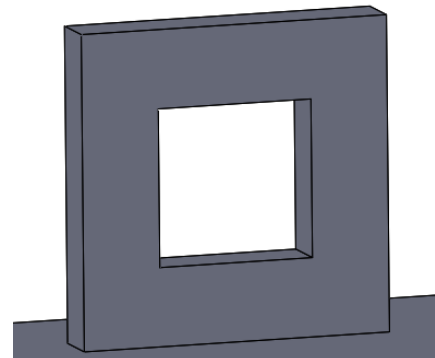
Figure 3.11: Both positions of the lever, for closed and open gas valve.

3.3.1 Overhanging Structures

One of the biggest challenges in WAAM is the manufacture of overhang structures, protruding structures without any supporting structures underneath. From within the overhanging structures, two types should be distinguished: Inclined walls and fully overhanging structures, as illustrated in figure 3.12. These types of structures present a challenge to this manufacturing technique, due to the forces inherent to its fabrication.



(a) Example of an inclined wall with 60°



(b) Example of a fully overhanging structure

Figure 3.12: Examples of overhanging structures.

As mentioned in the previous chapter, this type of additive manufacturing process relies on the generation of an electric arc, that will in turn melt the metal wire feedstock. The molten metal is then deposited, only solidifying after it's deposited on the substrate.

This means that as soon as the metal is deposited, the molten pool is subjected to not only the force exerted by gravity, but also the force created by the electric arc and the force produced by the impact of the metal droplet itself, all of which pulling in the downwards direction, towards the substrate. The only force in the molten pool that counters all of these downward pulling forces, is the surface tension of the

molten material. This means that in order to prevent the collapse of the overhanging molten pool, its surface tension must, at least, be equal to the all aforementioned forces, as represented in figure 3.13, in which G is the force produced by gravity, F_a is the arc force, F_d is the force of the droplets impact and σ is the force generated by the surface tension of the molten pool.

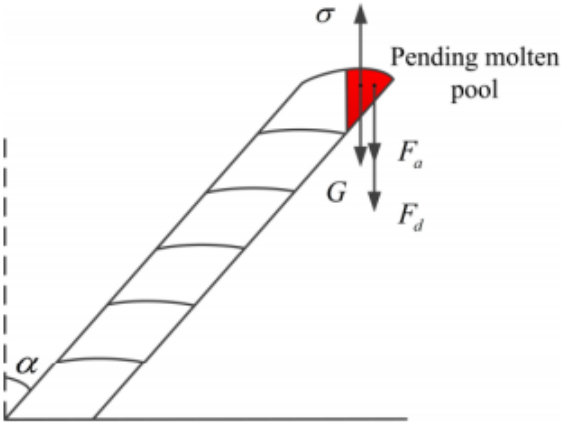


Figure 3.13: Representation of a force model during the fabrication of a inclined wall, [34].

Some ways to bypass this problem may involve using a more advanced software, with the option to use non-uniform layers or inclined slicing methods. These methods allow to change the layer height and angle in relation to the substrate. Another solution requires the use of a revolving table, permitting the torch to remain perpendicular to the section to deposit. However, as expressed at the beginning of this section, the objective was to overcome these challenges with a basic and easily accessible setup. That meant that none of those solutions could be implemented, and instead the focus remained on the process parameters.

These requirements meant that fully overhanging features would not be feasible. As stated by Ding et al. [35], parts with holes and depressions could be unbuildable, depending on the direction of the hole. Figure 3.14 illustrates such an example, presenting a wall with a hole, thus creating an overhanging section. As a result of the build direction (represented as B) and the hole's direction (represented as H), this section is classified as unbuildable, for it has no way to avoid collapse. Consequently, inclined walls were the type of geometries chosen for the study of overhanging structures.

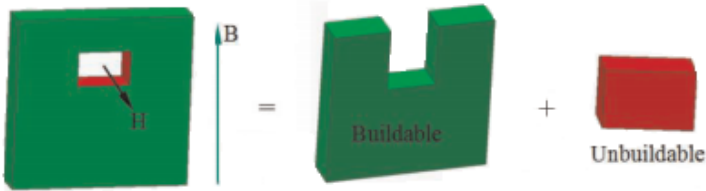


Figure 3.14: Structure with a fully overhanging feature decomposed into buildable and unbuildable sub-volumes, [35]

As a starting point, the 60° inclined wall represented in 3.12(a) was selected to attempt a successful build. The first approach was to vary the $\frac{WFS}{WTS}$ ratio, that indicates the quantity and accumulation of deposited material in the bead. The bigger the ratio, the more material, per unite of length, in the bead.

However, this parameter alone is not enough for the successful build of the inclined wall, as will be seen further on this work.

In order to achieve a fully successful deposition, several parameters were changed, noting their effects, and performing the changes necessary, until an acceptable 60° wall was created.

3.3.2 Thin Pins

Bearing in mind that WAAM is specially indicated for parts with medium to high dimensions, it's understandable that small sized details present a challenge for this additive manufacturing process.

As stated in section 2.3, depositing thin pins is an effective way to test the capabilities to create fine features and verify how its manufacture is affected by the processing software or even the diameter of the wire fed. It also lets the user know the dimensions of the smallest detail that can be printed in the vertical direction, ie, perpendicularly to the substrate.

For this purpose, a series of pins with progressively smaller diameter were designed (Figure 3.15), ranging from 10mm to 4mm, and all of which with a height of 30mm. A pin is considered satisfactorily built if it meets its geometrical requirements: Having a cylindrical shape, with a clearly round section, and accurate dimensions, when compared to its digital model.

After these requirements are accomplished, the diameter of the next pin should be reduced and the parameters optimized once more. The procedure was repeated until it was no longer possible to reduce the diameter obtain pins with the required dimensions, either due to software or equipment limitation.

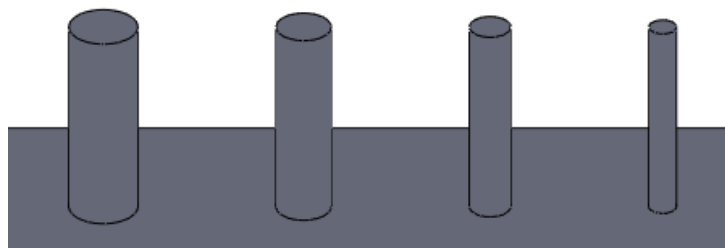


Figure 3.15: Thin pins with 10mm, 8mm, 6mm and 4mm respectively.

3.3.3 Thin Vertical Resolution Holes

Having determined the smallest detail that the setup could accurately print, with the smallest possible deviation from the CAD model, the next step was to verify what was the smallest hole that could be performed, under the same requirements presented in section 3.3.2. In order to do so, the geometry presented in figure 3.16 was selected, not only allowing to test the equipment's capability to deposit material around a progressively smaller circular perimeter, but also the setup's geometrical accuracy while depositing along the X, Y and Z axes.

The procedure selected for the analyses of this part was similar to the one used with the thin pins (section 3.3.2): An initial design with a certain internal hole diameter (in this case 15 mm) was selected

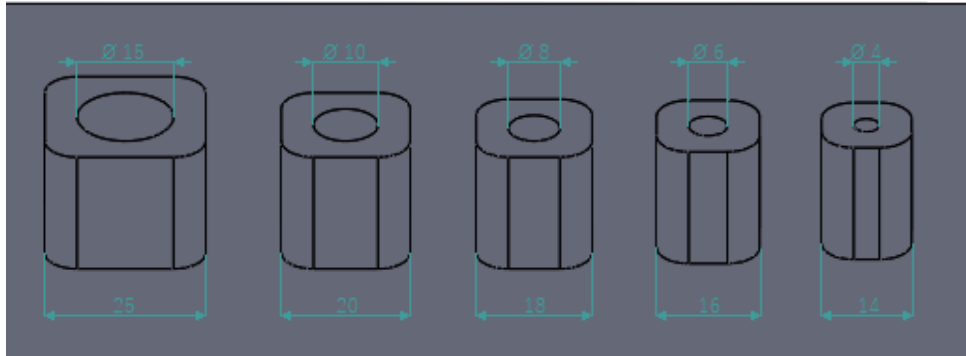


Figure 3.16: CAD model of the thin vertical resolution holes and respective dimensions in mm.

and tested, until admissible dimensions were achieved. At that point, the next design with a progressively smaller diameter was tested and so on, until it was no longer possible to achieve the desired measurements.

It should be noted that despite the diameter of the hole changing from part to part, the height and thickness of the parts were kept constant. The height was maintained at 20 mm and the thickness at 5 mm, to ensure that there were similar conditions between parts, regarding heat transfer. This design decision provides a direct comparison of each part's capability to extract heat, without collapsing nor flowing towards the inner resolution hole, and thus maintain the desired dimensions.

Furthermore, the radius of the fillet feature on the part's corner is constant on every part, but the distance between corners decreases, as a result of the decrease of the resolution hole's diameter. This ultimately means that separating the rounded corners from the straight portions of the outside walls, becomes increasingly harder. Thus, the user can also assess the process and set-up's geometrical precision, and the limits where the resulting geometry is no longer the one projected on the CAD model. Additionally, the existence of these rounded corners, allow the user to evaluate the setup's ability to handle changes to the deposition's linear speed. This becomes relevant as if no velocity compensation is performed during changes of direction such as these, the final part will end up with different amounts of deposited material on the straight and the corner sections.

Finally it's important to highlight that the primary objective of this test isn't to create the smallest hole possible with the equipment in question, but rather to accurately replicate the measurements of the CAD model, both of the diameter of the hole and the surrounding structure.

3.3.4 Straight Walls and Cross Shaped Intersection

Straight Walls

Despite being one of the simplest geometries possible to generate using WAAM, straight walls are fundamental for the planing of most parts. Their simple geometry allows the user to easily identify any lack of dimensional accuracy or equipment limitation during the deposition, whilst providing a concrete idea of how each parameter influences the geometry of the part. In other words, when depositing a straight wall, the user can inspect the machine's linear positioning accuracy along a certain direction.

The use of these geometries, both following the X and the Y axes, then become an effective way to test these properties and act as a linear element for the test artifact, as it was previously mentioned in section 2.3.

For this purpose, the walls represented in figure 3.17 (a) were projected with a length of 50 mm, width of 10 mm and a height of 20 mm, whilst making a 90° angle with the substrate. In the same figure, it's possible to observe two sets of walls in two different orientations. The different orientations were conceived with the intent of measuring the deposition precision alongside both the X and Y axes, as previously mentioned.

Complementary, each orientation contains a set of two walls, each one destined to test a different deposition strategy and let the user choose which one is the most indicated for his needs. These strategies test the performance of the deposition with a vertical and a horizontal guide line, ie, a deposition along the direction of the movement of the weld torch and a deposition perpendicular to that same direction, as illustrated in figure 3.17 (b). To further add to this, both the walls are strategically positioned parallel to each other, thus allowing to measure the parallelism between walls as suggested by Rebaioli and Fassi [36].

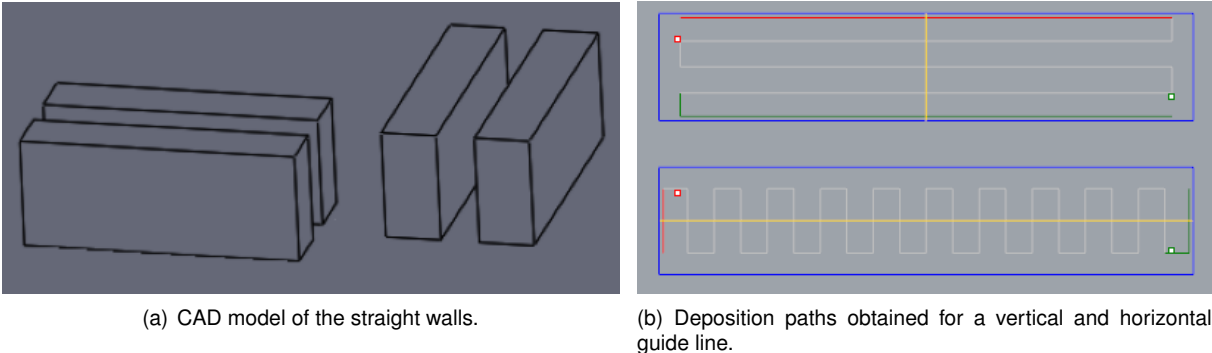


Figure 3.17: CAD model and respective deposition paths for the straight walls.

Cross Shaped Intersection

With the objective of further supplement the information obtained, two walls similar to the ones used in the previous section (length of 50 mm, width of 10 mm and a height of 20 mm), were designed perpendicularly to each other, generating a cross shape (figure 3.18).

This geometry allows to not only corroborate any previously obtained information regarding the X and Y axes deviations, but also to test how the setup performs intersections in which there is a complete overlap of two deposition segments, and whether or not that will effect the final dimensions of the part. A deposition with an excess of deposited material will result in the formation of a hump, while a lack of material on the junction area will promote a contraction and shrinkage of the part.

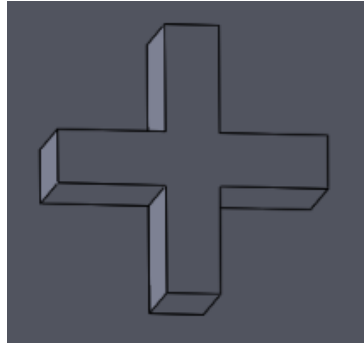


Figure 3.18: CAD model of the cross shaped intersection.

3.3.5 Staircase Vertical Increment

Finally, the last geometry selected was designed with the intent of testing how a constant vertical increment is affected by the increasing height of the part and consequent heat accumulation within it. For this purpose, the staircase shaped geometry shown in figure 3.19 was devised, where the first step, ie, the lowermost increment of the part, has a height of 10 mm while all other five increments measure 5 mm, thus comprising a total part height of 35 mm. Additionally, all steps both have a constant width and length of 10 mm, making up a total part length of 60 mm.

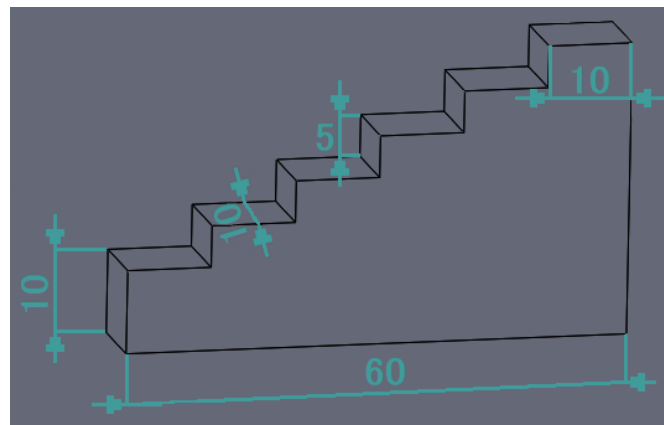


Figure 3.19: CAD model of the staircase vertical increment and key dimensions in mm.

Similarly to all other geometries, the main objective with this part is to replicate the dimensions of the CAD model as accurately as possible. For this reason, and despite the main focus when designing this part, being to evaluate the capability of performing constant vertical increments, every dimension of each step is equally as important for a successful deposition, and as such will also be used as an evaluating factor.

Chapter 4

Results and Analyses

This chapter is dedicated to the display of the results obtained, analyses and further discussion of the geometries presented in chapter 3, as well as displaying all the limitations found, either relative to the setup or the manufacturing process itself.

Additionally as every setup will perform differently, it's important to not only have base parameters that can serve as guide values, but also understand how each parameter affects the process and its resulting outcome. Thus, in this chapter, the influence of the most relevant parameters will be discussed as well.

Lastly, a proposal for a WAAM specific test artifact will be presented, accompanied by the respective ideal parameters and procedure.

4.1 Overhanging Structures

Regarding the wire feed speed (WFS), the velocity at which the torch provides the wire, two major events were identified. The first happened for low values of WFS, which meant there was not enough material per layer to create the desired section. This lack of material resulted in a cross-sectional deformation, as the part failed to have a rectangular section with the desired dimension. Since the software can't predict this deformation, the deposition will still take place as if there was no problem, leading to the deposition of material outside the part and onto the substrate. It's also worth noting that if the WFS is too low, there won't be enough voltage to start the electric arc and there won't be any deposition. This happens as the equipment used doesn't need the values for all the deposition parameters to be provided by the user. In the making of this work, the WFS was established, which automatically dictated the value of other parameters, such as arc voltage and current. This means that for low values of WFS, a low voltage will be selected, and might not be enough to stabilize the electric arc.

The other outcome, came for large WFS, presenting the opposite problem. The section had too much molten material, which eventually led to its collapse. Furthermore, when raising the value of the WFS, besides increasing the amount of material deposited per unit of time, the heat input is consequently

raised as well. Moreover, the weld penetration is also automatically increased, meaning that the bigger the value of WFS, and for a constant value of TS, the deeper the weld will reach into the inferior layers. An estimate on the weld penetration is presented on the display of the CMT remote controller, but this value does not account for the value of the TS and its respective impact on this property. The accumulated effects of having more molten material, more heat to dissipate (that will lead to an increase in the part's temperature), and further penetration into the previous layers that can lead them to remelt, all result in the structure's collapse. The part's temperature becomes too high to dissipate enough heat before the molten pool collapses. A higher penetration into the lower layers will also result in less solid material to support the molten pool above it.

Figure 4.1 presents the results obtained with variation of the WFS, and supports the previously stated conclusions.

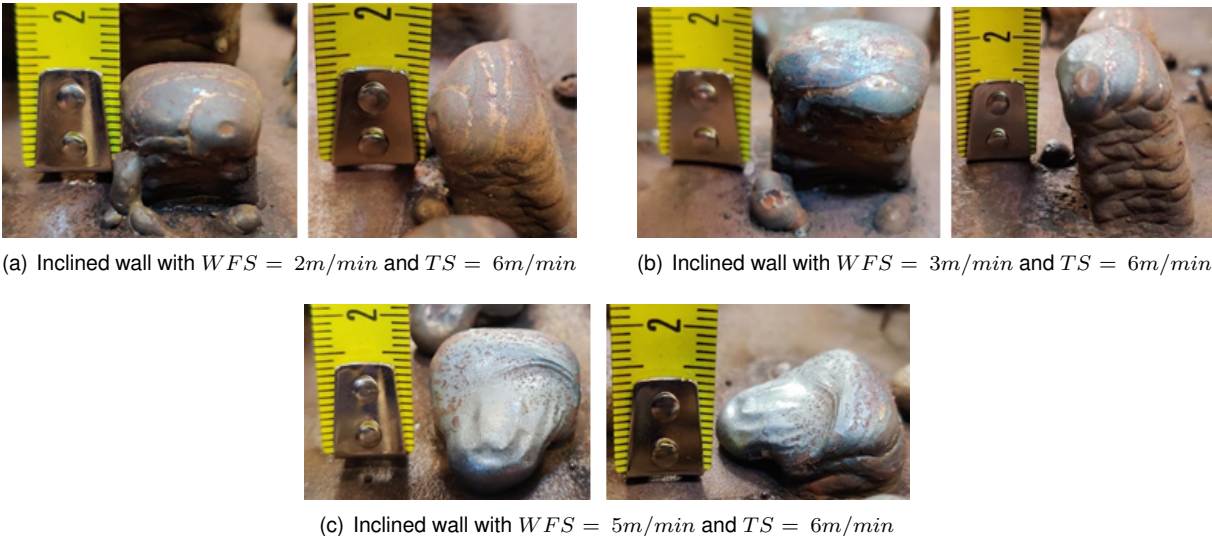


Figure 4.1: Effect of WFS in the deposition of inclined walls.

Advancing to the study of the wire travel speed (TS), the velocity at which the torch moves along the substrate, a different problem was identified. For high values of TS, as was the case for low WFS, there is not enough material being deposited, causing a deformation on the part. However, this deformation was smaller than the one occurring for low WFS, resulting in less material being deposited away from the part, and instead, portions of unmelted wire were attached to the part. This phenomena happened as, once again, the software can't predict these small deformations, thus starting the deposition slightly further away from the part. As the wire feed reaches and collides with the part, it breaks and is welded to the rest of the part, without fully melting. Besides this, the deformation of the part also causes an increase of the wire stick-out, that in turn, as stated in section 2.2, can also lead to the clustering of unmelted wire. This happens because when the stick-out is too long, the wire will bend slightly. The curvature will make the end of the wire to move away from the center of the arc, thus receiving less heat input than necessary to fully melt the wire, as discussed by Ji et al. [37].

The decrease of this velocity resulted in a lesser deformation and better results. It should also be stated that an excessive decrease of this property would result in a higher accumulation of material and

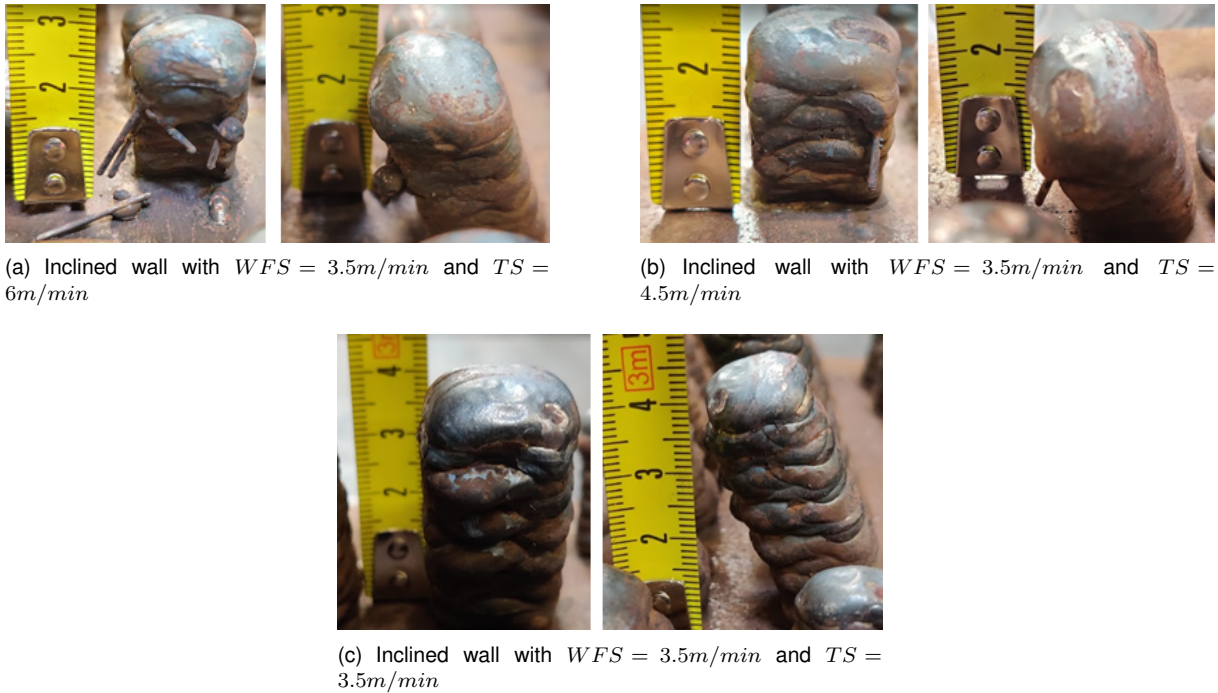


Figure 4.2: Effect of TS in the deposition of inclined walls.

internal temperature, that could lead to the weld pool's collapse. The outcome of the variation of the WTS is shown in figure 4.2.

Contrarily, an increase of the wire travel speed (TS), reduces the amount of material per unit of length, and also leads to a reduction of the part's temperature. Overall, the variation of the WFS was found to have a more predominant effect over the variation of the TS for the deposition of the inclined wall. This had become apparent not only due to the associated influence of the former on the weld penetration, but also because variations caused to the FS, lead to a bigger change to the process's heat input than a variation to the TS, as it will be analysed further on. The process's heat input [J/mm] refers to the amount of energy [J] that is provided by unit of length [mm] Table 4.1 shows data gathered from several identical depositions, only varying the WFS. Note that the heat input is determined using the equation 4.1, where V and I are the voltage and the current of the process respectively and η is the welding process efficiency. This last variable is dependent on the welding process selected and the equipment used, and for all calculations on this thesis a value of 0.85 was selected, in accordance with the source material found [38, 39].

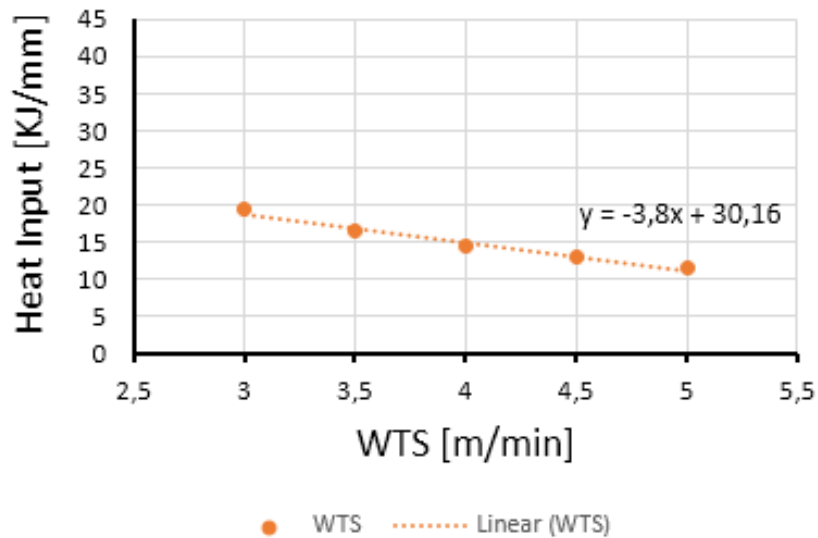
$$HI = \eta \frac{V \cdot I}{WTS} \quad (4.1)$$

With this, the heat input for a TS ranging from 3 m/min to 5 m/min was calculated, maintaining the WFS constant, at 3 m/min. Additionally, the heat input was also calculated for wire feed speeds of 3 m/min up to 5 m/min, but for a fixed value of TS at 3 m/min. The results are seen in figure 4.3, and it should be noted that for this calculation, the velocities must be converted to meters per second (m/s) .

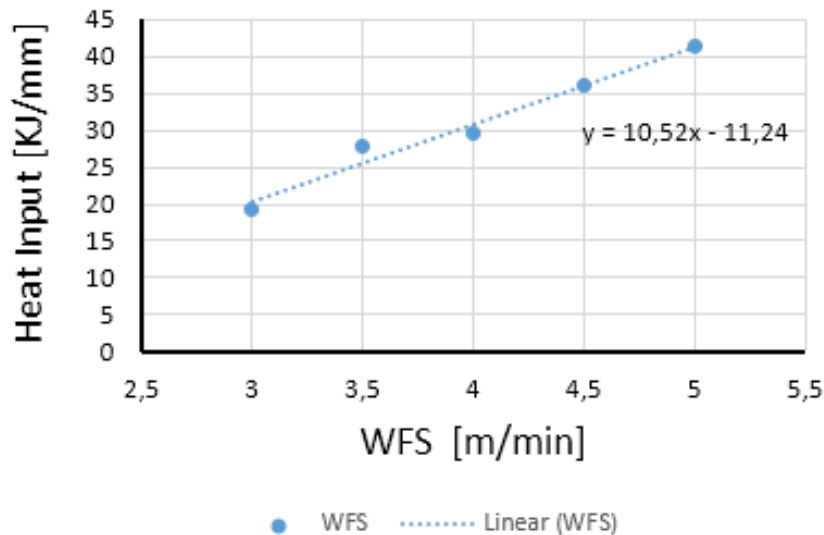
After inspection of the respective graphs, it then becomes clear that a variation to the WFS value has a higher impact in the variation of the heat input, than if the same variation was made to the TS.

Table 4.1: Voltage and current of several depositions at constant velocity.

| | I [A] | V [V] |
|-----------------|-------|-------|
| WFS = 3 m/min | 97 | 11.7 |
| WFS = 3.5 m/min | 126 | 13 |
| WFS = 4 m/min | 130 | 13.4 |
| WFS = 4.5 m/min | 150 | 14.1 |
| WFS = 5 m/min | 165 | 14.8 |



(a) Heat input variation for different values of TS and a constant WFS.



(b) Heat input variation for different values of WFS and a constant TS.

Figure 4.3: Heat input variation comparison for different values of TS and WFS.

This is corroborated when plotting a linear regression for both graphs, and then analysing the respective slopes. The results show that the Heat Input/TS slope is less than half of the slope of the Heat Input/WFS, indicating that the latter alters the heat input at a higher rate than the former.

Analyzing now the ratio of deposition to wire travel speed, or the $\frac{WFS}{TS}$ ratio, which provides the user

an indication of the material accumulation, ie, the amount of material that is deposited per unit of length of the part. A high value of the ratio indicates a high material accumulation, as it means that the rate at which the material is fed to the part is higher than the velocity at which the welding torch is travelling. Likewise, a lower value of this ratio will represent a low accumulation of material.

As stated previously on this section, an excess of material deposited on the part can lead to its collapse, thus showing that the $\frac{WFS}{TS}$ ratio can be of great importance to prevent collapse, by controlling the accumulation of material. However, the exclusive use of this parameter was proven to be insufficient to ensure a satisfactory deposition, or even to prevent the part's collapse.

The same part, built with the same ratio, but different WFS and WTS, will result in opposite results. This circumstance is illustrated in figure 4.4, in which all the parts have $\frac{WFS}{TS} = 1$, but the outcomes are very distinct from each other. While in figure 4.4 (a) there was no collapse, but the part had a big deformation and depositions outside the desired area, in figure 4.4 (c) the part collapsed, whilst in figure 4.4 (b) the structure doesn't present any defects.

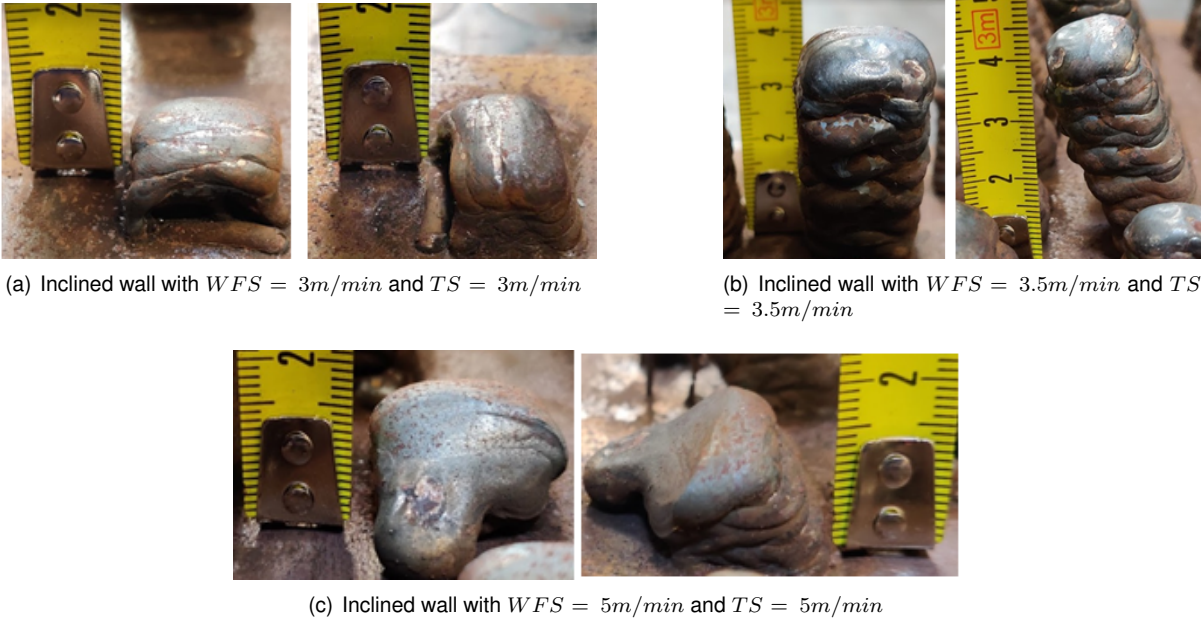


Figure 4.4: Examples of different outcomes for the same $\frac{WFS}{TS}$ ratio, in the deposition of inclined walls.

Analysing once more the heat input, it's possible to see that each of the previous cases have a distinct value, even though the $\frac{WFS}{TS}$ is the same (table 4.2). The wall seen in figure 4.4 (c), despite having the same amount of material as the other cases, also has a higher WFS and therefore, a higher weld penetration and heat input value, which culminates in its collapse. On the other hand, the trial shown in 4.4 (c) has the lowest WFS and heat input, however suffered a deformation due to lack of material, causing the deposit of an entire deposition parcel on the substrate. Despite this wall having the same amount of material as the one depicted in figure 4.4 (b), the latter has a slightly higher heat input, and although this could be problematic for high values, as it was the case of figure 4.4(c), if adjusted adjusted correctly, it can also promote a successful deposition. In the case of figure 4.4(b), the higher heat input and weld penetration led to a larger section, of the layer directly below the one just deposited,

to go back to the molten state, while simultaneously being subjected to a downwards force, caused by the layer of material above it. This effect causes the lower layer to flatten, thus offsetting the deformation that was found in figure 4.4(a). It then becomes apparent that the mutual use of the $\frac{WFS}{TS}$ ratio and the heat input, and consequently the weld penetration, is a more efficient method to prevent the collapse of the overhang, as well as other structural defects.

Table 4.2: Heat input for three distinct cases where WFS=TS

| | HI [KJ/mm] |
|--------------------|------------|
| WFS=WTS = 3 m/min | 19.3 |
| WFS=WTS= 3.5 m/min | 23.9 |
| WFS=WTS = 5 m/min | 24.9 |

Another parameter that can be changed by the user is the layer height. It allows to select the desired offset between layers, and is a way to control the stick-out during the deposition. As an example, if a layer height of two millimetres was to be selected, and knowing that the first layer is deposited on the substrate, the robot would increase its Z coordinate by two millimetres for the second layer, being Z the dimension perpendicular to the substrate. In the case of each layer deposited having a height of 2 mm, but the user selected layer height smaller than 2 mm, this would then culminate in a increment of the Z coordinate that's smaller than required, and consequently would lead to a smaller distance to the workpiece and lesser stick-out. This distance would however continue to decrease, with every deposited layer, and eventually could cause the welding torch to collide with the part. If this collision occurs against a molten section of the part, there's a risk that the torch could also weld itself to the part.

Otherwise, when selecting a layer height value that is greater than the increment of deposited material, the distance to the part will gradually increase, as well as the stick-out.

An increase of the stick-out will simultaneously reduce the weld penetration and raise the deposition rate, as a result of a higher electrical and, consequently, thermal resistances [40]. The deposition rate differs from the wire feed speed, as it only includes the metal that is actually deposited, excluding the material that turns into spatter or fumes [41].

Figure 4.5 demonstrates different outcomes for different values of layer height and ergo different stick-out values, while maintaining all other parameters constant. It's clear that the scenario with the higher layer height (figure 4.5 (b)) resulted in more misplaced depositions, seen as portions of unmelted wire on the substrate. Despite having a higher deposition rate, the added material only augments the parts vertical dimension, maintaining the same cross-section dimension, which in this case are smaller than intended, causing the appearance of unmelted wire. In opposition, figure 4.5 (a) has a smaller deposition rate, but also a higher weld penetration. This effect leads to the aggregation and flattening of both the deposited layer, and the one directly underneath it, culminating in an increase of the parts cross section measurements, thus compensating the previously existing deformation and reducing the misplaced depositions and portions of unmelted wire.

Finally, one last variable was found to be of great importance when building inclined walls: the cooling

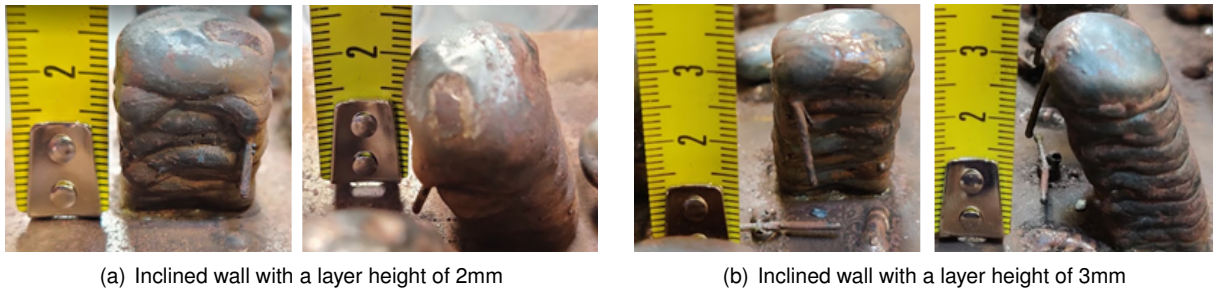


Figure 4.5: Influence of the layer height in the deposition of inclined walls.

time. If the part is not given enough time to exchange heat with its surroundings, its temperature will not reduce, ergo it will have less capability to remove heat from the weld pool and solidify it. This in turn, increases the probability of collapse of the weld pool, as the part couldn't cool the bead before there was any drippage or even collapse.

To optimize the part's capability to immediately extract heat from the weld pool, and to ensure a greater precision of the process, one can control the temperature of the part using a thermometer, instead of relying on a subjective time interval, which could vary depending on external conditions of each day.

Taking into consideration how these parameters influence the final geometry, a final deposition was made using a layer height of 2.75mm, $WFS = 3.5m/min$, $TS = 3.5m/min$ and thus, $\frac{WFS}{TS} = 1$. With these parameters, the inclined wall was built without any defects, as it can be seen in figure 4.6.



Figure 4.6: Final deposition of a 60° inclined wall, without defects.

As a final test, and to verify the precision of the process, the part was measured to ensure the dimensions required were met. As seen in figure 4.7, the rectangular section of the wall had the specified dimensions (20mm x 15mm), despite presenting rounded corners, instead of the sharp corner original design, which is a normal effect in WAAM. Regarding the height of the structure, its 4 millimeters higher than the originally intended height, however, this small excess could be corrected during a surface treatment process.

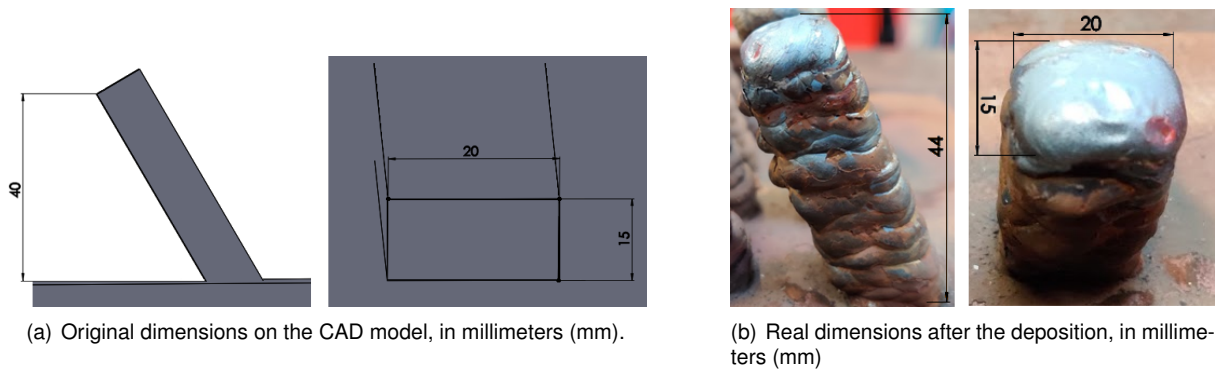


Figure 4.7: Original and final dimensions of the inclined wall, in millimeters (mm).

4.2 Thin Pins

The first parameter that should be selected to produce these structures is the wire feed speed. As the required diameters are small, a small WFS should be selected to prevent excess material deposition, and thus, a larger diameter than intended. As seen in the previous geometry (section 4.1), this parameter has a great influence in the resulting heat input of each layer. For a geometry such as this, where consistent and precise dimensions are required, in order to have the desired diameters, it's imperative that the heat input is low enough to prevent any possible deformations, caused by the drip of molten material, or an excessive weld penetration into the already deposited layers. Furthermore, a low WFS will also promote a smaller $\frac{WFS}{TS}$ ratio, meaning that there will be less deposited material accumulation, making it easier to achieve pins with a progressively smaller diameter.

However, as previously stated, for WFS values smaller than 3 m/min there was no consistent arc ignition and stabilization, which led to the selection of a wire feed speed of 3 m/min for the manufacture of all pins. The fact that the WFS was fixed throughout all depositions of this geometry, allowed for a better control of the part's geometry, decreasing the probability of over-depositing material and reducing a variable that needed further control and inspection.

As the WFS value was fixed to its minimal possible value, any adjustments to further regulate the amount of accumulated material, or in other words the $\frac{WFS}{TS}$ ratio, must be made via regulation of the wire travel speed. If the deposition produces a higher final diameter than wanted, the TS can be increased, leading to less material being deposited per unit of length, and ergo a smaller diameter. A higher value of TS will also induce a reduction of the heat input to the part, thus reducing any possible deformations caused by excess heat. Likewise, if the resulting pin is too thin, one can increase the TS, thus augmenting the final diameter, but also the heat input.

Although the amount of material deposited is crucial to the success of the manufacture of these elements, there are two more parameters which are equally as important.

First off, the proper layer height must be evaluated, as an incorrect value of this property can lead to a taller or smaller final geometry than intended. An incorrect layer height will also result in a different stick-out value, as explained in section 3.12. In that same section, it was discussed how an increase of the stick-out would lead to a higher deposition rate, due to the increase of electrical and thermal

resistances. It then becomes natural that a minimal layer height value should be selected, but bearing in mind that if this value was too small, the final part could fail to reach the desired height, or the weld gun could collide with the part. In order to accurately reach this value, at the end of each layer deposition the Z increment was measured, and the mean value of these measurements was used as the layer height. As the user advances to the deposition of progressively smaller diameter pins, it's expected that the decrease of the amount of deposited material is accompanied by a decrease of the layer height and subsequent increase in the total amount of layers.

Secondly there's the deposition pattern, the path that the software generates and the weld gun will follow, in order to achieve the desired geometry. As mentioned in section 3.1, despite being generated automatically by the software, it is possible to change this deposition pattern with alterations of the position of the guide line, seen in figure 4.8, as a yellow horizontal line. Both cases presented in 4.8 (a) and 4.8 (b) have the same parameters, only changing the position of the guide line, which results in a completely different deposition path.

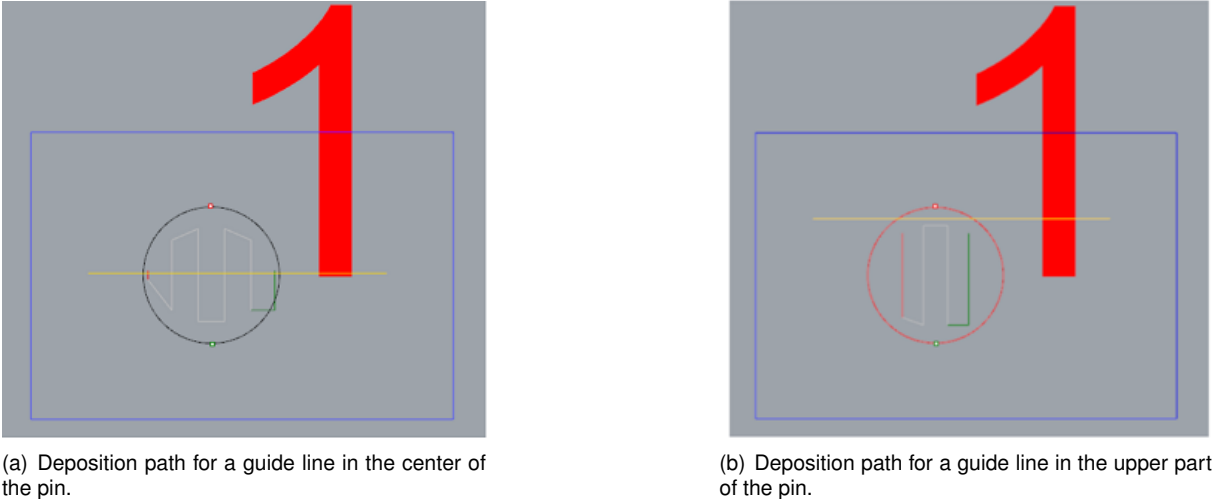


Figure 4.8: Two different deposition paths, for different positions of the guide line.

By inspection of the figure 4.9, in which the outcomes of the aforementioned deposition paths are presented, it's easy to see how the adjustment of the deposition guide can heavily influence the part's geometry. While the part in figure 4.9 (a) has an accentuated elliptical shape, the one in figure 4.9 (b) has a more circular shape, closer to the one desired.

A different way to change the deposition path is by altering the distance between each deposition parcel, ie, the distance between the white lines used to represent the projected deposition path. This property can, not only change the final shape of the part, but also the amount of material being deposited per unit of length, without altering the $\frac{WFS}{TS}$ ratio, as examined in figure 4.10. A small value of the deposition parcel distance will bring the parcels closer to each other, and consequently increases the number of parcels required to cover the same area of the part and with it, the amount of material deposited. This approximation thus leads to an increase to the beads overlap, causing an increase in the resulting layer height.

Once all parameters were optimized and the desired dimensions were reached, the diameter of the

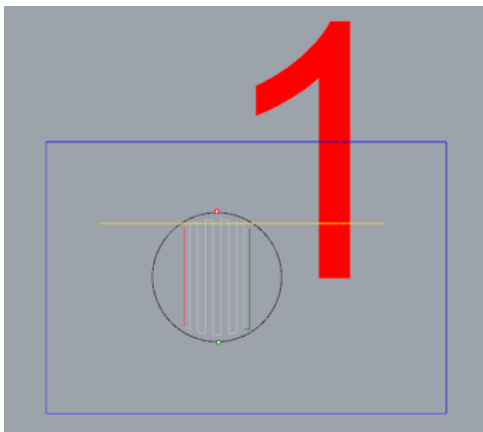


(a) Resulting pin profile using a guide line in the center of the pin.

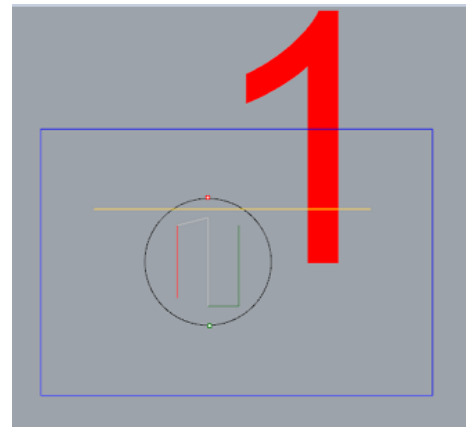


(b) Resulting pin profile using a guide line in the upper part of the pin.

Figure 4.9: Different geometrical outcomes, for different deposition paths.



(a) Deposition path for a segment distance of 1 mm.



(b) Deposition path for a segment distance of 3 mm.

Figure 4.10: Two different deposition paths, for different deposition segments distances.

pin was then reduced and the parameters adjusted as necessary once more, until it wasn't possible to reduce the diameter anymore. The dimension achieved is considered satisfactory if it has a deviation, from the original CAD dimension, that is smaller than 0.5 mm. Furthermore, the geometrical properties should also be respected, meaning that the part should have a well defined cylindrical shape, in which there are no big discrepancies between a diameter measured parallel to the X-axis and one measured parallel to the Y-axis. Note that the X-axis coincides with the slicing plane's horizontal direction and the Y-axis with the vertical direction, while the Z-axis corresponds to the height of the pin.

Table 4.3: Thin pins final parameters.

| | WFS [m/min] | TS [m/min] | Layer Height [mm] | Parcel Distance [mm] |
|-----------|-------------|------------|-------------------|----------------------|
| 10 mm pin | 3 | 6 | 1.7 | 2.5 |
| 8 mm pin | 3 | 6 | 1.5 | 3 |
| 6 mm pin | 3 | 10 | 1.2 | 3 |
| 4 mm pin | 3 | 30 | 0.9 | 2 |

Table 4.4: Thin pin's final measurements and respective deviations from the CAD.

| | 10 mm pin | 8 mm pin | 6 mm pin | 4 mm pin |
|-----------------------|-----------|----------|----------|----------|
| Part's Height [mm] | 30.6 | 29.5 | 30 | 30.6 |
| Height Deviation [mm] | 0.6 | -0.5 | 0 | 0.6 |
| X-Axis Diameter [mm] | 10.1 | 8.1 | 6.4 | 5.2 |
| X-Axis Deviation [mm] | 0.1 | 0.1 | 0.4 | 1.2 |
| Y-Axis Diameter [mm] | 9.7 | 8.1 | 6.2 | 5.2 |
| Y-Axis Deviation [mm] | -0.3 | 0.1 | 0.2 | 1.2 |

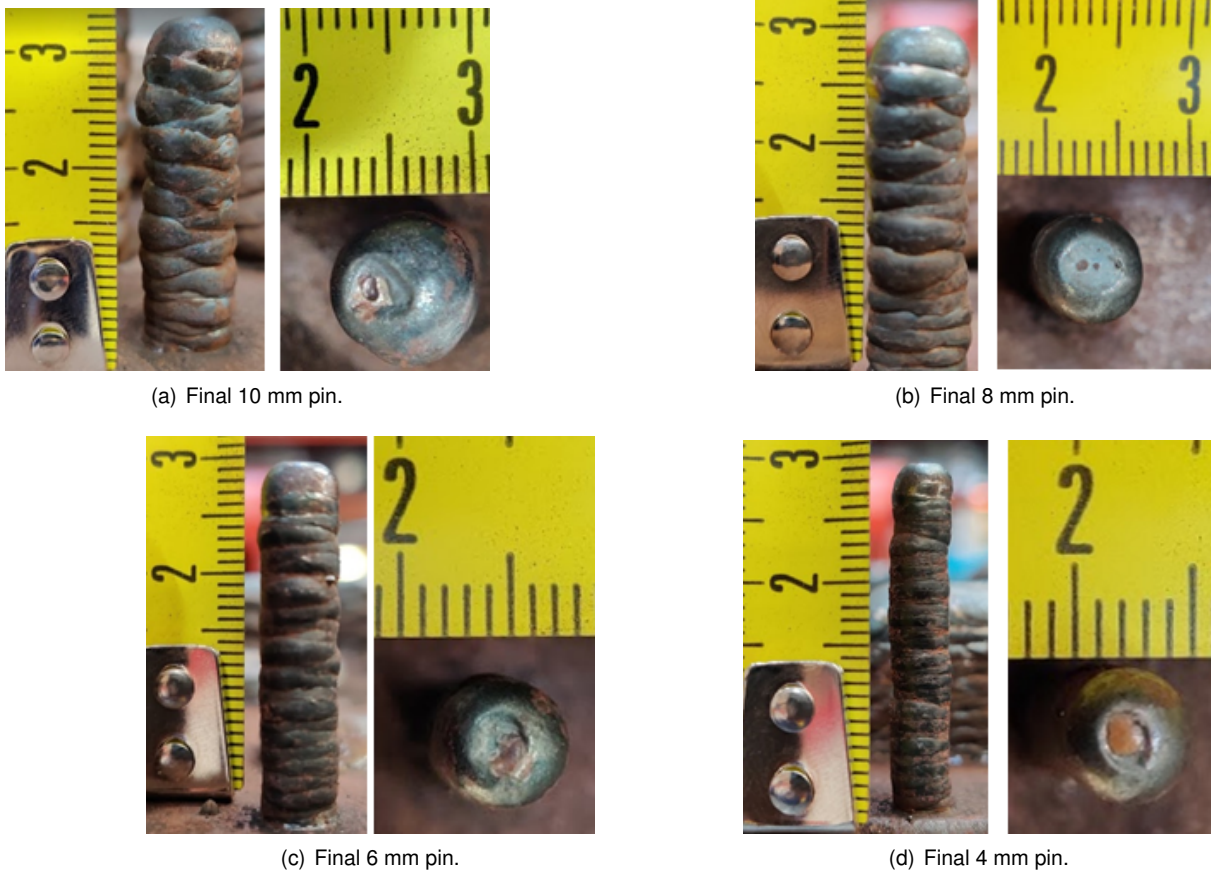


Figure 4.11: Final results for all the attempted pins.

Following this criteria, the process was repeated until failing to replicate the pin with a diameter of 4 mm. The smallest diameter achieved was 5.2 mm and it was not possible to reduce any further, whilst

still fulfilling the necessary requirements. Figure 4.11 presents the final thin pins manufactured, whose measurements and respective deviations are exhibited in table 4.4.

An overview of the selected trajectories can be found in Appendix A, noting that to achieve symmetry both in the X and Y axis, the software generates different paths for odd and even layers. The final parameters selected for each pin are presented in table 4.3. It's worth mentioning that the overall tendency was for the measurements deviation to increase with the decrease of the pin's diameter. This became more evident on the case of the last produced pin. Although part of this dimensional difference is caused by a software limitation that will be further discussed in section 4.6.2, it's also possible to assume that some additional vibrations and consequent uncertainty, were caused by the high travel speed selected in order to decrease the diameter of the pin.

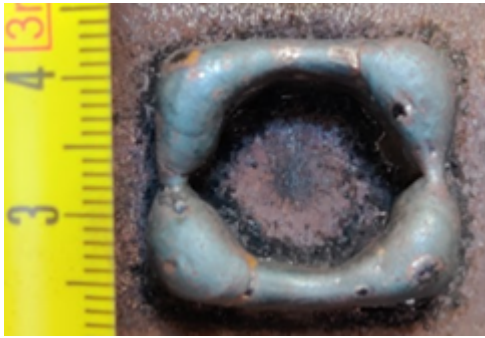
4.3 Thin Resolution Holes

Once again, it's beneficial to have the smallest WFS possible, in order to prevent any excessive deposition of material, thus affecting the geometry of the part. As an example, if too much material was deposited while performing the contour of the inner circumference, it would cause this area to have a smaller diameter than intended. Furthermore, a low WFS value will also result in a smaller heat input during the deposition and therefore, a smaller deformation due to the heat and consequent molten material drip. However, as previously explained, for very low values of WFS there isn't a consistent ignition of the electric arc, hence the selected value for WFS was 3m/min once more.

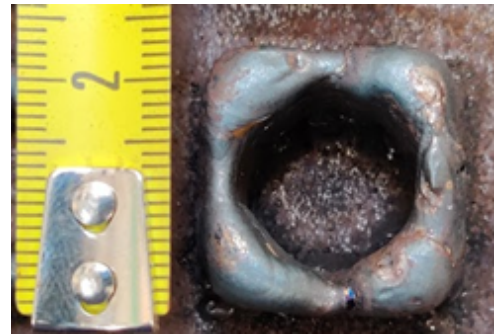
A parameter which influences heavily the outcome of this geometry is the deposition path selected. Firstly as of the version of WAAMSoft utilized for this work, it is not possible to generate a deposition path for a part with a hole within it, such as the one in selected geometry. The software couldn't recognize a segment that encompassed the entirety of the geometry. This meant that the part had to be separated into two distinct segments, creating a new problem: instead of one uniform part, this strategy generates two parts that must be connected in a somewhat seamless way. This was not successfully achieved using the same approach used in the previous cases, where one deposition path was selected and carried until the end of the deposition. As seen in the figure 4.12, both for a horizontal and a vertical guide line, the two segments struggle to connect properly, and areas with a clear lack of material can be spotted easily.

To overcome this problem, a new approach was selected using a combination of the two strategies mentioned previously. Instead of keeping the same two start and end points, and using only one guide line, which in turn, meant that the union of the two segments would be located on one section, this strategy would vary these parameters, to counter said effect. This was done by altering between a horizontal and a vertical guide line, every two layers, meaning that the start and end point, as well as the union of the two segments would change their positions every two layers, thus allowing to mitigate the geometrical depression which was found at the union of the segments.

The decision to change the strategies every two layers was influenced by how the software generates the deposition paths. As it can be seen in figure 4.13, each layer doesn't have to be identical to the

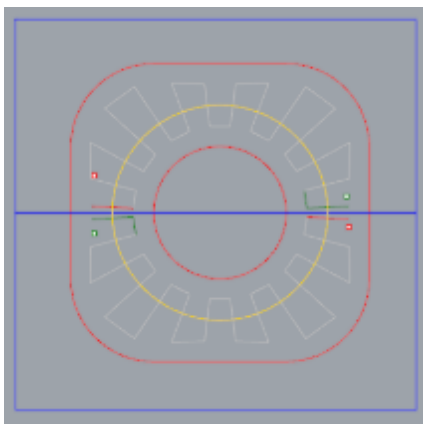


(a) Resulting part of a single deposition path strategy, with a horizontal guide line.

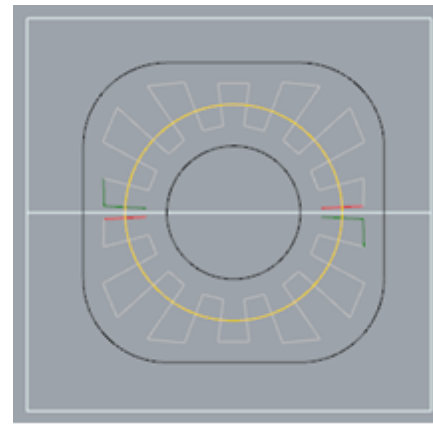


(b) Resulting part of a single deposition path strategy, with a vertical guide line.

Figure 4.12: Unsatisfactory connection of the two segments, both for a horizontal and vertical single deposition path strategy.



(a) Example of a first layer.



(b) Example of a second layer.

Figure 4.13: Example of the complementarity between odd and even layers.

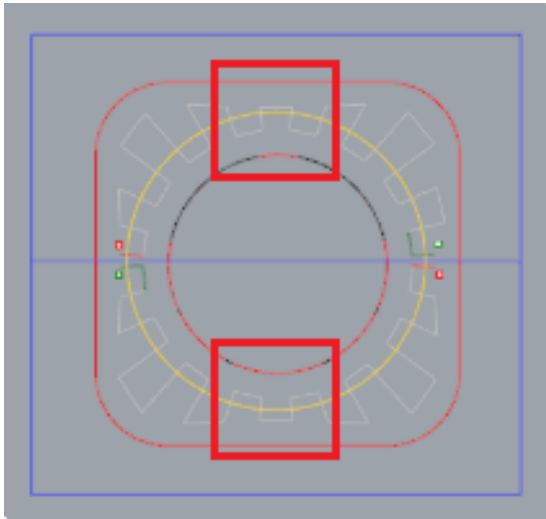
following or the previous one. Instead, the program might create two layers that complement each other, in order to produce a more accurate final shape.

As these complementary paths would occur every two layers, and in order to preserve the geometrical effect that they brought to the part, the alternation between the horizontal and the vertical guide line strategies was also done every two layers.

Regarding the deposition guide line, a straight and a semi-circumference, concentric with the resolution hole, were both tested. The results clearly indicated that the latter was the better option, not only allowing to achieve more accurate dimensions, but also generating a final geometry that was more true to the one projected in the CAD model.

Some additional features of the part that also require special attention, are the areas where the thickness of the wall is smaller. In these areas, the deposition path is considerably smaller than on the rest of the part, which might induce a lack of deposited material and affect the dimension of the part, as shown in figure 4.14. To counter this effect, custom zones (CZ) were implemented in said areas, reducing the wire travel speed only at those areas and ergo compensating the amount of material deposited.

Having taken care of all the particularities associated with this geometry, all that was left was to



(a) Areas with a smaller thickness and thus a shorter deposition path.



(b) Resulting geometry with less material being deposited in the highlighted areas.

Figure 4.14: Display of the deposition path in smaller thickness areas and consequent deposited geometry.

properly adjust the remaining deposition parameters in order to replicate the CAD's dimensions in the most accurate manner possible.

Unlike the thin pins, this geometry contains 3 different types of dimensions that need to be taken into consideration:

- **Internal dimensions:** the measurements of the hole in the X and Y axes;
- **External dimensions:** the measurements of the external structure that contains the hole, also both the X and Y axes;
- **Part's height.**

As stated at the beginning of this section, the main goal is to accurately replicate all of these dimensions presented in the CAD model. Therefore, if one of the dimensions is not achieved, then the part will be classified as not satisfactory and the test of this geometry will be concluded.

Advancing into the deposition tests, parameters such as the layer height, wire travel speed, costume zone speed, and the distance between deposition paths were modified, noting their effects in the geometry. The final and best depositions lead to the conclusion that both the 15 mm and the 10 mm parts were achieved successfully.

Table 4.5: Thin vertical resolution holes final parameters.

| | WFS [m/min] | TS [m/min] | CZ [m/min] | LH [mm] | Parcel Distance [mm] |
|------------|-------------|------------|------------|---------|----------------------|
| 15 mm hole | 3 | 13 | 7 | 1.5 | 3.5 |
| 10 mm hole | 3 | 16 | 9 | 1.25 | 3.5 |
| 8 mm hole | 3 | 28 | 16 | 1.25 | 2.5 |

However, during the deposition of the 8 mm part, a duality in the accuracy of the requested dimensions was found. This effect made it only possible to replicate either the external or the internal dimensions, but failing to replicate both. The issue was caused by a limitation imposed by the software used and will be further analysed in section 4.6. This limitation meant that in order to replicate the external dimensions of the part, the TS had to be reduced, thus increasing the amount of material deposited. However, the increased material made it harder to achieve the correct internal dimensions. As it was not possible to achieve both the internal and the external dimensions, the deposition for the 8 mm hole was not considered successful, and as such would not decrease the part's dimensions any further. Nevertheless, a decision was made to proceed testing the current part, in order to get as close as possible to the resolution hole's stipulated measurements, and then register the existing deviation of the external dimensions. The parameters used in the final depositions are exhibited in the table 4.5 as well as the respective deviations from the CAD's measurements (table 4.6) and a display of the final parts (figure 4.15).

Table 4.6: Thin vertical resolution hole's final measurements and respective deviations from the CAD.

| | 15 mm hole | 10 mm hole | 8 mm hole |
|---------------------------------------|------------|------------|-----------|
| Part's Height [mm] | 20.5 | 19.9 | 19.7 |
| Height Deviation [mm] | 0.5 | -0.1 | -0.3 |
| X-Axis Hole Diameter [mm] | 14.9 | 9.9 | 7.5 |
| X-Axis Hole Diameter Deviation [mm] | -0.1 | -0.1 | -0.5 |
| Y-Axis Hole Diameter [mm] | 14.2 | 9.8 | 7.8 |
| Y-Axis Hole Diameter Deviation [mm] | -0.8 | -0.2 | -0.3 |
| External X-Axis Length [mm] | 24.6 | 19.3 | 16.1 |
| External X-Axis Length Deviation [mm] | -0.4 | -0.7 | -1.9 |
| External Y-Axis Length [mm] | 24.5 | 19.3 | 15.4 |
| External Y-Axis Length Deviation [mm] | -0.5 | -0.7 | -2.6 |

Through further inspection to figure 4.15, it's possible to identify the software's increasing difficulty to clearly distinguish the part's straight walls from its rounded corners. As discussed in section 4.3, this is a consequence of the progressively smaller distance between the corners, which causes a reduction on the amount of deposition parcels, and with it a smaller ability to replicate details, such as changes of direction. Although decreasing the distance between the deposition parcels would increase the number of parcels, the length of the deposition becomes so small that, even with a minimum WFS, while using a wire feedstock of 1.2 mm both fillets will inevitably blend into each other, giving the appearance of a cylindrical exterior. Additionally, a decrease to the deposition parcels distance would increase the material overlap, accumulation and arc exposure time, thus inducing the molten material to drip and reduce the hole's diameter. Overall, the desired final shape was satisfactorily replicated for the produced parts, with however the 8 mm hole part showing the first signs of corner merging, and less distinct straight sections.

Continuing the final parts' evaluation, it's also possible to see that there were no significant differences in terms of deposited material on the areas of change of direction. Although an occasional hump appeared, it was not consistent within all changes of direction. Instead it only arose at the end of each

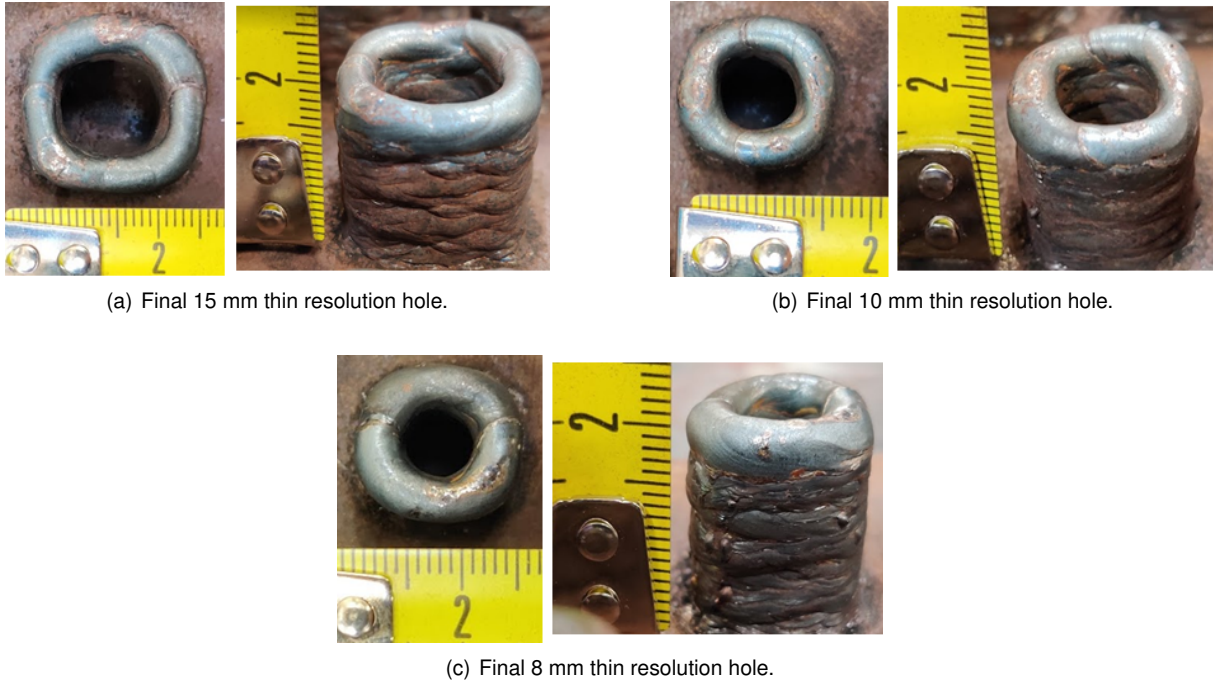


Figure 4.15: Final results for all the attempted thin resolution holes.

deposited layer, hence suggesting a different problem, that will in turn be discussed in section 4.6.2. It's then possible to infer that the present setup is adequate to perform changes of direction, as it is capable to compensate the differences in linear travel speed when doing so.

Focussing now only on the setup's ability to replicate the desired diameter, no limit was found, as the bottleneck limitation was on the external dimensions. To further corroborate this, the average heat input value was calculated for all three parts, and subsequently divided by the perimeter of each part's hole, in order to evaluate how much heat was disposed through the said holes (table 4.7).

Table 4.7: Heat input per square millimeter values for each part.

| | Heat Input [KJ/mm] | Heat Input/ Hole Perimeter [KJ/mm ²] |
|------------|--------------------|--|
| 15 mm hole | 6.1 | 0.129 |
| 10 mm hole | 4.7 | 0.150 |
| 8 mm hole | 2.6 | 0.103 |

Despite the available surface area to promote heat exchange reducing with each part, the heat input also suffered a reduction, specially in the part with 8 mm, where the ratio of heat input per hole perimeter actually decreases. However, it's important to note that this was caused by the use of a very high value of TS, meaning that in spite of the depositions not presenting a difficulty in removing the heat input, it will not be possible to repeat this with an increase of TS much further, as the limits of of travel speed of the robot will be reached eventually. It is expected that, once this point is reached, the heat exchange of the material encompassing the hole will be inhibited. As a result, the molten material will fail to solidify before dripping slightly, thus producing a smaller diameter than intended.

As a final remark, it was detected that the diameter of the hole decreased approximately 2 mm from the second to the third layers, in all parts. This reduction is developed by the deposition strategy introduced at the beginning of this section, where two different trajectories are combined to alternate the deposition's start and end points. These alternations lead to a spread of areas of accumulated material, reducing the hole's diameter, but also contribute to generation of a more uniform circumference.

Upon inspection of the table 4.6, it can be inferred that the part's X and Y axes deviations differ from each other, with a slight tendency to for the Y-axis to have the biggest deviation.

4.4 Straight Walls and Cross Shaped Intersection

Advancing now to the deposition of the straight walls, the evaluating factors differ from the previous geometries. As it's not expected to produce any small details, the WFS doesn't need to be fixed at low values. However, as Ayarkwa et al. [42] discussed, for higher values of WFS, the electric arc is more unstable, thus increasing the probability of defects arising, or a having a higher surface waviness. According to the author's findings, the best results for a defectless wall are obtained for values of WFS between 4 m/min and 8 m/min.

With these recommendations as a starting point, the WFS, TS and deposition parcel distance were adjusted, in order to meet the dimensions required. It was then found that depending on the deposition strategy selected, some consistent deviations, caused by the software, could be found (table 4.9).

Regarding the deposition with the horizontal guide line, there was an excess in the length of the part, consistently ranging around an extra 3 to 4 millimetres. On the other hand the part's width was successfully replicated using this strategy.

As for the case of the deposition with a vertical guide line, the part's length was shorter than intended, contrarily to what happened with the other strategy. Besides this, the width was consistently larger than projected, also with the same interval of an extra 3 to 4 millimetres.

These differences in the measurements were proven to be independent of the deposition parameters, hence suggesting that the dimensional discrepancy was caused by the deposition path generated and not excess or lack of deposited material. This effect could not be corrected in the software and it will be discussed further on section 4.6. As such, the focus turned into optimizing the rest of the part's geometry and then evaluate the dimensional deviations.

Despite this, it was still possible to evaluate how some of the part's dimensions are affected by the alteration of the deposition parameters.

First off, it was found that the width of the deposited walls are simultaneously dependent on the $\frac{WFS}{TS}$ ratio, the heat input and the deposition parcel distance. The $\frac{WFS}{TS}$ ratio, as established previously, indicates the deposited material accumulation per unit of length, so naturally a higher value of this ratio will result in a wider part. However, two parts with the same $\frac{WFS}{TS}$ ratio can have different values of width, despite having the same amount of material on the part. As an example, two different cases were tested:

- Case 1: $WFS = 5m/min$, $TS = 10m/min$, $\frac{WFS}{TS} = 0,5$, $width = 10mm$, $height = 17.4mm$;

- Case 2: $WFS = 4m/min$, $TS = 8m/min$, $\frac{WFS}{TS} = 0,5$, $width = 9.3mm$, $height = 19.1mm$;

As evidenced, although both cases have $\frac{WFS}{TS} = 0,5$, the width differs. This is a consequence of a change to the WFS value, that, as seen in section 4.1, greatly influences the resulting heat input. A higher WFS, will induce a higher heat input, that in turn will maintain the material molten and more fluid. This then causes the molten material to spread along the width of the part, increasing its width, but also decreasing its height. Additionally, changes to the deposition parcel distance, more specifically a decrease of this parameter, will lead to a higher overlap of the parcels, that can cause a slight increase of the part's width as well.

Moreover, the increase of the overlap will contribute to a higher part height, just as lowering the WFS while maintaining the $\frac{WFS}{TS} = 0,5$. It's then possible to surmise that the part's height is influenced by deposition parcel distance, the heat input and the manipulation of the layer height.

It was then found that the part required the development of two custom zones, causing the start and finish of each part to have a lower TS and consequently a higher material deposition. This was done to ensure a constant height on the entire part, and the reasoning behind it will also be further explained in section 4.6.2. Depending on the deposition strategy selected, the custom zone will require alterations, as the main objective with these custom zones is to slow down the TS at the first and last sections of the deposition parcels. As such, the following custom zones seen in figure (4.16) were selected for the depositions.

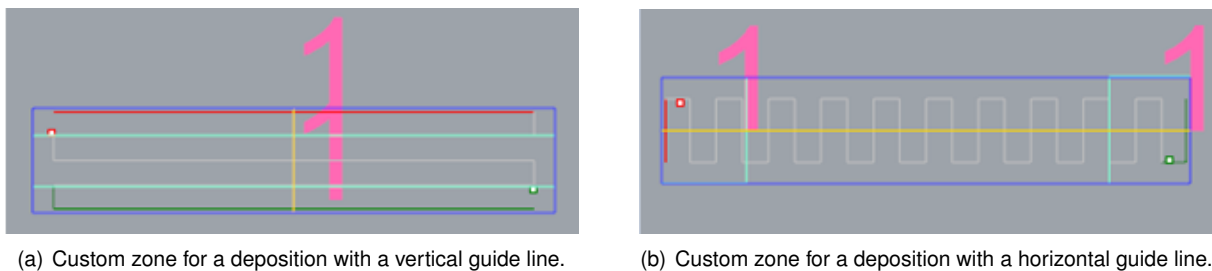


Figure 4.16: Different custom zones depending on the deposition guide line deposition.

The best possible outcomes for both deposition strategies were achieved (figure 4.17) and the respective deposition parameters were registered and presented in table 4.8.

Table 4.8: Final parameters for both the deposition strategies of the straight walls.

| | WFS [m/min] | TS [m/min] | CZ [m/min] | LH [mm] | Parcel Distance [mm] |
|----------------------------|-------------|------------|------------|---------|----------------------|
| Wall-Horizontal Guide Line | 4 | 6 | 5.5 | 2.25 | 5 |
| Wall-Vertical Guide Line | 4 | 7 | 6 | 2.25 | 4 |

When making a direct comparison between both the strategies while generating the same part, it's then clear that overall the deposition with the vertical deposition guide line was the most successful. Not only did it have a better finish, it was also the closest to the desired dimensions. Furthermore, it's possible to verify that there is a somewhat constant deviation in the direction of the deposition guide. In



(a) Final straight wall with a vertical deposition guide line.



(b) Final straight wall with a horizontal deposition guide line.

Figure 4.17: Final straight walls.

other words, the wall with the horizontal deposition guide line had a length deviation consistently similar to the width deviation of the wall with the vertical guide line.

Table 4.9: Straight wall's final measurements and respective deviations from the CAD.

| | Wall-Horizontal Guide Line | Wall-Vertical Guide Line |
|-----------------------|----------------------------|--------------------------|
| Lenght [mm] | 54.3 | 47.8 |
| Lenght Deviation [mm] | 4.3 | -2.2 |
| Width [mm] | 9.9 | 14.5 |
| Width Deviation [mm] | -0.1 | 4.5 |
| Heigth [mm] | 20.1 | 19.7 |
| Height Deviation [mm] | 0.1 | -0.3 |

Having gathered this information regarding the process parameters for simple linear walls, it's possible to take further advantage by using the results as a starting point for the parameter investigation of the cross shaped intersection. Since this geometry is an overlapping combination of two straight walls, the obtained results can be used and then adjusted as necessary in order to better fit this new geometry.

As expected, the area where this overlap occurs (the central area of the part) requires particular attention. If the parameters are not properly adjusted, this area would have double the amount of deposited material, as both segments would deposit the material at a constant speed. To correct this, a custom zone was created at that spot, at which the TS was much higher than at the rest of the part, thus compensating the overlapping effect. This custom zone is presented in figure 4.18, as well as two others per segment, inherited by the results of the study of straight walls, and with the objective to maintain the part's height as constant as possible.

Regarding the depositions strategy, the aforementioned horizontal guide line alternative was the one selected for three distinct reasons:

- It was concluded previously that this strategy produced the final geometry closest to the CAD's dimensions;

- Ding et al. [43] concluded that a deposition path with a higher oscillation would result in smaller necking effects on the intersections of the segments;
- There was a software incompatibility when trying to apply the other strategy. This will be further discussed in section 4.6.

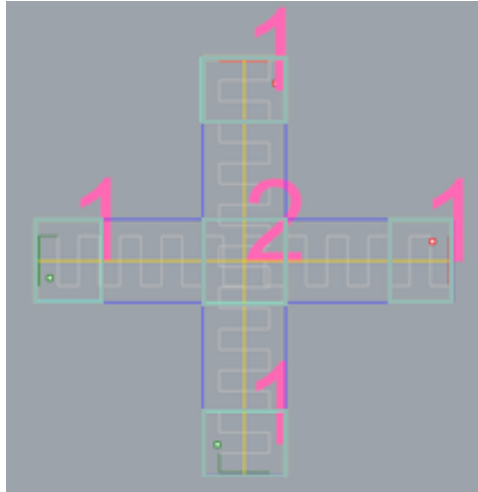


Figure 4.18: Representation of the custom zones necessary to the manufacture of the cross shaped intersection.

The final part is shown in figure and the respective deposition parameters were the following:
 $WFS = 4m/min$; $TS = 6m/min$; $CZ1 = 6.5m/min$; $CZ2 = 1.4m/min$; $LH = 2.25mm$; $SegmentDistance = 4mm$.



Figure 4.19: Final cross shaped intersection.

Unsurprisingly, the dimensions of the cross shaped intersection follow the same tendency of the straight wall's, seen in table 4.10, where V indicates that regards the vertical segment of the part (along the Y axis), and H the horizontal one (along the X axis). However, it's interesting to note that even though both the average width and height of both segments are identical, the length differed in about one millimetre. Regarding the intersection area, the primary objective was accomplished, as there was neither excess nor lack of material, meaning that this section had the same height as the rest of the part. There was however, a slight lack of material immediately after the intersection area. The suspected

reasons that lead to this effect and unsuccessful attempts to rectify it will be disclosed in section 4.6.

Table 4.10: Cross shaped intersection final dimensions and respective deviations from the CAD.

| | Length-V | Length-H | Width-V | Width-H | Height-V | Height-H |
|---------------------|----------|----------|---------|---------|----------|----------|
| Part Dimension [mm] | 54.6 | 55.6 | 10.4 | 10.4 | 20.5 | 20.5 |
| CAD Deviation [mm] | 4.6 | 5.6 | 0.4 | 0.4 | 0.5 | 0.5 |

4.5 Staircase Vertical Increment

Once again, when the part is divided into layers, the result is a rectangular section, with the same width as the previous geometries depicted in section 3.3.4. As such, the same parameters as the straight walls were once again used as a starting point, as well as the custom zones at the beginning and end of each segment.

It's very important to note that with each vertical increment, there's an associated decrease in the part's length, meaning that the area where the custom zone is designated also retracts and might also decrease its size. To match this effect, more than one segment must be defined so that changes can be made at each step of the part. To facilitate the generation of the segments, the layer height was set at 2,5 mm, making up half of each height increment between two consecutive steps. This meant that a new segment would be required at every two layers, with the exception of the first four layers of the part, as the first step has a height of 10 mm instead of 5 mm. To better understand the relative position of the deposition segments and how it benefits the part's geometry, figure 4.20 illustrates the position of each segment (S).

Furthermore, the decrease in length at each step compels the length of the custom zones to reduce a well. It was found that the most effective variation was to have two custom zones, covering the first and last 5 deposition parcels, from layers 1 to 10 and then two costume zones with 3 deposition parcels from layers 11 to 12. The final two layers did not require the use of costume zones, as it was unjustifiable due to their small size.

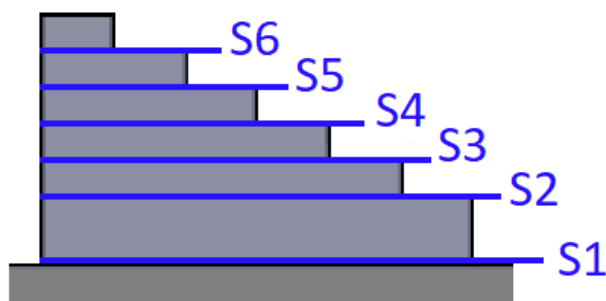


Figure 4.20: Profile representation of staircase vertical increment and each deposition segment (S).

After adjusting the parameters and listing the respective effects in the part's geometry, the following parameters were found to produce the best overall set of measurements: $WFS = 4m/min$; $TS =$

5.5m/min; CZ = 4m/min; LH = 2.5mm; Deposition Parcel Distance= 4mm. The final part can be seen in figure 4.21.



Figure 4.21: Different perspectives on the final staircase vertical increment.

Naturally, this geometry's deposition parameters, and respective influence on the part's final measurements, are analogous to the ones analysed when discussing the straight walls (4.4). For this reason, this correspondence will not be done once more. However, in this geometry there is a parameter that holds a higher level of importance: the heat input. As the part's Z coordinate increases, so does the accumulated heat, thanks to the consecutive depositions and a progressively smaller heat exchange surface. To control the influence of this effect on the part, all the dimensions were measured in every step and the results are presented in table 4.11, where "Step 1" represents the step closest to the substrate, and so forth.

During the depositions of this geometry, it was found that, when building up the steps, the process had a propensity to let the molten material slide at the end of each deposition, thus losing the characteristic staircase shape. This was aggravated by an involuntary event that will be analysed in section 4.6. In order to prevent such effect, the depositions were always planned in such a way that it was possible to "cover" the outcome of this effect. More specifically, and using as a reference image 4.20, knowing that all steps are comprised of an even number of layers, when starting the deposition from the left to the right side (ie, an odd number layer), this slide of material will be seen at the end of the right side of the part. However, when depositing the next layer (ie, an even number layer), this slide will be covered by the additional material and will now be seen at the leftmost side of the part instead. As this side marks the beginning of every step, when depositing the following step, the slide will be covered once more, while on the right side, where there's the distinction between steps, the slide is always covered at the end of every step.

Although some anomalies were found throughout the results, it was also possible to detect some tendencies in this part's geometry, and the versions that preceded it. For instances, there was an increase in each step's length and width, in spite of the appearance of some anomalous measurements. As discussed, this is a consequence of a constant heat input, with a simultaneous decrease in heat exchanged, leading to an augmented internal temperature. This in turn, just as the straight walls at

higher heat input values, causes the molten material to retain a higher temperature and spread itself more easily, causing an increase of the aforementioned dimensions.

Regarding the step's height, the overall tendency was to shorten with the increasing height, maintaining a height considered ideal from steps 2 to 5. On the very last step, there was however a big deviation from the CAD's measurements. In fact, in all three dimensions was measured a higher deviation from the CAD, on the last deposited step.

Table 4.11: Staircase vertical increment final dimensions and respective deviations from the CAD.

| | Step 1 | Step 2 | Step 3 | Step 4 | Step 5 | Step 6 |
|-----------------------|--------|--------|--------|--------|--------|--------|
| Length [mm] | 9.1 | 10.6 | 9.2 | 10.6 | 11.5 | 15.1 |
| Length Deviation [mm] | -0.9 | 0.6 | -0.8 | 0.6 | 1.5 | 5.1 |
| Width [mm] | 11.8 | 11.4 | 11.7 | 11.7 | 11.5 | 12.1 |
| Width Deviation [mm] | 1.8 | 1.4 | 1.7 | 1.7 | 1.5 | 2.1 |
| Height [mm] | 11.2 | 5.2 | 5.1 | 5 | 5 | 3.9 |
| Height Deviation [mm] | 1.2 | 0.2 | 0.1 | 0 | 0 | -1.1 |

4.6 Setup Limitations

As with any other test artifacts, the main objective is to not only analyze how well does each setup perform challenging geometries, but also to discover limitations associated with the setup. These limitations could be derived from the equipment used, such as the CMT arc wire feeder, the robotic arm, the type of metal wire selected, among other possibilities. There are also limitations associated with the software being used, as there aren't many programs developed for WAAM and most are in continuous development. Furthermore, the user could be using an outdated version that does not have the required features to control some parameters, as is the case with this master thesis. As such, in this section the limitations found during the creation of each geometry will be specified, separating the limits imposed by the mechanical components of the setup (hardware limitations) from the ones imposed by WAAM dedicated program (software limitations).

4.6.1 Hardware Limitations

One of these limitations, that was persistent throughout all of the performed geometries, was an unintended change of velocity during the last section of every deposition. Upon reaching the last deposition parcels, the robot would change the speed at which it was travelling (TS). This velocity change was most noticeable when the robotic arm was asked to perform either under low or high speed, creating an easily observable difference in the amount of material deposited. This effect can be noticed in figure 4.22 (a), where the area in the rightmost part of the picture has a greater amount of deposited material than the area in the leftmost part. This change in velocity is not intended by the end user, and as such, the code sent to the robotic arm doesn't reference any changes to the velocity. This means that there are no changes that could be made to the code in order to correct this, and is most likely a safety mechanism

employed in the programming of the robotic arm. Even when generating a custom zone to try to correct this effect, the robot would end up overriding it and kept depositing at a pre-defined velocity.

Although in some geometries this effect can be mitigated by the constant alteration of start and end of the deposition, there will always be a cumulative effect caused by the consequent lack of material. In figure 4.22(c) it's possible to observe, on the leftmost end of the wall, this cumulative effect, while on the rightmost side it's easy to spot the lack of material on the last layer.

In order to try and soothe this outcome in simple geometries, such as the straight walls, two custom zones were developed at the start and end of each layer. Although, as explained, the custom zone at the end of the layer was consistently ignored, the objective was to start each layer with a higher material accumulation, so as to when the following layer was deposited, the lack of material at the end was then compensated. However, this solutions also implies an increase of the heat input in that starting custom zone, causing that area to sink slightly, when compared to the rest of the part. This approach also isn't capable to cover the results of the very last deposition.

In other geometries, such as structures with an overhang, this effect encumbers the success of the deposition, as the lack of deposited material results in the deformation of cross-section of the part, thus diminishing the structure that holds the deposited molten material (figure 4.22 (b)). Besides this, the deformation caused by the lack of material can lead to the attachment of unmelted wire to the part, similarly to what happened for high values of WTS.



(a) Resulting deposited layer with a lower travel speed in the last deposition section.



(b) Part deformation due to the undesired velocity change.



(c) Straight wall aggravated dip, due to the increase of velocity at the end of each layer.

Figure 4.22: Effects of the undesired velocity alteration in the last segment of each layer.

Besides this, another problem was present through the manufacture off all geometries, although in a more irregular and unpredictable way. During the initial deposition phase, there was occasionally a slight delay with the electric arc ignition. As the robotic arm can't sense this delay, it begins the

designated trajectory, culminating in a slight bend and drag of the wire fed, during that fraction of time before arc ignition. Once the arc is ignited, the now distorted wire will melt and can lead to some material accumulations and shape distortions. This effect is specially problematic in parts with smaller dimensions, such as thin pins. Figure 4.23 demonstrates how this delay can end up altering the final geometry and consequently, the success of the deposition.



Figure 4.23: Material accumulation at the top of the thin pin, due to the arc ignition delay.

It's also worth taking into consideration that the diameter of the wire fed will also heavily influence the outcome of the depositions. A thinner wire would lead to a smaller deposition rate, thus enhancing the precision of the deposition and enabling the production of, as an example, thin pins with a higher aspect ratio, ie, pins with a smaller diameter. As of this work, although the diameter of the metal wire was not the main limitation responsible for the failure to further reduce the pin's diameter, it also contributes for this failure, thus presenting itself as a limitation. The main reason pointed as the principal culprit for the inability to further reduce the deposited diameter will be presented in section 4.6.2.

4.6.2 Software Limitations

As examined in previous chapters, the software used did not allow to control the deposition path, creating it automatically after defining the segment area, guide line and start and end points. The software would then recognize where it could create a path, making each segment perpendicular to the guide line and initiating and finalizing the deposition according to the relative position of the start and end points. Despite this, the program does not necessarily respect the actual coordinates of those points, instead recognizing their general vicinity and placing the points where it sees fit (figure 4.24). This obviously restricts the end user's ability to change the path trajectory, which can affect the part's geometry. Moreover, this lack of control over the deposition trajectory meant that it was not possible to test some strategies that were already proven to be far more optimal for certain geometries, such is the case of the strategies suggested by Venturini et al. [18] for the cross shaped intersections and Kazanas et al. [12] for the inclined walls.

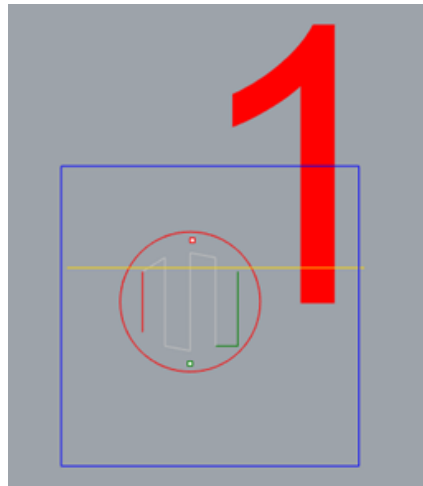
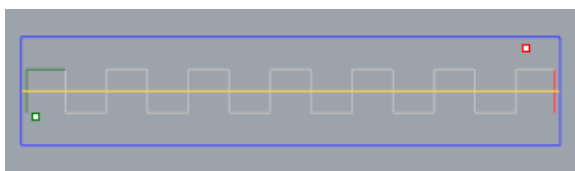


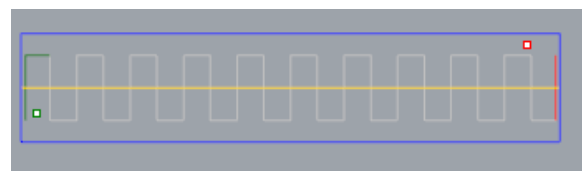
Figure 4.24: Example of a start and finish of deposition not coinciding with the ones defined by the user.

Going back to the production of the thin resolution holes, it was detected that there was a duality when trying to replicate both the internal and external dimensions of the part. This was in fact a result of a limitation when generating the deposition path. While the generated path was adequate to achieve the part's internal dimensions, the low values of WFS and TS made it necessary to reduce the distance between the deposition parcel and the end of the part, in order to reach the desired measurements. However, the software does not allow such changes to the deposition path. Even when changing the deposition parcel distance, it only resulted in an approximation of the parcels to each other, but never to the end of the part. The only way to increase the external dimensions was therefore to increase the amount of material deposited on the edges of the part, but this was not a satisfactory solution, as it would interfere with the other part's dimensions.

This problem also affected simpler geometries, such as the straight walls, and consequently the cross shaped intersection and the staircase vertical increment. For these geometries, a deposition path was created with a certain length that could not be altered. Changes to the deposition parameters only resulted in the alteration of the part's width, but not the length, as the first and last parcels distance to the part remained unchanged (figure 4.25).



(a) Deposition path for a straight wall, with a deposition parcel distance of 6 mm.



(b) [Deposition path for a straight wall, with a deposition parcel distance of 4 mm.

Figure 4.25: Similar distance between the deposition parcels and the ends of the part, for two distinct values of deposition parcel distance.

It's possible that this effect is intended by design, in order to allow the user to machine the final part. This is explained by Venturini et al. [44], when mentioning that the arc's irregularities at the beginning and end of the deposition. It's then defended that the part should be prolonged, so that it's possible to posteriorly machine the defective areas and still achieve the desired dimensions. This is represented

in figure 4.26, where the top leftmost wall was performed without an extension and the top rightmost wall with it. The lower images shown the respective results, where the red line represents the expected result by the user and the blue line the effective result, after machining the part. However, it was not possible to confirm whether or not this was an intentional feature within the software. Be that as it may, it's important to remember that ,during the fabrication of the thin resolution holes, the opposite effect was detected, where the external dimensions were actually smaller than intended, thus pointing to a probable miscalculation of deposited material, within the software

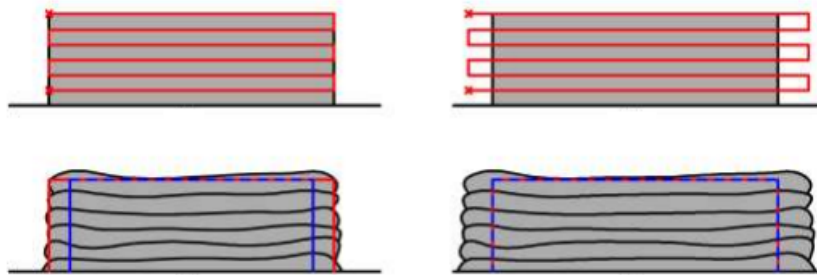
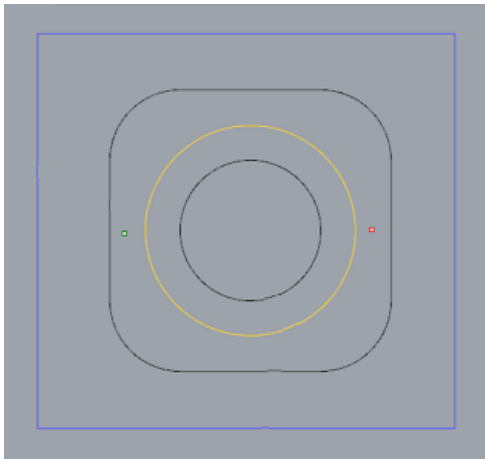


Figure 4.26: The importance of deposition path extensions in a straight wall [44].

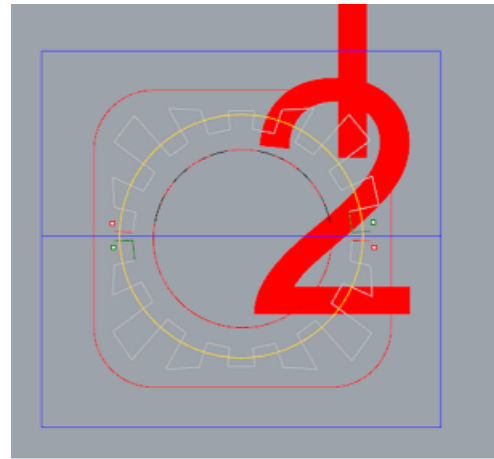
Another constraint found while generating these parts, was the fact that the program requires start and finish points in order to generate any deposition path. Therefore, it's not possible to make a single point deposition. The software will only create point-to-point depositions, which, as an example, will increase the resulting diameter of a thin pin when compared to a single point deposition.

In addition to this, the guide line must be an open contour so that the program can recognize it. In circular geometries, such as the thin vertical resolution hole, this requirement is not helpful as a circular deposition path is not recognized (figure 4.27 (a)), forcing the user to separate the part into several deposition segments, meaning that extra attention to the segment union areas is needed, in order to ensure a proper joint. As seen previously, a circular deposition guide provides better results than a straight one, so in order to overcome the open contour limitation, two depositions segments were created, each with a half circle deposition guide line (figure 4.27 (b)).

Besides closed contour guide lines, it was found that the software also failed to recognize some other features. During the build of the cross shaped intersection, it was noticed that the software did not allow the use of a single deposition segment for the entire shape. Instead, the user was forced to divide the part into two segments and deal with an overlap area. Furthermore, when trying to divide said part into two "L" shaped deposition segments, the software did not recognize it as well. Finally, it was attempted to combine the use of two rectangular deposition segments, but one with a vertical and the other with a horizontal deposition guide line. Once more, the software wasn't successful in generating the deposition paths, although it did recognize the segments. All of the aforementioned strategies were attempted as a way to emulate the results obtained by Venturini et al. [18] and Neto [45] for optimized crossing, thus reducing effects such as heat sink, but as just mentioned, all of the attempts were not allowed by the software. Moreover, the software also couldn't process a deposition path with vertical guide line. It was only capable of processing one of the segments with said strategy, but failed to do it on both of them.



(a) Full circular deposition guide not recognized by the software.



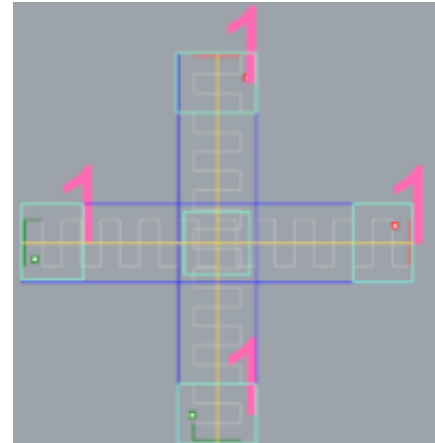
(b) Two half-circular deposition guide recognized by the software.

Figure 4.27: Deposition guide software limitations.

Still on the subject of the fabric of the cross shaped intersection, as seen in the previous section, the selected strategy encompassed the use of two rectangular deposition segments and a custom zone at their intersection. It was observed that the software did not interpret the custom zone as expected: instead of instantly changing the TS when reaching and exiting the custom, there was a slight delay relative to the change of velocities. This delay then led to a lack of material, adjacent to the custom zone, and caused the appearance of necking effects (figure 4.28).



(a) Necking effect derived of the TS change delay.



(b) Velocity custom zone not recognized by the software.

Figure 4.28: Deposition guide software limitations.

Trying to correct this effect, the custom zone was shrunk to attempt to compensate this delay. However, the program requires the segments that outline the custom zones, to intersect either the part or the deposition segment. This means that a custom zone that's completely enclosed, by the part or segment, will not be recognized by the system. This can be seen in figure 4.28, where while the custom zones at the beginning and end of each segment are recognized (indicated by the appearance of the custom zone identification number), the one on the center of the part isn't, as it doesn't intercept any deposition segment.

Another constraint inherent to the software was uncovered when planing depositions that required several deposition segments and velocity custom zones. As stated previously, developing the deposition strategy for the staircase vertical increment was such a case. During this process, despite no error message nor visible problem was presented in the program's interface, upon inspecting the resulting files, meant to be sent to the KUKA robot, it was found that they were correct only until a certain layer. From that layer onwards, all the remaining files would be blank, suggesting that the software possesses a maximum amount of deposition segments and custom zones, that is capable to process at once. To work around this setback, it was required to separate the deposition into several ones, as if it were different parts to deposit. With each deposition, different layer files are saved and then all of them are combined at the end to comprise the complete deposition.

It's also worth noting that the software version used did not allow changes to the deposition strategy, meaning that only the oscillation strategy could be implemented. As such, it wasn't possible to test the impact of other strategies such as uni-directional deposition or weaving. This specially affects the heat accumulation sensitive geometries because, as discussed previously in section 2.2.1, the oscillation strategy retained the most heat in the part, hence the need to test other strategies, with a higher cooling rate, such as the unidirectional deposition strategy. Additionally, features such as inclined slicing were not available within the software, nor any equivalent that allowed the inclination of the welding torch during the deposition. Changes to the deposition angle would result in a reduction of properties such as the weld penetration, and would then facilitate the manufacture of geometries with overhangs, as is the case of the inclined walls. Likewise, and as it was mentioned already in this work, it wasn't possible to set a value for the stick-out value on the software, meaning that all the depositions paths generated did not take the consequences of a wrong stick out value into consideration.

4.7 Test Artifact

Having analysed all the geometries that were planed and the information that each one provided, the last step was to combine all of the geometries into a single part, developed with the purpose to test the capacities of a simple WAAM setup, providing as much information regarding the process, hardware and software limitations as possible. As such, the test artifact presented in figure 4.29 was projected.

This final artifact has a length of 250 mm and a width of 200 mm, allowing the user to test a broad range of the setup's robot reach, without however requiring to big of a part, promoting an unnecessary waste of material. The motives as to why each geometry was included were already disclosed in section 3.3 and all deposition paths, as well as the location of the custom zones, are presented in appendix A . It's worth only highlighting that it's not expected of the user to deposit all of the presented geometries. For instance, while testing the setup's limits when generating the thin resolution holes, if a failure occurred for a diameter of 8 mm, then it's natural that the following holes cannot be successfully replicated. It's then unnecessary to proceed with the deposition of this geometry, and the user should instead advance to the deposition of the next one.

Regarding the measurements performed throughout the entirety of this work, they were all done in

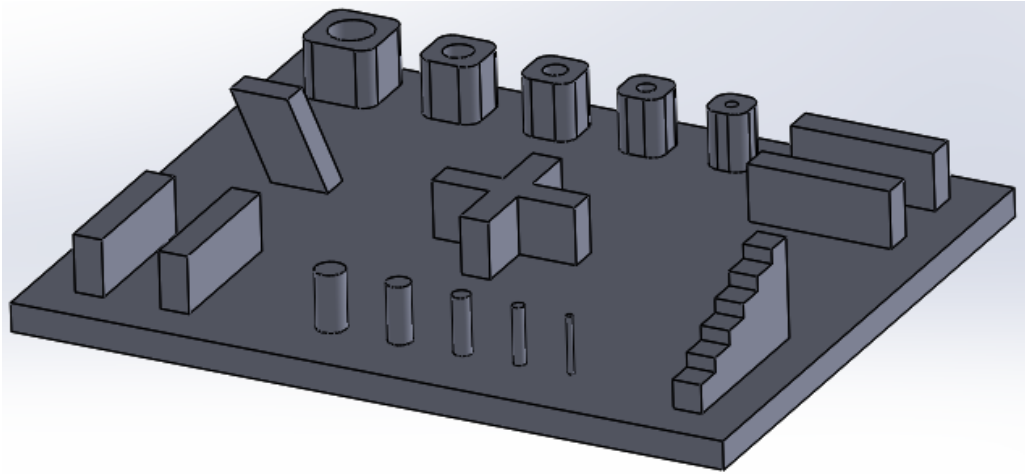


Figure 4.29: CAD model of the projected test artifact.

accordance with the ISO/ASTM 52902 standard, following the guide lines present in section 2.4. All measurements were made using a pair of digital callipers, that granted a dimensional uncertainty of 0,1 mm, hence fulfilling the requirement of a maximum permissible error (MPE) ≤ 2 , but only reaching a measurement grade of A (grade attributed by the ISO/ASTM 52902 standart and explained in section 2.4. Furthermore, a minimum of five measurements, per dimension to evaluate were performed, thereby surpassing the minimal requirements imposed by the international standart. These were taken on the beginning, middle and end of the feature to measure, just as demonstrated previously in figure 2.13, but also in the middle sections in between those three points.

It's also worth mentioning that in order to increase the accuracy of the measurements, for example of the part's height, all measurements should be conducted in relation to the same point. In other words, when measuring the height of hypothetical parts A, B and C, it should always be done starting from the same point, D, regardless of its position relative to the part to measure. This is advised as a means to avoid any deformations on the substrate derived of the resulting deposition heat.

However, the simple pair of callipers available did not allow for such flexibility when measuring, having instead used a fixed point within each part. This then permitted the existence of some uncertainty between two distinct parts, but not within the same part. It's therefore important to keep in mind, when analysing the final dimensions, that although comparisons regarding the X and Y axes deviations within the same geometry are accurate, the same cannot be said about comparisons between those same deviations between two different parts.

When searching for an axis specific deviation, possibly caused by a miss-calibration of the robotic arm, the results were not as straightforward as expected. Observing the final dimensions of all the parts, provided throughout this chapter, it first became apparent when constructing the thin pins and thin vertical holes, that there was a higher deviation following the Y axis. Be that as it may, upon the manufacture of the straight walls, cross shaped intersection and staircase vertical increment, the scenario changed and the X axis deviated more from the CAD's original dimensions. Nonetheless, it's important to remember that these final geometries had an associated deviation caused by the deposition

path generated by the software, so a clear judgement on axis deviation could not be made as the software's limitation ended up bottlenecking the setup's capacities. However, the information gathered from the first two geometries mentioned, comprised of small details, enables to see that the deviations are small when in comparison to the dimensions of the parts and only became relevant when caused by the software and not the robot itself.

In order to further complement this information, once both sets of straight walls were completed, it was possible to evaluate the parallelism between both walls. For this purpose, the distance between both the X-axis oriented and Y-axis oriented walls was measured at five distinct points. Upon inspecting the results gathered and presented in table 4.12, it's possible to infer that the majority of the distance differences between them are minimal, likely caused by the bead surface waviness, and therefore negligible. Both sets of walls also presented a significant distance difference at the end of the structures. This difference is likely associated with a material accumulation, generated at the beginning of each deposition. Lastly, it's possible to verify that while the average distance between the X-axis oriented walls was 17.98 mm, the one between the Y-axis oriented walls was 17.18 mm. This 0.8 mm difference could be correlated with an axis-specific deviation, but it's also important to mention that these two sets of walls were respectively the first and the last geometries being deposited on the final test artifact (figure 4.30). Consequently, it's normal that there are some differences between them, in regards to the heat extraction capacities, and consequently, in their width values, thus affecting the distance between them.

Table 4.12: Distances, in millimeters, between walls for both X-axis and Y-axis aligned walls.

| | | | | | |
|-------------------------------------|------|------|------|------|------|
| X-Axis Straight Walls Distance [mm] | 17.3 | 17.3 | 17.4 | 17.4 | 16.5 |
| Y-Axis Straight Walls Distance [mm] | 18.2 | 18.1 | 18.1 | 18.1 | 17.4 |

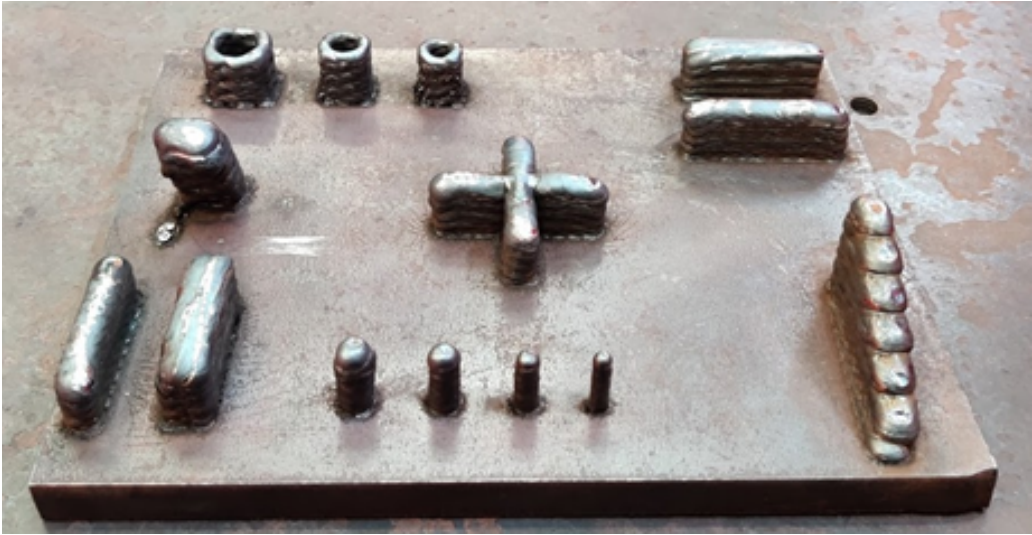


Figure 4.30: Final outcome of the test artifact.

Regarding the Z axis, it did not present any type of setback or deviation, mostly because as explained already, it's possible to adjust and correct the Z coordinate, or the part's height, via adjustment of the deposition parameters.

Ultimately, when taking everything into consideration, it's possible to state that the robot does not need the recalibration of any of its degrees of freedom. The only areas requiring maintenance are then the electric arc generation equipment, to prevent ignition delay, and a change to the robot's core programming, to correct the problem causing an increase in the wire travel speed on the last deposition parcels.

Additionally, for further use of this setup, the software induced limitations and deviations should be taken into consideration. Despite not being able to replicate the CAD's dimensions, after a certain point when the dimensions were too small, the user can account for these effects and alter the CAD model to better fit and compensate them. A simple example lies within the manufacture of the straight walls: as the software generated a deposition path, that would lead to a wall that was three to four millimetres bigger than desired, the user can prevent this by shortening the model by that same length and produce a part with the desired dimensions.

Finally, it's important to highlight once more that the results presented and the limits that were obtained are highly influenced by the setup and materials used. For instance, the use of a wire feed with a smaller diameter can lead to smaller depositions, thus leading to thinner parts. As such, a different setup will perform differently, with different limitations.

Chapter 5

Conclusions

The main objective that was set for this thesis, was to project and manufacture a test artifact that was specific to wire arc additive manufacturing (WAAM). In other words, the major goal was to create a test artifact that was better suited for geometries performed with WAAM and that accounted for the limitations inherent to the process. Additionally, this test artifact should provide the user with information regarding any geometrical limitation derived of the process from the setup, either regarding software or hardware.

As such, a set of benchmark geometries, selected in order to emulate WAAM built geometries, were gathered and their outcomes were promptly analysed. To summarize, the following evaluation presents a brief overview of the results obtained:

- **Overhanging structures:** Partial overhangs were proven to be feasible with this setup, as it was the case of the inclined wall that made a 60° with the substrate. However, as the manufacture of this geometry was pretty challenging and, as corroborated by previous investigations (namely by Ding et al. [35]), the build of a fully overhanging structure was not possible. It is then possible to state that the setup is capable to construct overhangs ranging from 60° from the substrate, up until 90° ;
- **Thin pins:** Successfully produced progressively thinner pins, with minimal deviations from the CAD's original model, up until the 4 mm pin. The minimal diameter was imposed by a software limitation, as the hardware itself was capable to reduce even further this diameter. The minimal diameter achieved was of 5.2 mm;
- **Thin resolution holes:** Similarly to the thin pins, recreated accurately up until a point where a software induced limitation prevented a decrease of the resolution hole, while maintaining all the required dimensions as intended. This point coincided with the build of the geometry with the 8 mm hole, thus failing to recreate it. The distinction between the straight sections and the rounded corners was sufficiently performed, presenting however the first signs of merge between them, on the last built hole (8 mm hole). There was also no lack nor excess of material in the part's corners, caused by the change of direction of the torch, and consequent change in linear velocity;

- **Straight walls:** A possible miscalculation within the software, led to an excessive generation of deposition parcels and thus, a length higher than expected. As it was not possible to change the location of the first and last deposition parcels, the length could not be corrected. However, the part's width was correct, with negligible deviations, when regarding the horizontal guide line strategy. In regards to the vertical guide line strategy, the length was smaller than expected, contrasting with the higher than expected wall width, both suspected to be a consequence of said miscalculation within the software. Both of the strategies presented an accurate height replication. Furthermore, both sets of walls also presented satisfactory results regarding the parallelism between walls;
- **Cross shaped intersection:** The dimensions followed the same tendencies presented when building the straight walls, as the geometries were similar. Furthermore, it was possible to produce a homogeneous intersection, without any lack or excess of material;
- **Staircase vertical increment:** Once more, this geometry inherited the same problem presented in the straight walls, as the geometries were similar. Furthermore, the width was higher than the two previous geometries, as well as the length, due to heat input accumulation, as the amount of steps progressed. The height of each step however, tended to decrease the higher the step, for the same reasons.

Ultimately, it was found that few restriction were imposed by the setup's hardware components. No significant deviations following the X, Y or Z axes were found, during the manufacture of the test artifact, hence suggesting that no recalibration, to the robotic arm's axes, is required. There were however some problems regarding the timing of the electric arc ignition, as well as an undesired wire travel speed alteration, during the last deposition segments. These problems ended up affecting the final geometry of the parts and, in order to ensure the most precise deposition possible using this setup, said problems should be corrected.

However, most of the setup imposed geometrical limitations were caused by the software used to generate the deposition paths. The inability to manually alter the path provided, along side a suspected miscalculation of deposited material within the software, prevented to further decrease the dimensions of geometries like the thin pins and thin resolution holes. The straight walls, cross shaped intersection and staircase vertical increment were affected as well, as it was not possible to adjust the parts' width.

Concluding, a successful WAAM specific test artifact was created, that allowed to adequately evaluate the manufacturing capabilities of the setup. The results provided, allowed to infer that, as it stands, the setup test is adequate for WAAM, although a more recent version of the WAAMSoft is advised.

5.1 Future Work

The test artifact that was presented in this thesis, is merely a stepping stone for the future work that can still be done on this subject. Examples of such work, go through some of the following topics:

- Incorporation of different types of overhangs, not only through the production of inclined walls, but

also different shaped protrusions on vertical walls or elbow shaped vertical increments. Different aspect ratios for such overhangs could also be applied;

- Addition of the analysis of thin ribs, with increasingly smaller aspect ratios, in order to determine the finest wall possible to produce;
- Complementing the previous point, the study of resolution slots, also with increasingly smaller aspect ratios, should also be performed;
- Further development of linear artifacts, not only aiming at the analysis of X, Y and Z axes deviations, but also incorporating diagonally positioned elements;
- Addition of artifacts dedicated to the evaluation of the surface finish, allowing the comparison between several deposition strategies.
- Once more benchmark geometries have been tested, the aggregation of specific geometries for distinct purposes might be pertinent. In other words, it might be useful to promote the creation of a test artifact, as an example, with the specific purpose of revealing the thinnest features possible to create, or one that focuses on analysing axis specific deviations;
- The test of other deposition path planing programs should also be performed. This will grant the user with a comparison between softwares, from which it's possible to select the one that best fits the geometry intended to manufacture. Furthermore, it can also allow to reveal other setup limitations that were otherwise unknown, caused by the bottlenecking generated by a software limitation.

Bibliography

- [1] S. W. Williams, F. Martina, A. C. Addison, J. Ding, G. Pardal, and P. Colegrove. Wire+ arc additive manufacturing. *Materials Science and Technology*, 32(7):641–647, 2016.
- [2] G. N. Levy, R. Schindel, and J.-P. Kruth. Rapid manufacturing and rapid tooling with layer manufacturing (lm) technologies, state of the art and future perspectives. *CIRP annals*, 52(2):589–609, 2003.
- [3] W. J. Sames, F. List, S. Pannala, R. R. Dehoff, and S. S. Babu. The metallurgy and processing science of metal additive manufacturing. *International Materials Reviews*, 61(5):315–360, 2016.
- [4] P. Almeida and S. Williams. Innovative process model of ti–6al–4v additive layer manufacturing using cold metal transfer (cmt). In *Proceedings of the twenty-first annual international solid freeform fabrication symposium, University of Texas at Austin, Austin, TX, USA*, 2010.
- [5] S. Selvi, A. Vishvaksenan, and E. Rajasekar. Cold metal transfer (cmt) technology-an overview. *Defence technology*, 14(1):28–44, 2018.
- [6] TWI-Global. Current and voltage fluctuations during the dip-transfer mode of mig/mag welding. URL <https://www.twi-global.com/technical-knowledge/job-knowledge/mig-mag-developments-in-low-heat-input-transfer-modes-133>. viewed on 2019-11-08.
- [7] J. Oliveira, T. Santos, and R. Miranda. Revisiting fundamental welding concepts to improve additive manufacturing: From theory to practice. *Progress in Materials Science*, page 100590, 2019.
- [8] J. Roman, P. Colegrove, and S. Williams. Analytical Model for Distortion Prediction in Wire + Arc Additive Manufacturing. 6:277–282, 2018.
- [9] L. Martin. Giant satellite fuel tank sets new record for 3-d printed space parts, 2018. URL https://news.lockheedmartin.com/2018-07-11-Giant-Satellite-Fuel-Tank-Sets-New-Record-for-3-D-Printed-Space-Parts#assets_all. viewed on 2020-02-11.
- [10] E. Berger. Relativity space reveals its ambitions with big nasa deal, 2018. URL <https://arstechnica.com/science/2018/03/relativity-space-reveals-its-ambitions-with-big-nasa-deal/>. viewed on 2020-02-12.
- [11] R. Space. URL <https://www.relativityspace.com/stargate>. viewed on 2020-02-12.

- [12] P. Kazanas, P. Deherkar, P. Almeida, H. Lockett, and S. Williams. Fabrication of geometrical features using wire and arc additive manufacture. *Proceedings of the Institution of Mechanical Engineers, Part B: Journal of Engineering Manufacture*, 226(6):1042–1051, 2012.
- [13] X. Xu, J. Ding, S. Ganguly, C. Diao, and S. Williams. Preliminary investigation of building strategies of maraging steel bulk material using wire+ arc additive manufacture. *Journal of Materials Engineering and Performance*, 28(2):594–600, 2019.
- [14] G. Venturini, F. Montevercchi, A. Scippa, and G. Campatelli. Optimization of waam deposition patterns for t-crossing features. *Procedia CIRP*, 55:95–100, 2016.
- [15] R. Israr, J. Buhl, L. Elze, and M. Bambach. Simulation of different path strategies for wire-arc additive manufacturing with lagrangian finite element methods. In *LS-DYNA Forum*, 2018.
- [16] T. A. Rodrigues, V. Duarte, R. Miranda, T. G. Santos, and J. Oliveira. Current status and perspectives on wire and arc additive manufacturing (waam). *Materials*, 12(7):1121, 2019.
- [17] J. Mehnen, J. Ding, H. Lockett, and P. Kazanas. Design study for wire and arc additive manufacture. *International Journal of Product Development* 20, 19(1-3):2–20, 2014.
- [18] G. Venturini, F. Montevercchi, A. Scippa, and G. Campatelli. Optimization of waam deposition patterns for t-crossing features. *Procedia CIRP*, 55:95–100, 2016.
- [19] B. S. Rupal, R. Ahmad, and A. J. Qureshi. Feature-based methodology for design of geometric benchmark test artifacts for additive manufacturing processes. *Procedia Cirp*, 70:84–89, 2018.
- [20] S. Moylan, A. Cooke, M. A. Donmez, K. Jurrens, S. Moylan, and J. Slotwinski. *A review of test artifacts for additive manufacturing*. US Department of Commerce, National Institute of Standards and Technology, 2012.
- [21] M. Mahesh, Y. Wong, J. Fuh, and H. Loh. Benchmarking for comparative evaluation of rp systems and processes. *Rapid Prototyping Journal*, 2004.
- [22] J.-P. Kruth, B. Vandenbroucke, J. Van Vaerenbergh, and P. Mercelis. Benchmarking of different sls/slm processes as rapid manufacturing techniques. In *Proceedings of the International Conference Polymers & Moulds Innovations PMI 2005*, 2005.
- [23] L. Castillo. Study about the rapid manufacturing of complex parts of stainless steel and titanium. *TNO report with the collaboration of AIMME*, 2005.
- [24] L. Rebaioli and I. Fassi. A review on benchmark artifacts for evaluating the geometrical performance of additive manufacturing processes. *The International Journal of Advanced Manufacturing Technology*, 93(5-8):2571–2598, 2017.
- [25] S. W. Williams, F. Martina, A. C. Addison, J. Ding, G. Pardal, and P. Colegrove. Wire+ arc additive manufacturing. *Materials Science and Technology*, 32(7):641–647, 2016.

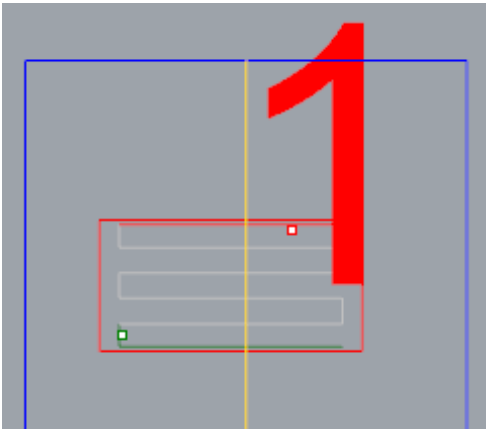
- [26] A. Addison, J. Ding, F. Martina, H. Lockett, S. Williams, and X. Zhang. Manufacture of complex titanium parts using wire+ arc additive manufacture. *Titanium Europe*, 2015.
- [27] L. Neto. Studying the application of additive manufacturing to large parts. Master's thesis, Instituto Superior Técnico, 2017.
- [28] C. Cunningham, S. Wikshåland, F. Xu, N. Kemakolam, A. Shokrani, V. Dhokia, and S. Newman. Cost modelling and sensitivity analysis of wire and arc additive manufacturing. *Procedia Manufacturing*, 11:650–657, 2017.
- [29] L. Fialho. Development of wire arc additive manufacturing (waam) procedures that allow depositing very complex structures without support. Master's thesis, Instituto Superior Técnico, 2019.
- [30] J. Prado-Cerqueira, A. Camacho, J. Diéguez, Á. Rodríguez-Prieto, A. Aragón, C. Lorenzo-Martín, and Á. Yanguas-Gil. Analysis of favorable process conditions for the manufacturing of thin-wall pieces of mild steel obtained by wire and arc additive manufacturing (waam). *Materials*, 11(8): 1449, 2018.
- [31] Iso/astm 52902, 2019, “ additive manufacturing—test artefacts—standard guideline for geometric capability assessment of additive manufacturing systems,” astm international, west conshohocken, pa, standard no. iso/astm 52902:2019.
- [32] Kuka kr 16 industrial robots with its 6 axes shown. URL https://www.researchgate.net/figure/Kuka-KR-16-Industrial-Robots-with-its-6-Axes-shown_fig11_200101490. viewed on 2020-07-21.
- [33] D. Ding, Z. Pan, D. Cuiuri, and H. Li. A multi-bead overlapping model for robotic wire and arc additive manufacturing (waam). *Robotics and Computer-Integrated Manufacturing*, 31:101–110, 2015.
- [34] J. Xiong, Y. Lei, H. Chen, and G. Zhang. Fabrication of inclined thin-walled parts in multi-layer single-pass gmaw-based additive manufacturing with flat position deposition. *Journal of Materials Processing Technology*, 240:397–403, 2017.
- [35] D. Ding, Z. Pan, D. Cuiuri, H. Li, N. Larkin, and S. Van Duin. Automatic multi-direction slicing algorithms for wire based additive manufacturing. *Robotics and Computer-Integrated Manufacturing*, 37:139–150, 2016.
- [36] L. Rebaioli and I. Fassi. A review on benchmark artifacts for evaluating the geometrical performance of additive manufacturing processes. *The International Journal of Advanced Manufacturing Technology*, 93(5-8):2571–2598, 2017.
- [37] L. Ji, J. Lu, S. Tang, Q. Wu, J. Wang, S. Ma, H. Fan, and C. Liu. Research on mechanisms and controlling methods of macro defects in tc4 alloy fabricated by wire additive manufacturing. *Materials*, 11(7):1104, 2018.

- [38] N. Pépe, S. Egerland, P. A. Colegrove, D. Yapp, A. Leonhartsberger, and A. Scotti. Measuring the process efficiency of controlled gas metal arc welding processes. *Science and Technology of Welding and Joining*, 16(5):412–417, 2011.
- [39] Joining processes: Physics of welding arc. URL <https://fenix.tecnico.ulisboa.pt/disciplinas/PLig3645111326/2018-2019/2-semester/slides>. viewed on 2020-03-19.
- [40] Joining processes: Gas metal arc welding (gmaw) metal active/inert gas(mig/mag) welding. URL <https://fenix.tecnico.ulisboa.pt/disciplinas/PLig3645111326/2018-2019/2-semester/slides>. viewed on 2020-03-19.
- [41] W. Galverly, F. Marlow, and P. Tallman. *Welding Essentials: Questions & Answers*. Industrial Press, 2001. ISBN 9780831131517. URL <https://books.google.pt/books?id=jNxCxwp2fHoC>.
- [42] K. Ayarkwa, S. Williams, and J. Ding. Investigation of pulse advance cold metal transfer on aluminium wire arc additive manufacturing. *International Journal of Rapid Manufacturing*, 5(1):44–57, 2015.
- [43] J. Ding, F. Martina, and S. Williams. Production of large metallic components by additive manufacture—issues and achievements. In *Conf. Pap., nov*, 2015.
- [44] G. Venturini, F. Montevicchi, F. Bandini, A. Scippa, and G. Campatelli. Feature based three axes computer aided manufacturing software for wire arc additive manufacturing dedicated to thin walled components. *Additive Manufacturing*, 22:643–657, 2018.
- [45] L. M. S. C. Neto. Studying the application of additive manufacturing to large parts. *Universidade de Lisboa, Lisbon*, 2017.

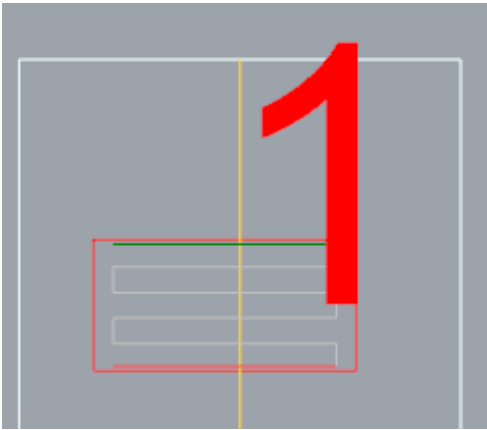
Appendix A

Deposition paths

A.1 Inclined Walls



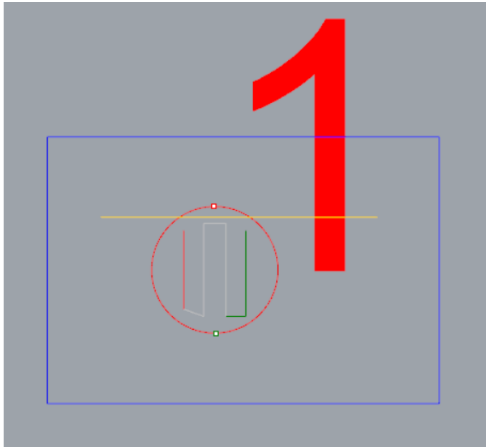
(a) Deposition path for the 60° inclined wall, for even layers.



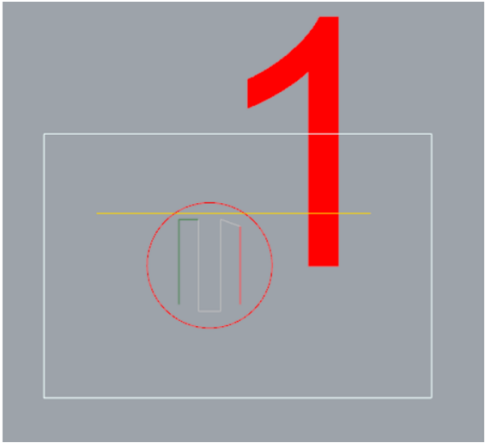
(b) Deposition path for the 60° inclined wall, for odd layers.

Figure A.1: Deposition paths for the 60° inclined wall.

A.2 Thin Pins

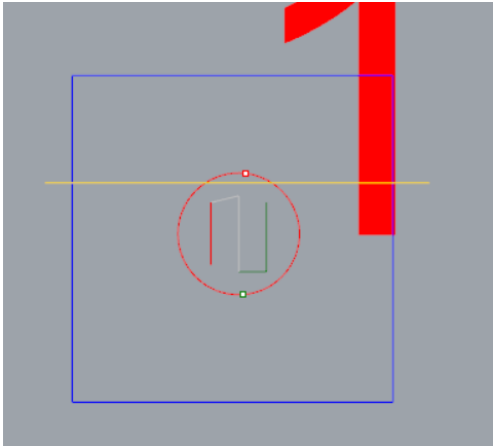


(a) Deposition path for the 10 mm pin, for even layers.

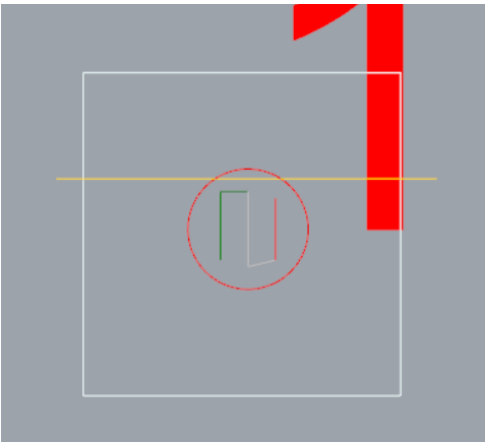


(b) Deposition path for the 10 mm pin, for odd layers.

Figure A.2: Deposition paths for the 10 mm pin.

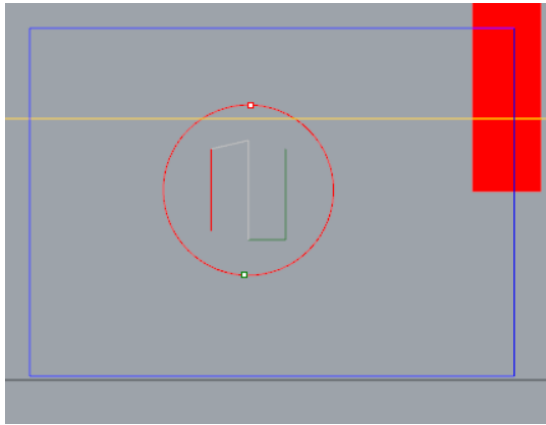


(a) Deposition path for the 8 mm pin, for even layers.

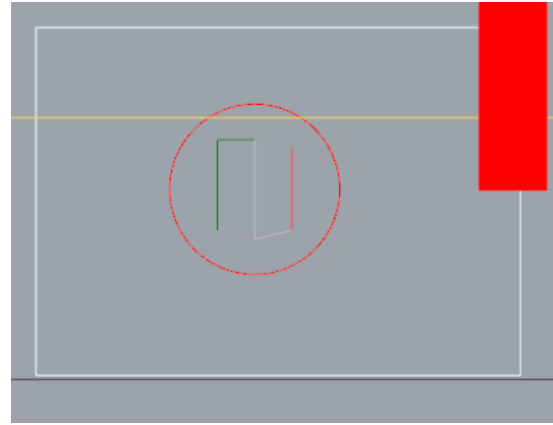


(b) Deposition path for the 8 mm pin, for odd layers.

Figure A.3: Deposition paths for the 8 mm pin.

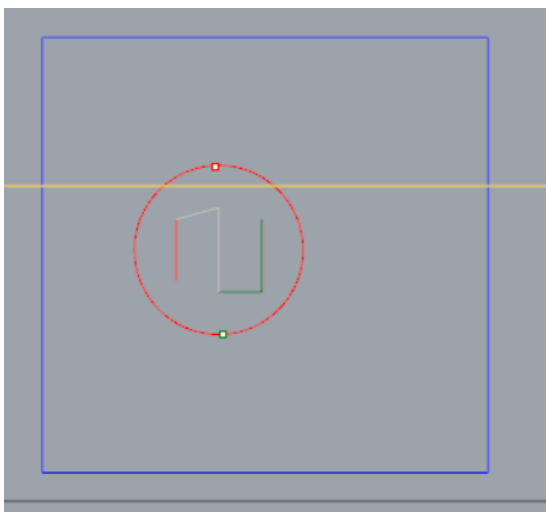


(a) Deposition path for the 6 mm pin, for even layers.

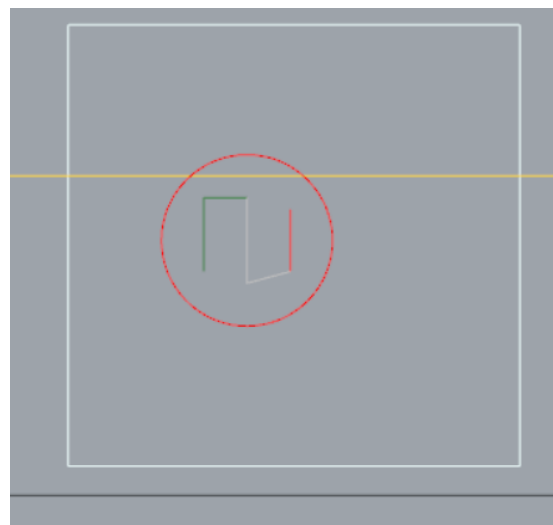


(b) Deposition path for the 6 mm pin, for odd layers.

Figure A.4: Deposition paths for the 6 mm pin.



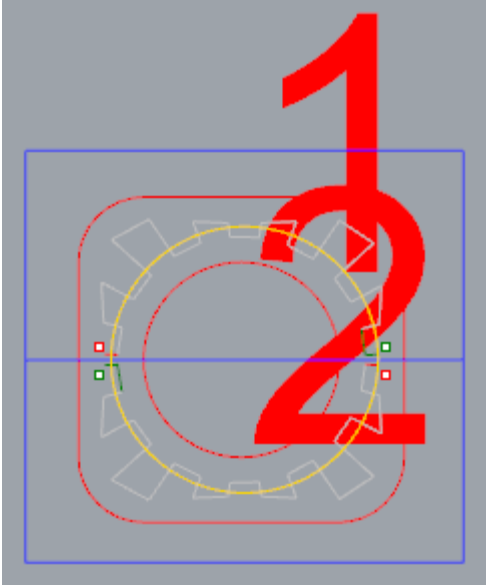
(a) Deposition path for the 4 mm pin, for even layers.



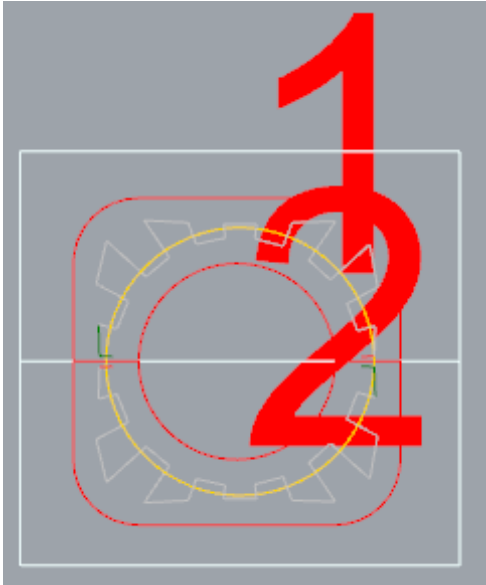
(b) Deposition path for the 4 mm pin, for odd layers.

Figure A.5: Deposition paths for the 4 mm pin.

A.3 Thin Resolution Holes

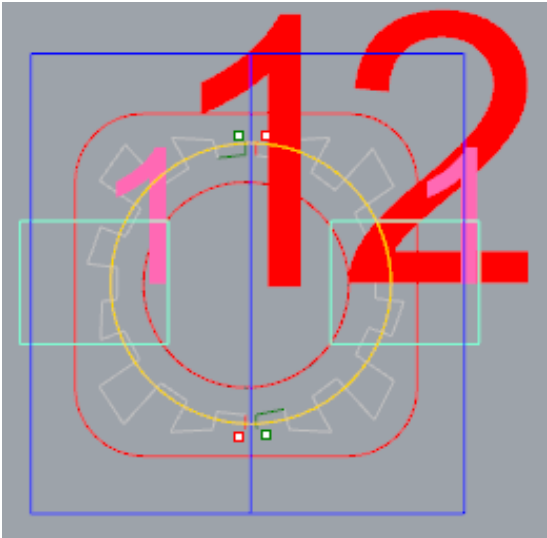


(a) Deposition path for the 15 mm thin resolution hole, with a horizontal guide line, for even layers.

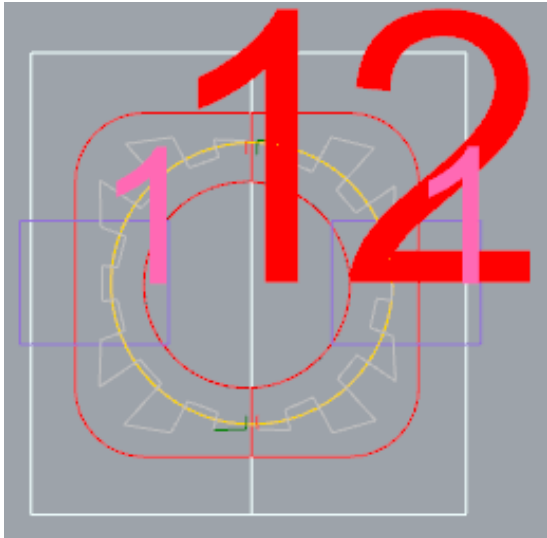


(b) Deposition path for the 15 mm thin resolution hole, with a horizontal guide line, for odd layers.

Figure A.6: Deposition paths for the 15 mm thin resolution hole, with a horizontal guide line.

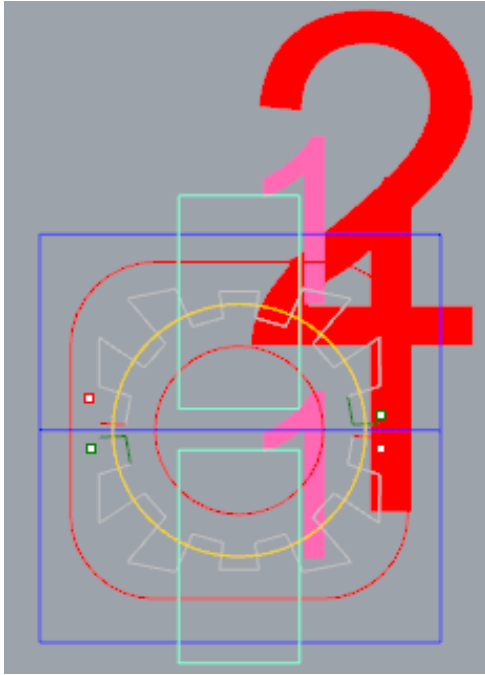


(a) Deposition path for the 15 mm thin resolution hole, with a vertical guide line, for even layers.

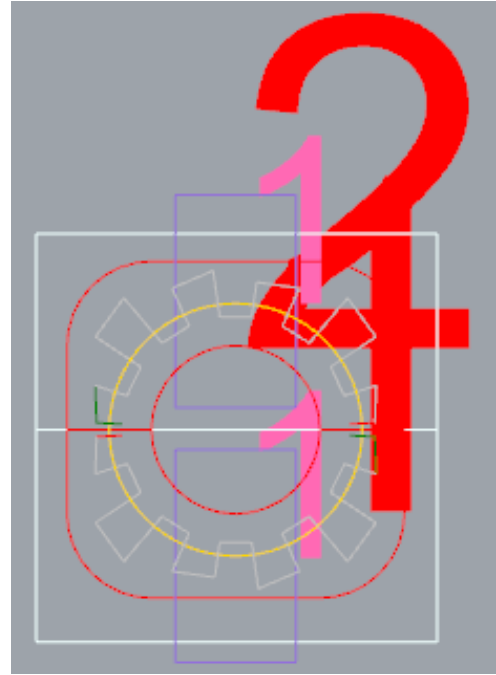


(b) Deposition path for the 15 mm thin resolution hole, with a vertical guide line, for odd layers.

Figure A.7: Deposition paths for the 15 mm thin resolution hole, with a vertical guide line.

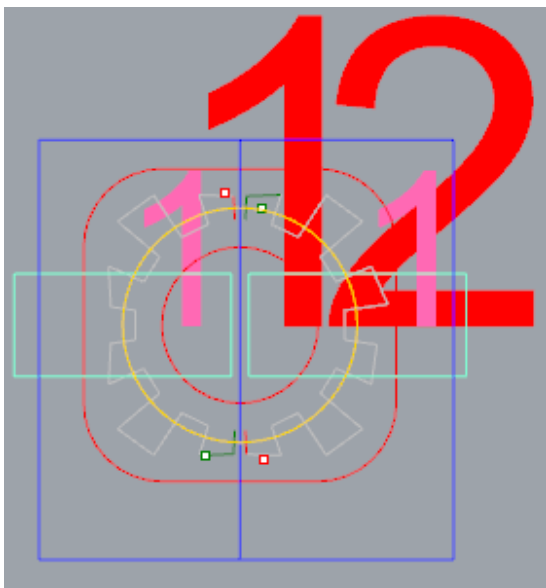


(a) Deposition path for the 10 mm thin resolution hole, with a horizontal guide line, for even layers.

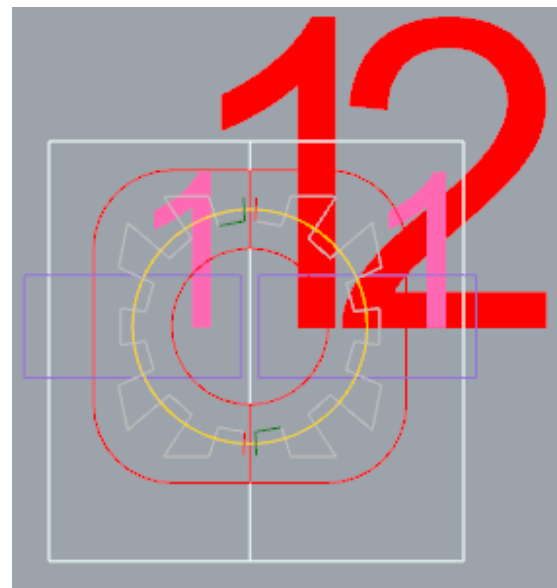


(b) Deposition path for the 1 mm thin resolution hole, with a horizontal guide line, for odd layers.

Figure A.8: Deposition paths for the 10 mm thin resolution hole, with a horizontal guide line.

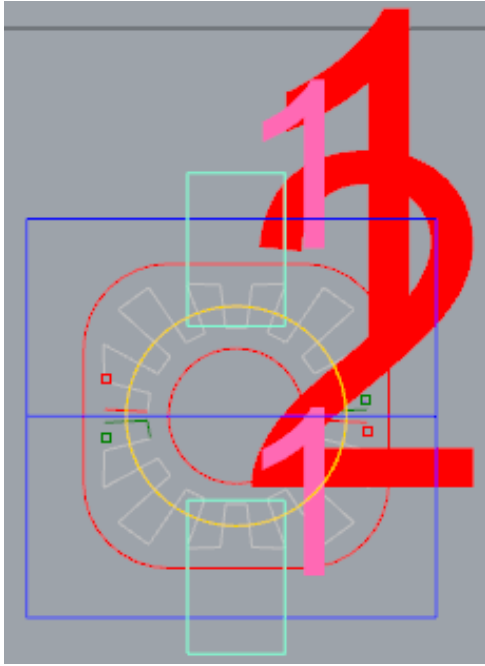


(a) Deposition path for the 10 mm thin resolution hole, with a vertical guide line, for even layers.

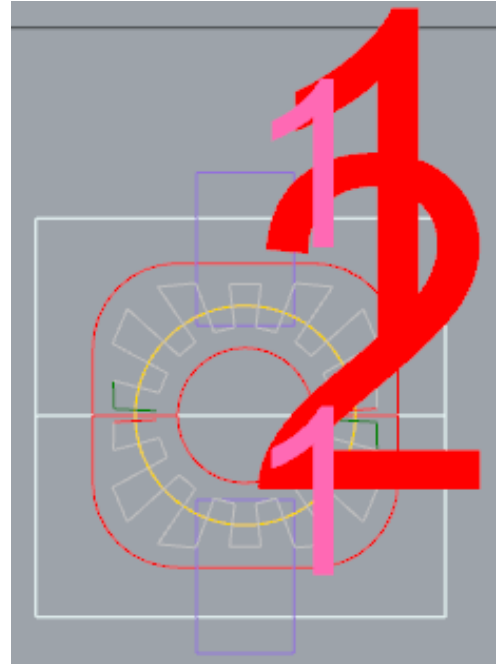


(b) Deposition path for the 10 mm thin resolution hole, with a vertical guide line, for odd layers.

Figure A.9: Deposition paths for the 10 mm thin resolution hole, with a vertical guide line.

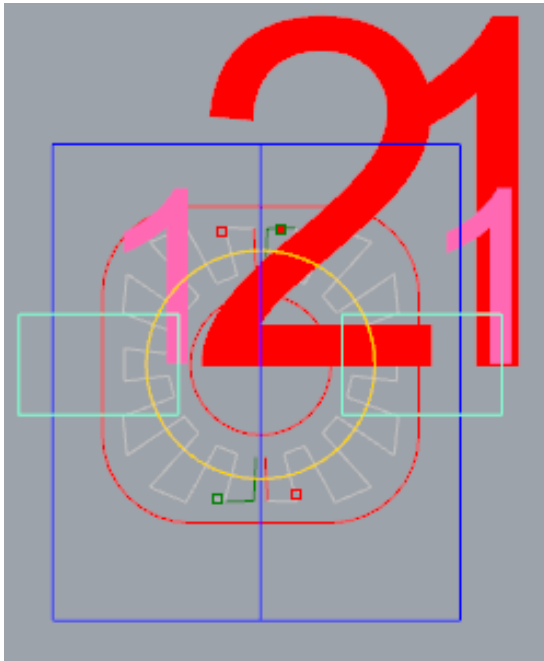


(a) Deposition path for the 8 mm thin resolution hole, with a horizontal guide line, for even layers.

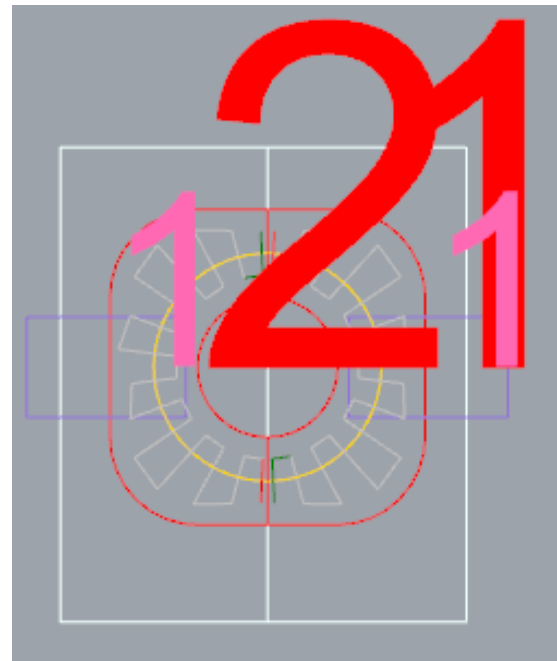


(b) Deposition path for the 8 mm thin resolution hole, with a horizontal guide line, for odd layers.

Figure A.10: Deposition paths for the 8 mm thin resolution hole, with a horizontal guide line.



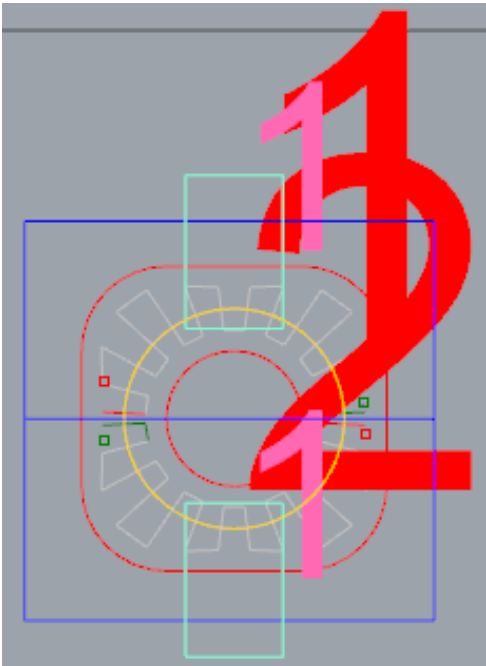
(a) Deposition path for the 8 mm thin resolution hole, with a vertical guide line, for even layers.



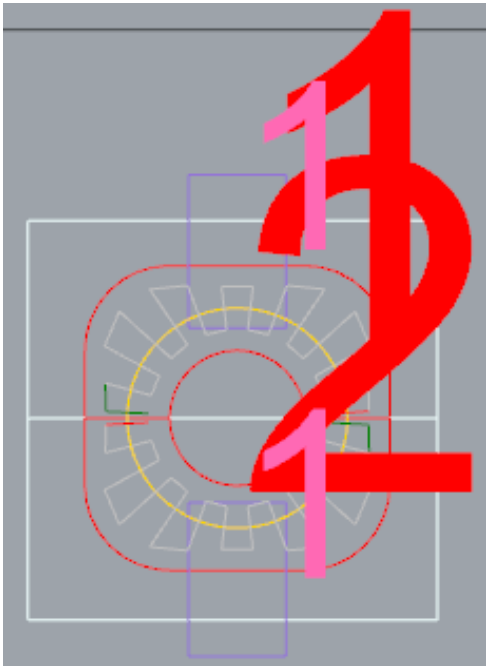
(b) Deposition path for the 8 mm thin resolution hole, with a vertical guide line, for odd layers.

Figure A.11: Deposition paths for the 8 mm thin resolution hole, with a vertical guide line.

A.4 Straight Walls

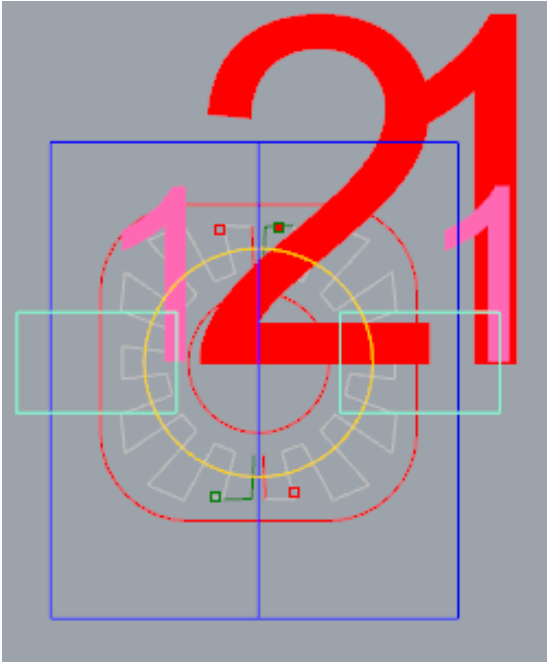


(a) Deposition path for the straight wall, with a horizontal guide line, for even layers.

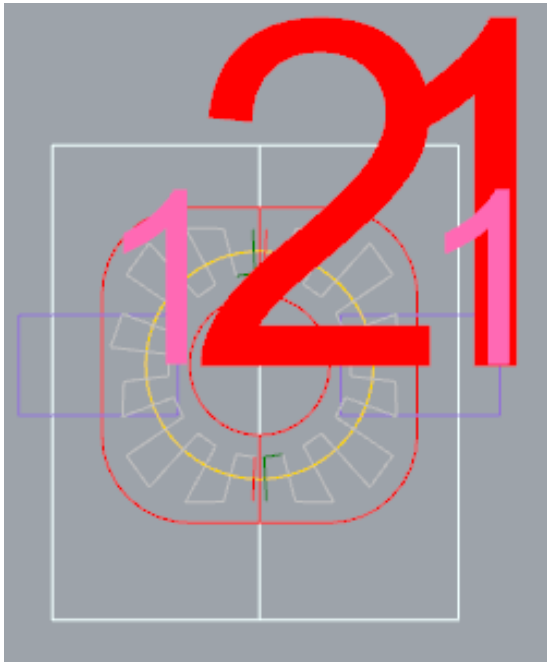


(b) Deposition path for the straight wall, with a horizontal guide line, for odd layers.

Figure A.12: Deposition paths for the straight wall, with a horizontal guide line.



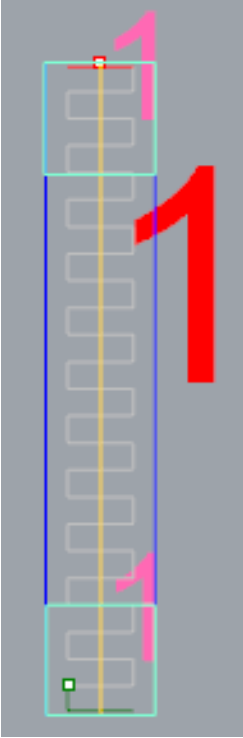
(a) Deposition path for the straight wall, with a vertical guide line, for even layers.



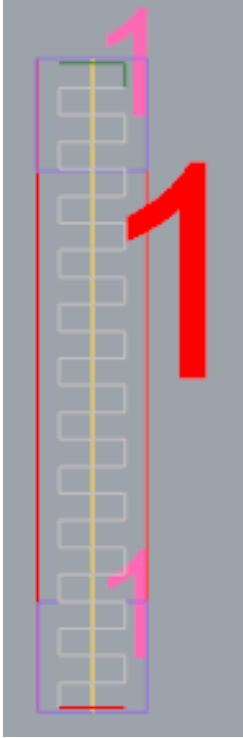
(b) Deposition path for the straight wall, with a vertical guide line, for odd layers.

Figure A.13: Deposition paths for the straight wall, with a vertical guide line.

A.6 Staircase Vertical Increment

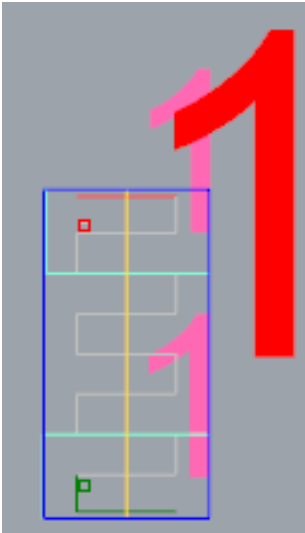


(a) Deposition path for the staircase vertical increment, for the even layers up until layer 9.

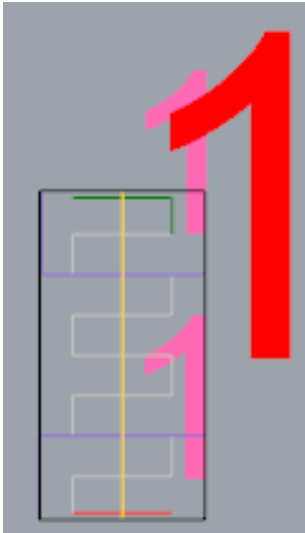


(b) Deposition path for the staircase vertical increment, for odd layers until layer 10.

Figure A.15: Deposition paths for the staircase vertical increment, up until layer 10.

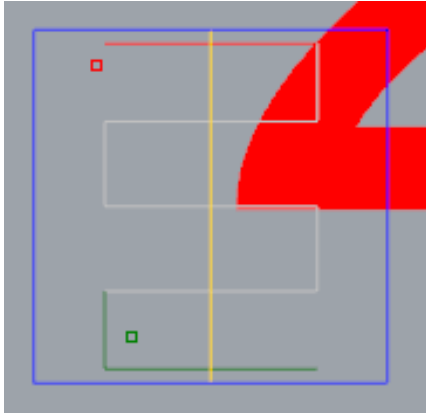


(a) Deposition path for the staircase vertical increment, for layer 11.

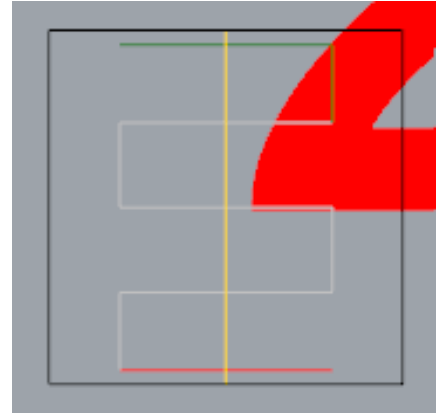


(b) Deposition path for the staircase vertical increment, for layer 12.

Figure A.16: Deposition paths for the staircase vertical increment, for layers 11 e 12.



(a) Deposition path for the staircase vertical increment, for layer 13.



(b) Deposition path for the staircase vertical increment, for layer 14.

Figure A.17: Deposition paths for the staircase vertical increment, for layers 13 e 14.